DEVELOPMENT OF BIO-COMPOSITE BLADES FOR STRAIGHT DARRIEUS WIND TURBINES

A Thesis Submitted in

Partial Fulfillment of the Requirements

for the Degree of

DOCTOR OF PHILOSOPHY

By

MRIDUSMITA BORA

(Roll No.186151005)

SCHOOL OF ENERGY SCIENCE AND ENGINEERING

INDIAN INSTITUTE OF TECHNOLOGY GUWAHATI

GUWAHATI-781039, ASSAM, INDIA

SEPTEMBER, 2024

Dedicated to my parents and siblings for their endless love, support, and encouragement throughout my pursuit of this academic endeavor.

I hope this achievement will fulfill the dream they envisioned for me.

Certificate

This is to certify that the thesis entitled "**Development of Bio-Composite Blades for Straight Darrieus Wind Turbines**" being submitted by **Miss. Mridusmita Bora** to the Indian Institute of Technology, Guwahati, for the award of the degree of Doctor of Philosophy in the School of Energy Science and Engineering is a record of original bonafide research work carried out by her under our supervision and guidance. The thesis work, in our opinion, has reached the requisite standard fulfilling the requirements for the degree of Doctor of Philosophy.

The results contained in this thesis have not been submitted in part or full to any other University or Institute for the award of any degree or diploma.

Dr. Niranjan Sahoo
(Thesis Supervisor),
Department of Mechanical Engineering,
IIT Guwahati-781039, Assam India.

Dr. Poonam Kumari
(Thesis Co-Supervisor),
Department of Mechanical Engineering,
IIT Guwahati-781039, Assam India.

Declaration

I, Mridusmita Bora (Roll No: 186151005) declare that the present written submission is my thoughts in my own words. I have adequately cited and referenced the original sources, where other's ideas have been involved. I also declare that I have adhered to all principles of academic honesty and integrity and have neither fabricated nor falsified any idea/data/fact/source in my submission. I understand that any violation of the above will be cause for disciplinary action by the Institute and can also evoke penal action from the sources which have thus not been properly cited or from whom proper permission has not been taken when needed.

Date: Mridusmita Bora

Place: IIT Guwahati Roll No. 186151005

Acknowledgements

First and foremost, I want to express my sincere gratitude toward my Ph.D. supervisor, Prof. Niranjan Sahoo and co-supervisor Dr. Poonam Kumari, for providing me an opportunity to work under their supervision. I am grateful to them for their consistent guidance, motivation, patience, kindness, over these years. They have always made available themselves for discussions besides their busy schedules. Their enthusiasm, sublime work ethics, analytical abilities, and never-say-die attitude toward research and life as well, has natured my scientific skills and also inspired me immensely to work hard. I am proud to have them as my Ph.D. supervisor and co-supervisor. Thank you, Sir and Ma'am, for all your help, advice, and support.

I want to thank my doctoral committee member, Prof., Ujjwal Kumar Saha, Prof. Vinayak Kulkarni, and Dr. Pankaj Kalita, for their encouragement, insightful comments, and suggestions which have helped me to refine and widen my research from various perspectives. My sincere gratitude also goes to the Head of School of Energy Science and Engineering, Prof. Vaibhav V Goud, for providing all the resources needed for my research. I also thankful to all faculty and staff members of the School of Energy Science and Engineering who help me whenever I needed. Without their help, it would not have been possible to conduct my research. It is an honor for me to thank the Indian Institute of Technology Guwahati for giving me such an excellent opportunity for undergoing my research.

I gratefully acknowledge the ADMECA Design and Engineering Soultions, India for providing financial support to support this research work.

I want to thank my labmates, and my seniors Dr. Agyapal Singh, Dr. Satish, Mr. Dhirendra, Dr. Devamallika, Dr. Shiv Sahaya Shukla for their timely help, suggestions,

and encouragements. I am indebted to my colleagues, Sikha Moni Nath, and Joyshree Das with whom I had a very good time. My special gratitude goes to my family for their role in my life. I offer my regards to my loving parents, Mr. Nripendra Kumar Bora and Mrs. Mala Rani Bora, whose love, teachings, sacrifices, and blessings brought me this far. Their unconditional love, support, and trust on me are the most precious gift that I have. I am thankful to my younger brothers, Mr. Bitupan Bora and Mr. Bedabrata Bora for their eternal love and all kind of support. Their inspiration, understating, and faith in me have been my greatest strength.

I extend my sincere thank to my friends Khyati Manjari Choudhary, Sonam Kalita, Bhargab Bora, Devismita Sanjay who helped me emotionally, socially during the tough time of my life. Thanks for being what you are. My parents, and my brothers are the backbone of my happiness, and I dedicate my thesis to them.

Finally, I thank God for always being with me.

Mridusmita Bora

Abstract

In the present modernized world, with the increase in energy demand, conventional energy sources are not only towards the depletion stage but also causing serious adverse effects on the environment. The escalating environmental concerns and the urgent need for sustainable energy solutions have intensified the quest for renewable energy sources. Among the various renewable sources, wind is the most viable and practical form, generating a large amount of usable electricity. However, the conventional materials used in the construction of wind turbine blades such as glass/carbon fiber reinforced polymers (FRPs) have raised serious environmental concerns due to their non-biodegradable nature and reliance on fossil fuels during manufacturing. To address these challenges, the development of bio-composite materials represents an environmentally friendly alternative for wind turbine blades. These composites possess several advantages over conventional composites, including a low carbon footprint, better recyclability, and possible improved mechanical properties.

The research aims to investigate the mechanical properties of bio-based composites developed from natural material (bamboo) for wind turbine blade application. Different bamboo species are selected from the North-Eastern region of India and the developed composites are tested for mechanical strength. The elastic material properties of the bamboo composite is evaluated using representative volume element (RVE) homogenization technique. These material properties are utilized for determining the static strength of bamboo composite turbine blades on two standard airfoils. The model is developed in ANSYS and detailed structural analysis is done to get the optimum layup. Free and

forced vibration of the bamboo composite blade is also studied. A three-dimensional model of the straight Darrieus wind turbine is modelled to study the real-time interaction between the blade and the surrounding airflow and finally a prototype of the bamboo blade is fabricated. The results of the experimental investigated demonstrated that the developed bamboo composite has a high specific strength of 245 $MPa.m^3/g$ compared to glass composites with specific strength of 239 $MPa.m^3/g$. Further it is observed that the non-symmetric blade with angle-ply layup showed better structural performance in terms of stress and deflection. The bamboo composite blade have 70.98% and 1.11% less stress and deflection values compared to the glass composite wind turbine blade. The natural frequency values of bamboo composite blades are higher which represents stiffer blades with reduced risk of structural failure. The value of maximum stress from the fluid-structure interaction is 32.26 MPa which is less than the allowable safe stress limit of 96.14 MPa obtained from the experimental results.

It is concluded that bamboo has a high strength-to-weight ratio, which is a crucial factor in designing efficient wind turbine blades. Bamboo is also an attractive substitute for replacing traditional composites like carbon and glass fiber composites in the construction of blades because of its remarkable mechanical properties, low cost, quick growth rate, and availability. Moreover, the density of bamboo is very less compared to traditional glass/carbon fiber composites, which can withstand the mechanical stresses and large deflections associated with wind energy production. The application of bamboo composites in wind turbine blades is a novel and sustainable solution for enhancing the environmental friendliness and efficiency of wind turbine systems.

Contents

List of Figures

List of Tables

List of Abbreviations

AR = Aspect ratio

BC = Boundary condition

BEM = Blade element momentum

BFRC = Bamboo fiber-reinforced composite

BL = Boundary layer

CFD = Computational fluid dynamics

CFRP = Carbon fiber-reinforced polymer

CLT = Classical laminated theory

DOF = Degree of freedom

1D = One dimensional

2D = Two dimensional

3D = Three dimensional

FE = Finite element

FEA = Finite element analysis

FEM = Finite element method

FESEM = Field emission scanning microscopy

FRC = Fiber-reinforced composite

FRF = Frequency response function

FSI = Fluid-structure interaction

FTIR = Fourier transform infrared spectroscopic

GA = Genetic algorithm

GFRP = Glass fiber-reinforced polymer

HAWT = Horizonatal axis wind turbine

LBL = Laminated bamboo lumber

LBC = Laminated bamboo composite

LCC = Lignin-carbohydrate complex

LE = Leading edge

MOE = Modulus of elasticity

MOR = Modulus of rupture

NF = Natural fiber

NFC = Natural fiber composite

NFRC = Natural fiber-reinforced composite

-OH = Hydroxyl

PBC = Periodic boundary condition

RANS = Reynolds Averaged Navier Stroke

ROM = Rule of mixture

RVE = Representative volume element

SB-VAWT = Straight-bladed vertical axis wind turbine

SST = Shear stress transport

SWT = Small wind turbine

TE = Trailing edge

TSR = Tip speed ratio

UC = Unit cell

UTS = Ultimate tensile strength

VARTM = Vacumm assisted resin transfer molding

VAWT = Vertical axis wind turbine

WTB =Wind turbine blade

WT = Wind turbine

List of ASTM standard

Standard	Dimensions	Test
ASTM-D-570-98	(20×20×3) mm^3	Water absorption test
ASTM-D-570-98	(160×14×3) mm^3	Tensile test
ASTM-3479	(250×25×5) mm^3	Fatigue test
ASTM-D-790-3	(130×14×3) mm^3	3-point bending test
ASTM-D-3410	(25×25×15) mm^3	Compression test
ASTM-D-792-12	(20×20×3) mm^3	Density of the composites
ASTM-D-6110	(64×12.7×3.2) mm^3	Charpy Impact test

List of machines used for different testing

FTIR spectrometer - (PerkinELmer, Model: Spectrum-2, Singapore)

Hot oven - (IKON, Model: IK-109,India)

Impact testing machine - (IT-30, Maker: FIE, India)

Sigma Field emission microscopy - (Make: Zeiss, Germany)

Tensile testing machine (Shimadzu, model: AGX-V, Japan)

Weighing balance - (Sartorius, Model: Cubis®, Germany)

Chapter 1

Introduction

1.1 Preface

Energy is the backbone for the economy of any country, and it plays a significant role in the growth and development of that. The rapid advancement of industrialization and the intensive developments of human civilization have had profound detrimental effects on the environment and as well as energy resources. The traditional energy sources such as petroleum crude oil, and natural gas which are the primary energy essentials since the industrial revolution are progressively causing serious environmental concerns and threats to human life. The increasing environmental concerns and the urgent need for sustainable energy solutions have intensified the quest for renewable energy sources such as solar, wind, hydro, and geothermal is growing constantly.

Among these renewable energy sources, wind is one of the primary contributors to the country renewable energy portfolio and has been widely used to satisfy the increasing demand for affordable and clean energy. It is also the key feature to mitigate the adverse consequences of carbon emissions from traditional fossil fuels to fight against increasing global warming. Rotor blades are solely responsible for converting the kinetic energy from wind into electrical power generation. The increasing demand for clean energy has led to a significant rise in the development and installation of wind turbines. The annual installed wind generation capacity has increased from 25 GW to 200 GW in 10 years from 2001 to 2010 [1], and is expected to increase up to 2110 GW by the end of

2030 [2]. The extensive rise in rated power is directly proportional to the blade material usage. During the early nineties, aluminium is used as the blade material for vertical axis wind turbine (VAWT). It is reported that due to a lack of knowledge on fatigue loading characteristics, these extruded aluminium blades showed premature fatigue damage to the ultimate collapse of the structure [3]. Steel is also reported to be utilized as a blade material, however, these blades for electricity generation were considered a failure as one of the blades failed within a few hours of operation [4]. Thus, a new path towards the blade material leads to the introduction of composite materials. Gedser turbine is the first successful wind turbine with composite blades which run for 11 years [5]. Since that, composites have always been the material choice for turbine blades due to their superior fatigue performance compared to other materials.

Blades are the most critical part of the entire system and therefore they must be designed structurally strong to withstand the various external loads during its operation. To meet the response to such critical requirements, composites such as glass-fiber and carbon-fiber composites have emerged as highly suitable materials for high-load structural applications such as wind turbine blade (WTB). These composites have exceptional mechanical properties including high-strength and stiffness, better resistance to fatigue loading, and are lighter in weight. Even though wind energy is claimed to be clean and renewable energy with no adverse impacts during operation, the manufacturing of wind turbine components especially wind blades is very energy-intensive. A wide range of chemical usage and non-biodegradable wastes are associated with the manufacturing of wind turbines. Nowadays about 90% of the blade material is made of fiber-reinforced composites (FRCs). Glass-fiber composites play a primary role in blade manufacturing due to their low cost, higher tensile strength and durability, excellent fatigue resistance,

and impact strength. As these composite blades approach their end of service life, their disposal becomes a crucial aspect of sustainability waste management due to their non-biodegradable nature. Significant amounts of blade waste are being accumulated every year causing serious landfill and disposal problems. Total blade waste of 50,000 tonnes has been reported in the year 2020 which is further expected to increase to 200000 *tonnes* between (2030-2040) and 800000 *tonnes* by the year 2050 as shown in Fig. 1.1 [6]. The growing concern regarding the hazardous blade waste in the landfill/environment and its future disposal problems has shifted the attention toward the development and utilization of cellulose-based fiber composites.

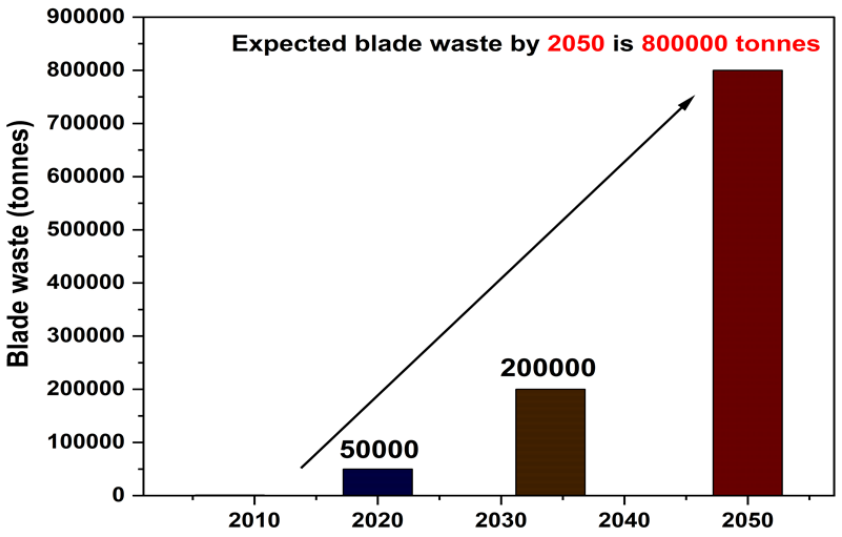

Figure 1.1: Increment in blade waste between 2010-2050.

Natural fiber-reinforced composites (NFRC) offer several benefits such as renewability, recyclability, and biodegradability which makes them superior to synthetic fibers [7]. Natural fibers are suitable for structural applications like wind turbine blades as they are lightweight and carry better mechanical, thermal, and damping properties. However, the biodegradability nature of natural fiber composite is hindered due to the due to the presence of polymer matrix. Despite recycling problems, other economic factors must also be considered for shaping wind energy technology such as material availability,

raw material cost, and manufacturing cost and waste [8]. For these reasons, special attention is focused on developing natural composites for wind turbine as these materials are reliable and cost-effective. The biodegradability issue can be addressed by introducing fully biodegradable or bio-based polymers for composite materials in developing more environmentally friendly solutions for turbine blade manufacturing and disposal. They also offers the potential to capture onsite wind energy generation by manufacturing wind blades using locally produced composite materials. Thus, the selection process for suitable blade material also plays an important role in determining the efficiency of the wind turbine blade.

1.2 Historical development of wind turbines

History of wind power is 3000 years old but people began to use it for generating electricity 120 years ago [9]. The immense potential of the inexhaustible wind flowing through the seas is utilized to generate useful energy for humans. This concept of using wind as a source of energy is expended to land in the form of windmills. Vertical-axis windmills were the first practical windmills developed in the 7^{th} century in Iran [10]. The early designs of vertical axis wind turbines originated in 2000 B.C in Persia. Originally these machines were used for pumping water and then later evolved into windmills for grinding grains. The first windmill to produce electricity is developed by Prof. James Bylth [11]. Meanwhile, in the year 1888, Bruch and his colleagues successfully developed a wind machine that is put into operation on the Atlantic coast. From that time onwards, wind power technology began to develop step by step and people started generating electricity from windmills.

During the early 1920s and 1930s, America widely developed small wind machines and

windmills to produce 5 kW to 2 kW of power in its rural remote locations. A prototype of the modern horizontal axis wind turbine is built in the US in the year 1941 and these turbines were widely used to provide electricity to the farms where electric lines could not reach. However, at the beginning of 1950, the widespread development of electric power lines, the wind market is seen to be gradually diminished [12]. While examining the development of wind power history, it is understood that the popularity of wind energy has always been fluctuating with the price of fossil fuels. The oil crises in the early 1970s lead to wind power development and a boom took take place in 1995. Since the beginning of the 21^{st} century, the world wind electricity generation capacity has been observed to be doubled approximately every three and a half years [9].

1.3 Classification of wind turbines

Wind turbines (WT) are classified into various categories to take advantage of wind power. There are several ways to classify the wind turbines [13]. Fig. 1.2 shows the classification of wind turbines. Among them, the major classification depends on the axis of rotation and aerodynamic forces, and rotor capacity as shown below-

- Based on the axis of rotation

Based on rotational axis, the wind turbines are classified into vertical axis wind turbine (VAWT) and horizontal axis wind turbine (HAWT). The horizontal axis wind turbines are used in big wind farm applications in the offshore loactions where the undisturbed and clean wind is obtained. Whereas, vertical turbines can be installed in built environment where the nature of wind is turbulent.

- Based aerodynamic forces on the blade

According to the aerodynamic forces, wind turbines are categorized into drag-based, lift-based and combined drag and lift based turbines. The aerodynamic forces in the drag-based WTs are in the direction of airflow, while the aerodynamic forces in lift-based WTs are perpendicular to the wind flow.

- Based wind stream

The wind turbines are also differentiated into upwind and downwind turbines. Upwind turbines are the most common wind turbines. It allows the blades to intercept the wind first, enabling to capture the wind energy efficiently. In contrast, downwind turbines position the rotor behind the tower, facing away from the wind.

- Based rotor diameter and power rating

Based on the rotor diameter and power rating, six types of WT are available such as micro-turbine, mini-turbine, domestic-turbine, commercial-turbine, medium turbine, and large turbine. According to the capacity, modern WT are classified as small WT (below 50 kW), medium WT (50 kW-250 kW), and large WT (above 250 kW).

1.3.1 Horizontal axis wind turbine

Horizontal axis wind turbines are the traditional design of wind turbines which usually consist of two to three blades that are connected at the top of the tower. Generally, the rotor of the HAWT should always face towards the direction of the wind. Thus, a yawing system and self-starting mechanism are necessary for turning the blades towards the flow direction. Under steady flow conditions, the ideal efficiency of the HAWTs is reported to be in the range of (40-55)% [14]. The energy output of these turbines mainly depends on the turbulence and average wind speed of the specific site. They are highly suitable for

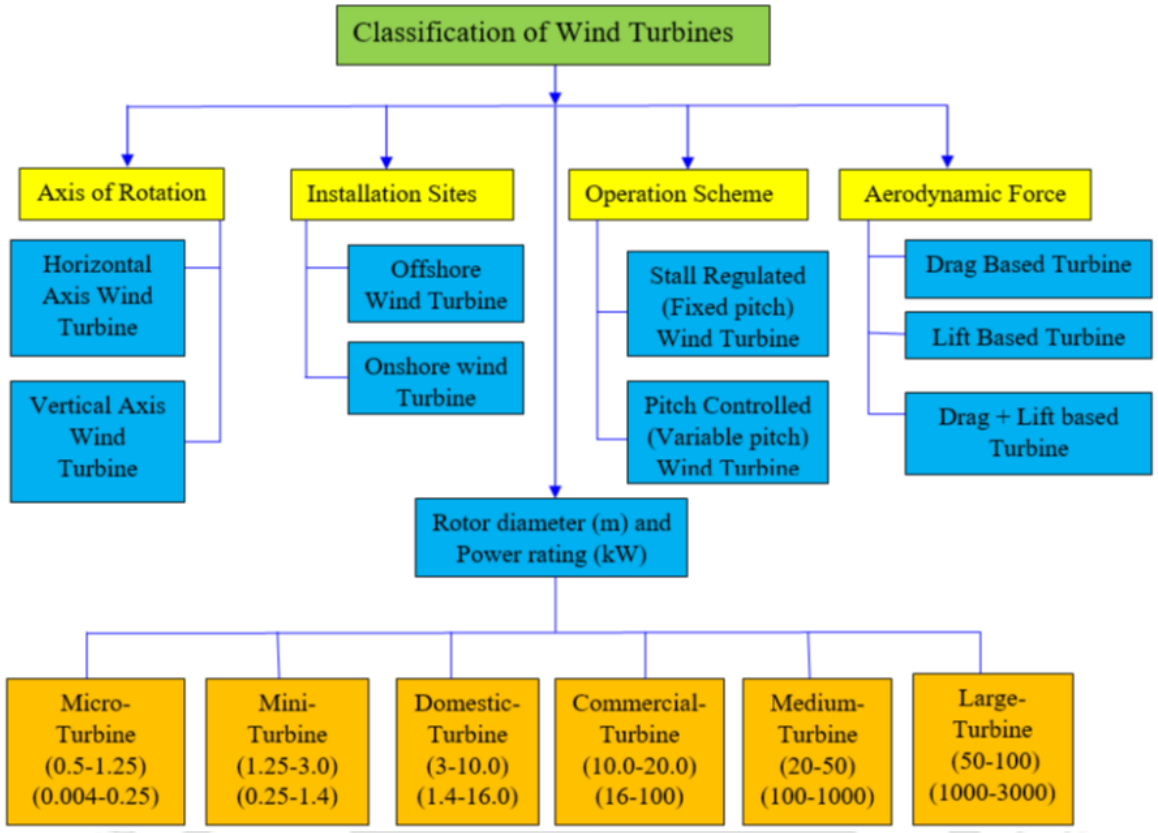

Figure 1.2: Schematic of classification of various wind turbines.

installation in big onshore and offshore wind farms to achieve maximum energy efficiency. However, these turbines are not suitable for built-up or urban surroundings as they require larger space to operate efficiently. In urban environments the space is limited and the presence of high-rise buildings causes wind turbulence which affects the performance of the HAWT.

1.3.2 Vertical axis wind turbine

A vertical axis wind turbine is a turbine whose axis of rotation is perpendicular to the ground. These turbines can capture air-flow from any direction and do not require any yaw mechanism. The VAWT can operate in highly turbulent regions with low cut-in wind speeds. These turbines emit less noise than the traditional HAWT and can be integrated into the built environment/ buildings. The VAWT mainly operates on the principle

of aerodynamic drag. The designs of VAWT is primarily categorized into Savonius and Darrieus. Savonius is the first vertical axis wind turbine developed in the year 1920 by the French engineer J Savonius [15]. It usually consists of connecting two half cylinders face to face resembling the letter "S". These turbines have low cut-in speed and their output efficiency is significantly less. Subsequently, in the year 1930, the French engineer G.J.M Darrieus invented and patented a new design known as Darrieus wind turbines [16]. These turbines operate according to the principle of aerodynamic lift and have comparatively higher efficiency than the Savonius turbines.

1.3.3 Darrieus wind turbine

Darrieus-type VAWT is the most typical type of wind turbines as it is insensitive to the changing wind direction. These turbines are patented into two major configurations – curved and straight blades. The curved design is known as an Egg-beater and the straight-bladed design is known as an H-rotor. The detailed description of various Darreius configurations is documented by Tiju *et al.* [17]. The straight-bladed turbines achieved greater popularity due to their simple design, low manufacturing, and maintenance cost as compared to the curved blades. The straight-bladed turbines are preferably built with two or three blades. The basic two configurations of a straight Darrieus turbine are depicted in Fig. 1.3. The blades are directly connected to the rotating shaft using the blade-strut connectors. Due to the easy accessibility, these turbines are installed not only in offshore areas but also in the building rooftops both urban and remote areas [18]. These turbines are mostly suitable for small-scale applications such as battery charging, electrifying schools, colleges, individual homes, powering highways, and streetlights, etc [19]. The specific advantage of the straight-bladed wind turbine is that they do not require any yaw

mechanism, and the electrical and mechanical components can be installed at the ground level for easy maintenance. Compared to other VAWT, the straight-bladed turbine has a higher power coefficient [20], however, these designs suffered from delays in self-starting capabilities.

1.4 Biocomposites

Biocomposites are extensively used as structural elements as these composites can be disposed of without much harming the environment. Biocomposites comprise bio-fibers and polymer matrices. Bio-fibers are classified into non-wood fibers (known as natural fibers) and wood fibers as shown in Fig. 1.4 [21, 22]. In the late 1980s, the development of biocomposites started evolving in the exploration of sustainable replacements for traditional synthetic materials. Wood plastics are the first developed biocomposites that offered better physical and mechanical properties compared to plastics [23]. However, with time various natural fibers (NF) are introduced which showed fairly better mechanical properties such as high specific strength, stiffness, impact resistance, and flexibility. These fibers are categorized into plant-based fibers such as flax, hemp, kenaf, sisal, jute, and

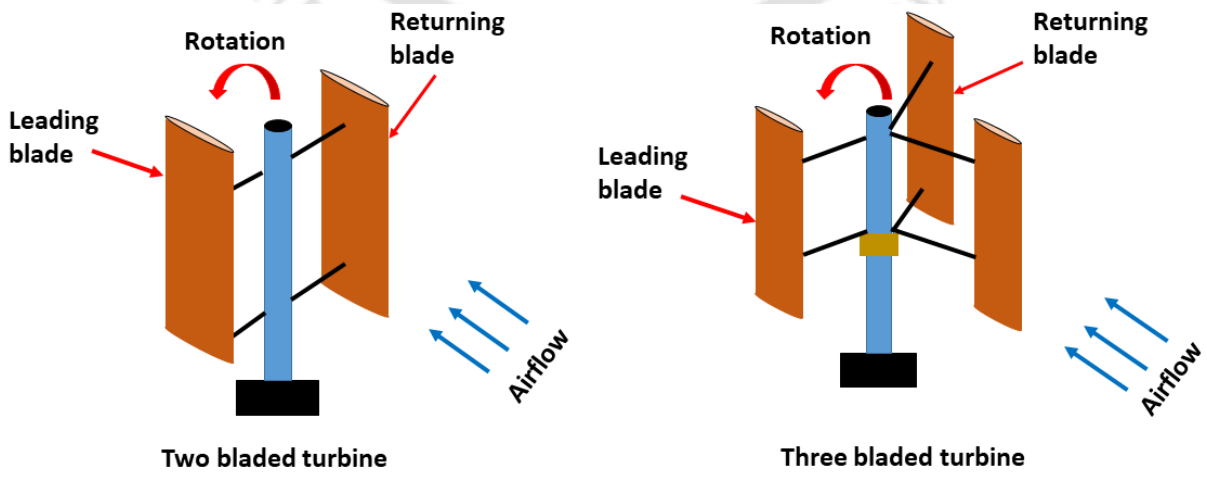

Figure 1.3: Two and three-bladed H-rotor Darrieus turbine.

animal-based fibers such as wool and silk. These fibers are low cost, lighter in weight, easily available, and have better strength due to high cellulose content than wood fibers [24]. Cellulose is mainly responsible for the mechanical strength of the natural plant fibers.

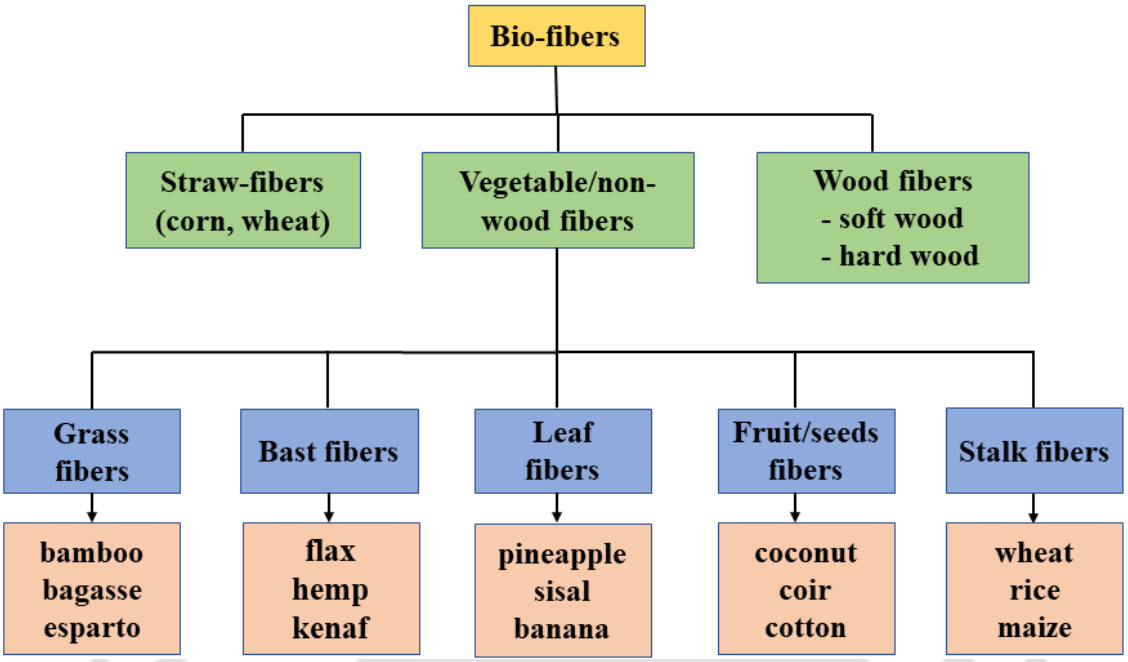

Figure 1.4: Broad classification of bio/natural fibers [21,22].

The NFRC are formed with natural fibers as reinforcement embedded in polymer matrices. The major role of the reinforcement is to carry the loads and provide adequate strength and stiffness to the composite. Usually, polymers are categorized into thermoset and thermoplastic. Thermoset polymer resins such as polyester and epoxy are the most widely for the fabrication of biocomposites [25]. Natural fiber composites are being increasingly used in various industrial applications including aerospace, textiles, automobiles, military, sports, construction, etc. The performance of natural composite depends primarily on the strength of the fiber itself. The quality of fiber depends on various parameters such as such type of fiber (short/long), fiber extraction method, region of fiber extraction, type of soil, climatic condition of the plant, and maturity of the plant species [26, 27].

The mechanical strength and stiffness of the natural composite are also affected by the hydrophilic nature of fibers and the amount of fiber loading. The advantages and disadvantages of natural composites over traditional composites are presented in Table. 1.1. Since natural fibers are hydrophilic, composites developed using these fibers are extremely sensitive to moisture. This results in weak interfacial bonding strength between the fibers and the matrix affecting the composite mechanical characteristics [28]. Thus, chemical treatments/surface modifications are necessary to achieve better interfacial bonding. Among all the methods, alkali treatment with a percentage (%) value between (4-6)% can considerably improve the fiber-matrix interfacial bonding [29, 30]. Apart from the drawbacks, the plant fibers also exhibit comparable specific strength and stiffness as compared to synthetic glass fibers [31]. These fibers can replace synthetic-based composites as eco-friendly, lightweight, and sustainable composites to the rising concerns regarding future biodegradability.

Table 1.1: Advantages and disadvantages of NFC over synthetic fibers.

Advantages	Disadvantages
• Low density and high specific strength and stiffness	• Less durable than synthetic composites, but can be increased significantly with treatment
• They are easy to recycle and produce less hazards during manufacturing	• Moisture absorption is high resulting in fiber swelling
• They produce biodegradable and eco-friendly composites	• Greater variability of mechanical properties
• Emits less toxic flumes when they are subjected to heating or land disposal at the end of life	• They are limited to low-temperature applications compared to synthetic composites
• Non-abrasive to composite processing equipment	• It possesses lower impact strength than synthetic composites

1.5 Bamboo-based polymer composites

Bamboo is a type of plant-based fiber that is rapidly renewable, biodegradable, and used for carbon sequestration. Bamboo-based composites are preferred over wood/timber due to their high mechanical strength, high stiffness, and rapid growth rate [32]. Bamboo plants have a higher strength-to-weight ratio than wood and plain steel. Bamboo culms are hard, flexible, wear-resistant, and have less density [33] compared to wood/timber. Moreover, due to global biomass production, the supply of availability and quality of wood/ timber are subsequently declining at a faster rate. In that case, an alternative material, bamboo as short growth industrial crop (3-5) years with better tensile properties than wood and of the same density is highly appreciated. Bamboo is one of the fastest-growing plants in the world at a growing rate of 3 *cm/hour*. Various studies reported that bamboo can grow (11-21) *cm/day* or up to 2 *inches/hour* [34]. However, depending on the types of species, bamboo can attain maturity in (4-5) years from the time of plantation compared to timber, which takes decades. Over the past four decades, significant development has been reported on bamboo-based composites, particularly, bamboo-fiber composites [35], bamboo ply boards [36], bamboo scrimber [37], and bamboo strip-based composites [38].

1.5.1 Anatomical features of bamboo

The anatomical structure of bamboo determines its physical and mechanical properties. Bamboo plant has a hollow cylindrical shape culm that is filled with woody material. The culm is divided into several nodes and internodes. The woody culm is in the form of a tapered hollow section with the largest diameter and wall thickness at the bottom.

The anatomical characteristic features of bamboo culm are shown in Fig. 1.5 [39]. The diameter and wall thickness of the bamboo culm decrease from the bottom towards the top of the plant. The bamboo is composed of different organic composition groups such as cellulose (60%), lignin (32%), and hemicellulose (12%) [40]. The properties of bamboo fibers are highly dependent on these organic constituents. The bamboo culm consists of cellulosic fibers aligned along its length which gives bamboo ultimate tensile-flexural strength and rigidity in that direction as shown in Fig. 1.5.

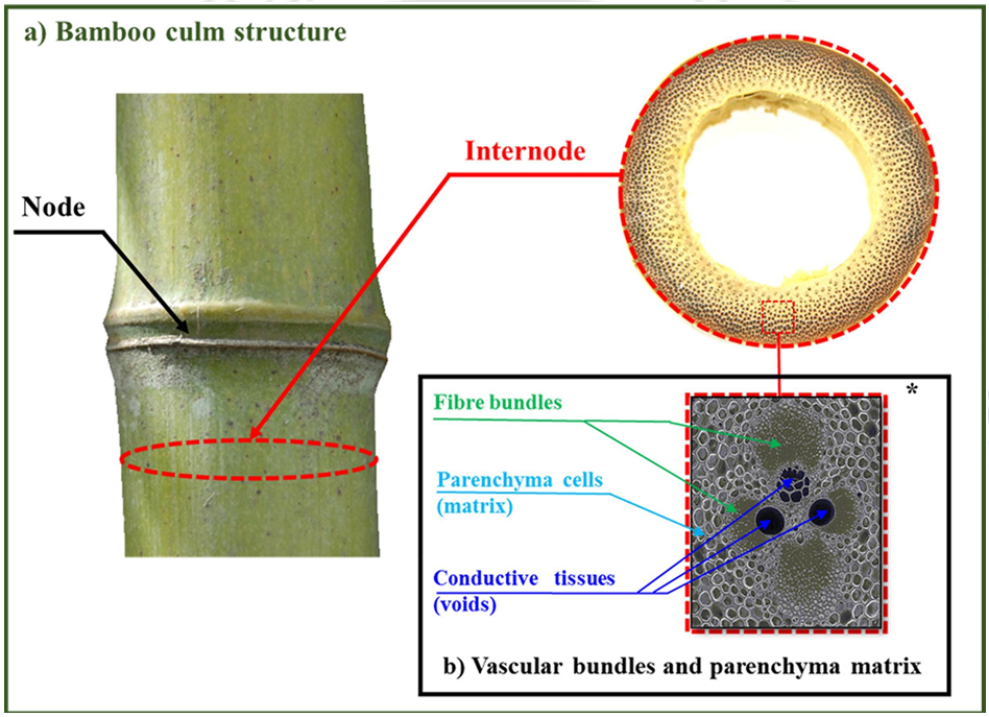

Figure 1.5: Characteristic features of bamboo (a) bamboo culm (b) vascular fiber bundles [39].

These cellulosic fibers are embedded in lignin which acts as a matrix. The cellulose fibers are the reinforcement while the lignin is the matrix which ultimately makes the bamboo a natural composite. However, the non-cellulosic components, such as hemicellulose and lignin tend to decrease the strength of the fibers. The higher fiber moisture absorption is due to the presence of hemicellulose whereas lignin provides hardness and rigidity to the plant. The presence of lignin also makes the bamboo fibers brittle. The

distribution of the fiber bundles is denser in the outer radial region of the bamboo culm compared to the inner region. As a result of the increase in fiber bundles from inner to outer, the strength of the outer portion is higher than the inner.

1.5.2 Distribution of bamboo

Bamboo is a versatile and fast-growing plant belonging to the Bambusoideae grass family. A total of 1,662 species of bamboo are available worldwide [41]. The growth of bamboo depends on the climatic and soil conditions and is mostly favorable in tropical and sub-tropical climatic conditions. The distribution of bamboo is extensive in specific continents of the world such as Asia-Pacific, Africa, North America, and Europe. The cultivation of Bamboo forests covers a total area of 38,000 million hectares, which is approximately 3.2% of the total forest area around the world [42]. The Asian countries Vietnam, China, India, Myanmar, and Indonesia are the largest producers of bamboo. It has been identified by different names in these regions, namely "wood of the poor" in India, "the brother" in Vietnam, and "People friend" in China [43]. China is the largest bamboo-producing country with more than 500 species followed by India with 145 species [44]. The distribution of bamboo production by different states of India is shown in Fig. 1.6 [45]. It is observed that the North-Eastern (NE) region of India is one of the richest reservoirs of genetic diversity as it supports about 50% of the total genetic resources of bamboo in India. Dendrocalamus and Bambusa are the two most predominant bamboo species found in the North-Eastern region of India. Fig. 1.7 presents the distribution of bamboo species in different North-Eastern states, among which Assam records the highest cultivation of bamboo [46]. Even though the potential of bamboo cultivation in the North-Eastern region is quite impressive, the commercialized development

of bamboo is understated and is used for developing local products and in construction industries.

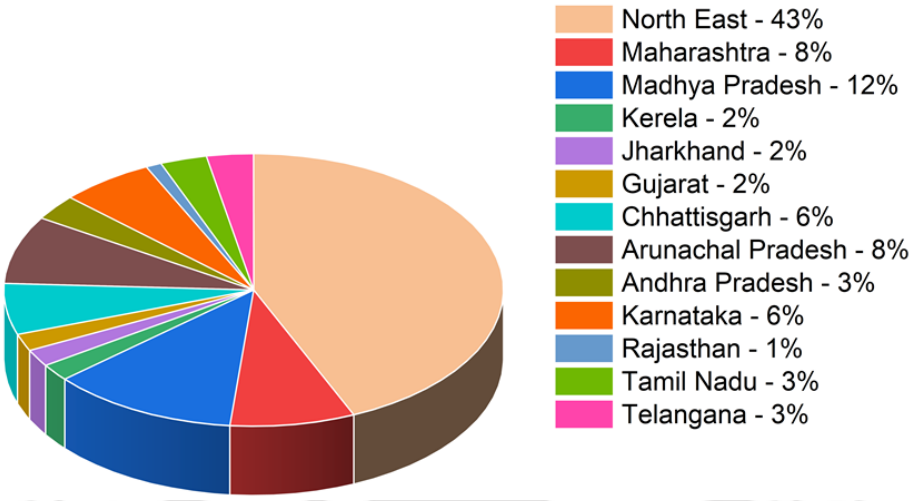

Figure 1.6: Bamboo distribution in protected forests in states of India [45].

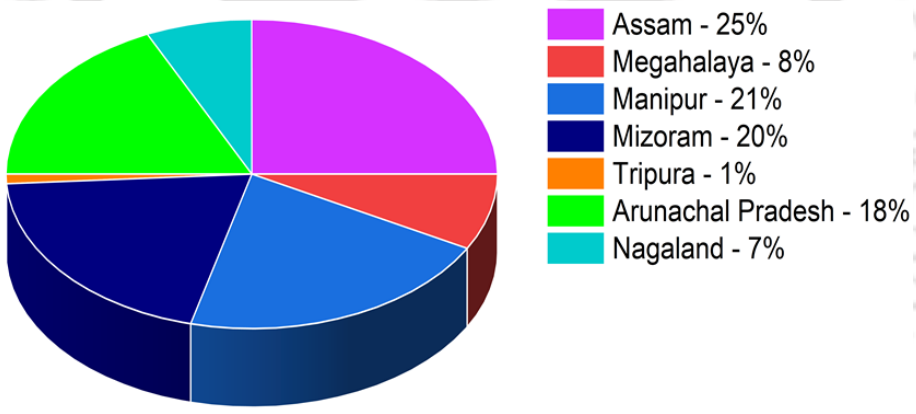

Figure 1.7: Bamboo distribution in the North-Eastern states [46].

1.5.3 Extraction of bamboo fibers

The extraction of bamboo fibers efficiently is a challenging task as the fibers are linked with a complex organic constituent called lignin. Lignin provides rigidity to the bamboo plant cell walls. Bamboo fibers are brittle due to high lignin content which reduces the effectiveness of resin impregnation into the fibers. Therefore, it is necessary to remove the maximum amount of lignin from the bamboo fiber surface to achieve the desired

mechanical strength and stiffness. There are several techniques by which bamboo fibers can be extracted. Bamboo is extracted in different forms for composite fabrication such as single fibers, long strips, and bamboo powder particles as shown in Fig. 1.8. The quality and strength of fiber are directly affected by the type of fiber extraction method. The raw bamboo fibers are extracted using three procedures, namely mechanical extraction, chemical extraction, and their combination [47].

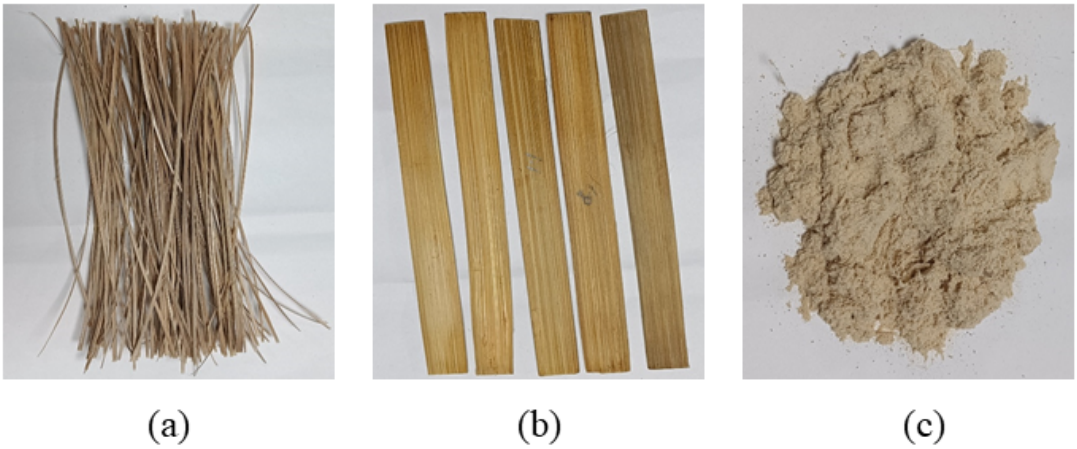

Figure 1.8: Extraction of bamboo in different forms (a) single fibers, (b) long strips, and (c) bamboo powder.

Mechanical extraction:

This method involves different procedures such as steam explosion, retting, crushing, grinding and, rolling mill. Steam explosion is a physicochemical method that uses high-pressure steam to disrupt bonding between polymeric components to break the structural components of cellulose. Okubo *et al.* [48] applied steam explosion method to extract bamboo fibers from bamboo tree. In this process, the cell wall of the fibers is cracked and the bamboo fibers become soft enabling extraction. Results showed that the tensile strength and modulus of bamboo composites using steam explosion increased up to (15-30)%. They concluded the steam explosion technique as an efficient method to extract

bamboo fibers for reinforcing thermoplastic. This process is appropriate in removing lignin from the surface, the resulting fibers are dark and rigid, however, the cost of equipment and energy consumption for the steam explosion method is relatively higher [47]. In retting process, the bamboo strips are dipped in water for (3-4) days, and then beaten and scraped using sharp knife [49]. This process of knife scraping had a strong effect on the quality of fibers. In a study, the authors reported that using the retting process the fibers can be extracted in any desired length [50], whereas in crushing method, pin rollers are used to extract the fibers [51]. This process is relatively expensive and the extracted fibers are short in length. Ashimori *et al.* [52] mechanically extracted bamboo fibers by a rotating rotor to extract the bamboo fibers. The authors reported that the major drawback of with this method is that it yields short fibers which become powdered after mechanical over-processing. Similarly, the fibers extracted using rolling and grinding mill are in short fiber bundles and powdered form [47]. Among these, the steam explosion method is the most efficient as it able to achieve long and rough fibers for composite fabrication [48].

Chemical extraction:

The chemical extraction procedures use degumming, alkali or acid retting, and chemical retting to remove the non-cellulosic parts, lignin, and hemicellulose from the fiber surface. In this process is used to reduce the lignin and water content in the fibers. The bamboo strips/chips are dipped in different acidic chemicals and alkaline solutions for a range of time intervals. It is reported that the alkali treatment in the category of chemical extraction, has shown the best efficiency for fiber modification by enhancing the interfacial bonding between fiber and the matrix. The bamboo fibers treated with NaOH solution

with (4-6)% caused less damage to the fibers by preserving the microstructure and alignment of the fiber bundles [53]. The lignin and hemicellulose are significantly removed from the NaOH-treated fibers which is the major factor of brittleness and hydrophilicity of fibers [54], whereas, Kaur *et al.* [55] treated the bamboo fibers with different concentrations of $Zn(NO_3)_2$ and found that the lignin content of the fibers are greater removed compared to alkaline solution, but the water content of the fibers are high. The surface of the treated fiber becomes rough which further improves the interfacial bonding of the composite.

Combined mechanical and chemical extraction:

In this procedure, the bamboo chips are first dipped in alkaline solution and then the treated bamboo strips are processed mechanically to extract the fibers. The compression molding technique and the roller mill method is usually used to mechanically extract the treated fibers. The mechanical extraction methods are eco-friendly and cause less damage to the microstructure of the fibers compared to chemical methods [56], [57]. Thus, the composites prepared by mechanically extracting the fibers and chemically treating the same with different concentrations of alkali enhanced the fiber-matrix bonding with improved mechanical strength.

1.6 Applications of bamboo composites

Bamboo a naturally occurring versatile composite material growing abundantly in most tropical countries has found popularity across various industries contributing to environment sustainability and eco-friendly products. Its excellent and unique properties such as mechanical strength, durability, and heat resistance have widened its application in

various sectors like ranging from construction industries to textiles, automobiles, marine, military, etc [58, 59]. It is also emerging as a good substitute for engineering timber products for furniture such as laminated sheets, and bamboo scimber. Due to its remarkable strength-to-weight ratio, bamboo has achieved major applications in meeting different structural and commercial elements such as longhouses, scaffoldings, bamboo flooring. The impressive qualities of bamboo as a lightweight, high-strength, and sustainable material along with good interfacial bonding with polymeric matrices have extended its applications in sports goods, electronic and electrical appliances, such as snowboards,

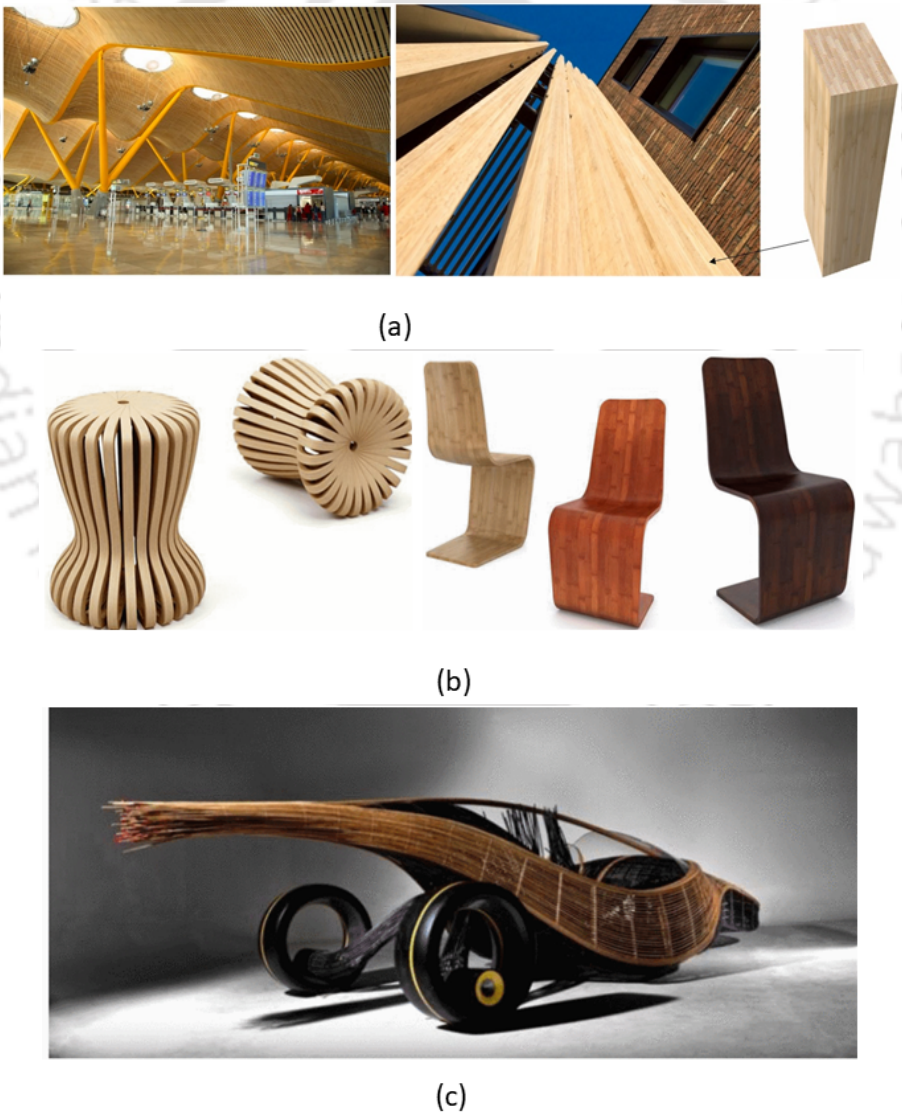

Figure 1.9: Application of bamboo composites (a) interior and exterior structural design (b) furniture (c) automotive [33, 58].

computer shells, flexible electronic sensors, motion detection systems, composite deck and fencing etc [60, 61]. Bamboo has proven to be a safe and durable material for structures such as bridges, laminated panels, and roof architecture in many countries worldwide. Moreover, door panels in automobiles, wall ceilings, decks, and other interior materials prepared by non-woven bamboo mats and hot pressed have reached a mature state in the construction industries [62]. The continuous unidirectional bamboo-reinforced thermosetting composites possess outstanding mechanical properties. These composites have the potential to replace synthetic composites such as glass/ carbon and other petroleum-based composites in high-load applications including wind turbine blades, ship and submarine materials, highway fence materials, etc [63]. Bamboo columns are also used as replacements for steel bars for concrete frameworks such as beams, and columns [64]. Compared to steel, bamboo is nine times lighter and its strength-to-weight ratio is approximately five to six times higher than mild steel [65]. A few of the examples of bamboo-composites in real-life applications have been presented in Fig. 1.9 [33, 58].

Chapter 2

Literature Survey

2.1 Introduction

As discussed previously in Chapter 1, the significant growth and high demand for clean energy generation have led to the development of wind turbines. The literature on wind turbine blades covers a wide range of areas including material science, structural mechanics, aerodynamics, etc. The major area of attention is material selection and characterization as substitutes for conventional fiber-reinforced polymer composites. Structural mechanics and dynamics are also crucial to ensure blade safety and reliability under various operating conditions. In this Chapter, the literature on various aspects of wind turbines such as material selection, material properties of bamboo composites, standards for turbine blades, and static and dynamic behavior of wind blades will be reviewed.

2.2 Evolution of natural materials for wind turbine blade

Blades are primarily composed of steel, aluminum, copper, glass, and carbon fiber composites. Over time the materials for wind turbines have undergone tremendous change from steel to lightweight polymeric composites. This is mainly to reduce the effects of gravitational and fatigue loads. Presently, the turbine blades are manufactured from

glass-carbon fibers, thermoset resin (epoxy, polyester, and vinyl ester), and structural adhesives. Compared to glass-fibers, carbon fibers are lightweight with high stiffness which makes them create thinner and lighter blades [66]. Despite these advantages, carbon fibers are expensive and highly sensitive to misalignment of fibers as they can lead to a significant reduction in compressive and fatigue strength [4]. Aramid and basalt fibers are the second alternatives to glass/carbon fibers known for their exceptional mechanical properties and heat resistance [67]. Basalt fibers are a compelling material choice for small wind turbines as they have demonstrated much higher mechanical characteristics i.e. 9% lighter, 30% harder, and (15-20)% stiffer than conventional glass fiber composites [68, 69]. Basalt fibers are mineral-based, and their environmental impact, especially in terms of decomposition, is an important consideration. Unlike plant fibers, which can degrade relatively quickly under natural conditions, basalt fibers contains high amount of chemical contents which slow their degradation process [70]. Various disposal methods as such landfill, mechanical, chemical, and thermal degradation recycling methods have been studied in the literature. However, none of these techniques are perfect as each one has its limitations [71–73]. These drawbacks have led to the utilization of natural and sustainable fibers. In comparison to synthetic composites, natural/ green composites are less expensive and abundantly available.

Natural fibers-based composites fabrication and testing are the hot topics of research. It has the potential to replace the widely used synthetic fiber-reinforced polymer composites [26]. Thus, bio-composite materials will help to develop more environmentally friendly small wind turbine (SWT) blades as an alternative to the current material system. Several investigations have been carried out to study the feasibility of wooden/ timber composites for wind turbine blades. Mishnaevsky *et al.* [74] conducted the mechanical test of wood

to explore the applicability of timber/timber composites for small-scale wind turbine blades. The results of the study included mechanical strength analysis and environmental degradation of timber. Based on various recommendations and considerations from the strength and other environmental factors, wind turbines with timber wind blades are produced as shown in Fig. 2.1, and tested. Astle *et al.* [75] studied the material properties

Figure 2.1: Installed wind turbine with timber wind blades in the country Nepal [74]).

of Douglas fir, a North American timber species, and Sitka spruce, and European species in terms of strength and fatigue life. Both timber have excellent fatigue life crossing over 1 million cycles. Further, analyzing the results experimentally, it is recommended that these timbers be suitable for SWT blades. Pourrajabian *et al.* [76] experimentally tested four species of Iranian timber for small wind turbine blades. Based on the mechanical properties, a design optimization is performed to study the suitability of the timbers for solid and hollow blades. Alder and beech timber demonstrated better performance for hollow blades in high windy areas. Similarly, Peterson *et al.* [77], and Sinha *et al.* [78] studied the suitability of different timber/ wood for wind turbine blades. The criteria of their selection process involved mechanical properties, price, growth, and availability of timber. Despite the advantages of low prices, these timbers are high in moisture absorption. To improve the durability different water-resistant coatings are studied [74, 78].

Green composites such as wood, and Douglas fir have received approval for wind turbine application in the U.S. [79]. However, the increased cost of timber and shortage in global supply chains have shifted academic attention toward investigating different types of natural fibers for developing wind turbine blades.

Numerous attempts have been made to show that natural fiber-composites (NFCs) are suitable for wind turbine blade applications. Kalagi *et al.* [80] presented a review of the mechanical properties, constituents, and manufacturing processes of natural fiber-reinforced composites. The authors reported that the basic material requirements for wind turbine blades are high strength-to-weight ratio, better fatigue resistance, and high stiffness. Batu *et al.* [81] investigated eleven different natural fiber-reinforced composites for SWT blade applications. The designed blades are analyzed for stress, and deflection under different loading conditions, and the results are compared with the existing E-glass/epoxy blade. The hemp fiber composites are also tested for tension, flexure, and impact strength. As reported, natural hemp composites are suitable candidates for use as turbine blade material [82]. Holmes *et al.* [83] performed the static and dynamic test on the bamboo-epoxy laminates and suggested that bamboo composites can be used for wind turbine blade application. Huang *et al.* [84] investigated the mechanical properties of timber and bamboo composites for turbine blades. The authors reported that bamboo-composite has better properties than wood/timber. Similarly, Shah *et al.* [85] confirmed the suitability of natural flax composite for wind turbine applications. However, there are certain drawbacks associated with the performance of NFs such as their hydrophilic nature, and low thermal stability [86]. This nature affects the microstructure of the composite. The structure of the wind turbine blade can be improved by hybridizing the mechanical properties of the NFCs. Miliket *et al.* [8] investigated the mechanical

properties of sisal/nacha/glass fibers hybrid composite and suggested that the composite with a fiber volume ratio of (20:5) has adequate potential to be used for blade design.

2.3 Experimental investigation on bamboo-based composites

The investigation of mechanical properties of bamboo and bamboo fiber-reinforced composites (BFRC) has gained significant interest due to the growing recognition as lightweight, sustainable, biodegradable, and low carbon content material. Various experiments are being conducted such as tensile, flexural, compressive, impact, etc to have an in-depth visualization of how these materials behave in different loading and atmospheric conditions. Further, the exploration extends to the development of bamboo composites i.e. bamboo fibers embedded in different polymeric matrices or resins. This helps in enhancing the specific strength and stiffness of bamboo for high-load applications.

2.3.1 Material characterization under static loading

Mohanty and Nayak [87] developed bamboo fiber-reinforced polyester composites with different fiber content. It is observed that the composites with fiber content between (10-30)% possess excellent tensile and flexural strength and beyond that content, there is a decline in the values of mechanical strength. Lokesh *et al.* [88] investigated the mechanical properties of untreated bamboo and bamboo epoxy composites. The bamboo species is not known in their work. Results demonstrated that the composites showed higher strength and stiffness compared to the untreated samples. The tensile strength increased from 16.51 *MPa* to 18 *MPa* for the composite samples. The infiltration of hy-

drophobic epoxy resin facilitates improved dimensional stability against moisture attack, high strength and stiffness, and waterproof coating to the composites [89–91] fabricated composites with Gigantochlea scotechini (bamboo species from Malaysia). They studied the performance of BFRC with different portions of fiber content. It is observed that the bamboo epoxy composites with 40% fiber content exhibited the highest tensile and flexural strength. Hou *et al.* [92] performed the tensile and compressive test of BFRC. The tensile strength of the composite parallel to the reinforcing direction is reported to be 148.53 MPa which is almost 26.47 times higher than the reinforcing fibers in the perpendicular direction. Barman *et al.* [93] investigated the mechanical properties of Bambusa Tulda fiber-reinforced composites. The composites are fabricated using compression molding and hand layup methods. The compression-molded composites exhibited better mechanical strength and surface smoothness. The flexural characterization of the bamboo species Guadua angustifolia and its composites is performed by Osorio *et al.* [94]. It is observed that the experimental flexural strength reaches nearly 78% of the theoretical value. It indicates good fiber-matrix bonding which is mainly responsible for high strength and stiffness. The mechanical strength of bamboo varies from species to species. An experimental study is carried out by Awalluddin *et al.* [95] by comparing five different species from different parts of the world. The tensile strength of the bamboo species namely, Bambusa Vulgaris, Dendrocalamus Asper, Schizostachyum Grande, and Gigantochloa Scortechinii differed from 145 N/mm^2 to 233.98 N/mm^2. There is an increasing global interest in developing bamboo as a substitute for structural steel [96], but its direct utilization is restricted to construction and structural applications.

Bamboo is highly susceptible to insect attack and fungal decay, dimensional instability with a reduction in strength due to moisture absorption, poor corrosion, and thermal resis-

tance [97]. Literature supports that after certain chemical modifications, low-cost bamboo develops itself in a high-efficiency composite structure such as bamboo plastic composite material [98] and green eco-friendly bamboo composite material [53]. Alkali modification is an effective treatment for lignocellulosic fibers as the composite tensile strength is unaffected and an increase in its concentration increases the fiber stiffness [99]. Manalo *et al.* [100] investigated the effect of alkali concentration on the mechanical strength of bamboo polyester composites. An alkali concentration of 6% is found optimum and resulted in the best mechanical performance for the bamboo composites. Further, a reduction in mechanical properties is observed at the alkali concentration of 8%. Behera *et al.* [101] studied the mechanical properties of the composites with varying alkali concentrations from (1-4)%. The fibers treated with 4% NaOH demonstrated improved tensile strength. Wang *et al.* [102] experimentally studied the different concentrations of NaOH treatment of bamboo fibers and found 4% as the optimum value with good mechanical properties. The authors suggested through their experiment that alkali concentration of 5% does not affect the tensile strength of bamboo fibers, whereas beyond that the tensile strength dramatically decreased [103]. Zang *et al.* [104] reported that the bamboo fibers treated with 6% NaOH are more suitable for composite fabrication with improved tensile strength. The (4-6)% alkaline treatment of bamboo fibers is the most suitable range for achieving the best mechanical properties. However, most of the literature on the characterization of bamboo composites is based on the reinforcement of bamboo fibers in polymeric composites. The characterization of bamboo composites on laminae/ strips is limited.

Verma *et al.* [35] carried out the mechanical characterization of bamboo laminae under different loading conditions and found that laminated bamboo composites (LBCs) have

better strength than wood-based polymeric composites. A four-year-old green bamboo species Dendrocalamus strictus is selected for the study. The tensile strength of LBC is found in the range of (169-205) *MPa*. Asif *et al.* [105] compared the mechanical properties of bamboo strip composite and bamboo strip hybrid glass composite. It is observed that the flexural strength increased by 22.49% for the hybrid composites however, there is no significant effect on the tensile properties. Bako *et al.* [106] studied the effect of the tensile strength of bamboo woven strip composite on various immersion time of the composite. It is found that the composite immersed in sulfur water and seawater had the highest tensile strength compared to immersion in pure sulfur water. Sumardi *et al.* [107] studied the mechanical properties of bamboo laminated composites using bamboo strips and bamboo zephyrs and found that laminated bamboo boards using bamboo strips have better dimensional stability and shear strength. Similarly, Rassiah *et al.* [38] experimentally studied the mechanical properties of laminated bamboo strips. The strips from the middle portion of the bamboo culm have better strength, whereas the outer culm strips provide higher hardness. The authors revealed that bamboo strip composites have good mechanical characteristics than pure bamboo and these composites can be a good alternative to composite-based reinforcing fibers.

2.3.2 Material characterization under dynamic loading

Fatigue stress is another major factor affecting the lifetime of a structure. Natural bamboo plants are flexible compared to other plant fibers which allows them to withstand dynamic loads and vibration. This inherent characteristic makes natural bamboo and its composites suitable for applications where dynamic loads are considered such as wind turbine blades. Keogh *et al.* [108] investigated the fatigue behavior of raw bamboo culm

subjected to compression-compression fatigue loading in the axial and diametral direction of the bamboo culm. The results demonstrated that the bamboo culm undergo fatigue failure when the samples are loaded under diametral compression whereas, no fatigue behavior is recorded when the samples are loaded under axial compression. For fiber composites, the fatigue range for unidirectional fiber composites loaded parallel to fibers is less as the applied stress is largely borne by the fibers, showing brittle failure. However, the composites loaded perpendicular to the fibers showcased large fatigue cycles due to the fiber/matrix interfacial bonding [108]. Song *et al.* [109] investigated the fatigue behavior of raw bamboo strips subjected to three-point flexural loading. Crack propagation, flexural fatigue life, and residual stiffness under different loading conditions are studied. Test results demonstrated that the samples with high fiber density displayed liner anisotropic flexural fatigue behavior than the low fiber density samples.

Ali *et al.* [110] studied the fracture and fatigue behavior of composite bamboo strips. They reported excellent fatigue properties with a fatigue limit of 30 MPa with 10^6 cycles. Onche *et al.* [111] studied the fracture and fatigue behavior of Bambusa Vulgaris-Schrad bamboo under monotonic and cyclic loading. Cracks are initiated in the perpendicular direction of the applied force under the flexural fracture test, whereas fatigue failure occurred when the applied stress exceeded the critical buckling stress. Amada and Untao [112] studied the effect of fracture toughness on the volume fraction of bamboo fibers. Test results demonstrated that the bamboo region having low fiber density has less toughening value compared to the region with higher fiber volume. Numerous experimental investigations have also been carried out to study the fracture characterization of bamboo-based polymer composites [113–115], and it is concluded that an increment in fiber content deteriorates the fracture toughness of the composites leading to matrix

cracking, fiber breakage, and fiber pull. Scherer *et al.* [116] studied the fatigue behavior of bamboo-epoxy composites under torsional fatigue loading. Fatigue test results of bamboo composites revealed that torsional fatigue is strongly related to the epoxy resin. Crack initiation is observed at the interfacial region between the matrix and the fibers. Thwe and Liao [117] conducted a fatigue assessment of bamboo/glass fiber hybrid composites. They concluded that hybridizing a small percentage of glass fiber can significantly improve the fatigue life and damage resistance of the composites than pure bamboo-based composites.

2.4 Effect of airfoil for vertical axis wind turbine blade

Wind blades are designed keeping in concern the unpredictable environmental climatic consequences and never less failed to deliver satisfactory performance during their lifetime. Based on the aerodynamic theory, the efficiency of the wind turbine largely depends on the selection of a suitable airfoil profile cross-section and shape. Analysis of VAWT started being carried out using various types of airfoils to exhibit useful results in terms of aerodynamic performance.

Subramanian *et al.* [118] investigated the aerodynamic performance of the symmetrical airfoils NACA 0012, NACA 0015, and NACA 0030 for its use in VAWTs. The numerical results demonstrated that VAWTs deliver better performance with thinner airfoils at a high TSR which shows that NACA 0015 is the best-performing airfoil. Mohamed [119] performed the aerodynamic investigation on 20 different airfoils both symmetric and non-symmetric and found that the symmetric airfoils have a better power coefficient. Wang *et*

al. [120] investigated the power coefficient of different symmetric NACA series airfoils and found that the value of the power coefficient increases with an increase in airfoil thickness and attains the highest value of 39.47% when the airfoil thickness is 15%, and further decrease with increase in thickness. Further, it is reported that NACA 0018 airfoils perform better at TSR lower than 2.33, whereas at TSR greater than 2.33 NACA 0015 is the best option for VAWTs. The aerodynamic performance of different series of airfoils such as airfoils with different thicknesses (symmetric NACA series) and airfoils with different camber thicknesses (non-symmetric NACA series and S series) are summarised by Wang *et al.* [120]. Kanyako and Janajreh [121] numerically analyzed the two-dimensional aerodynamic performance using airfoils DU-06-W-200, NACA 0015, NACA 0018, and S 1046. The results showed that NACA 0015 is the best-performing airfoil for the tip speed ratio range of 1 to 4. Mohamed *et al.* [122] investigated the aerodynamic performance of the H-Darrieus rotor with 25 different airfoils. The authors concluded that the non-symmetric airfoils for this turbine increased the efficiency by 10% compared to standard symmetric shapes. Blade pitch is also included in the study and results demonstrated that zero pitch angle is the best configuration. Recently, Dastjerdi *et al.* [123] revealed that non-symmetric airfoils have better self-starting capabilities and exhibited 79.80% higher torque than symmetric profiles, whereas, the symmetric airfoils have a higher power coefficient of 68.70% than the non-symmetric airfoils. Subsequently, Kumar and Sarkar [124] reported that the non-symmetric NACA 4415 airfoil demonstrated better performance approximately 1.4 times higher compared to other cambered airfoils.

2.5 Structural reliability of composite blades

Wind turbine blades are the most crucial and costly components of the whole system. The turbine efficiency mainly depends on aerodynamic shape as well as the blade materials [80]. The aerodynamics of the straight-bladed vertical axis wind turbine (SB-VAWT) has received appreciable recognition in the literature [125, 126]. However, only a few works concern the structural design of VAWT blades. The major cause of blade failure is due to increased centrifugal forces. The VAWT blades rotate freely at high rpm which increases the centrifugal forces. At high rpm, these forces counter the lift force causing bending of the blade away from the optimum bending angle and decreasing the overall power output [127]. Moreover, these forces significantly contribute to the magnitude of overall forces acting on the blade [128]. Thus the blade structure is desired to be designed with lightweight materials to reduce the dominance of the centrifugal force and also to reduce the material cost. Natural fiber composites are much lighter than synthetic composites as shown in Fig. 2.2 [129] and the blades produced from these composites will result in reduced centrifugal and gravity forces.

Wind turbine blades have complex structural layouts to meet the structural design requirements. These blades include one or more shear webs and numerous composite plies arranged at various ply angles. The structural performance of the composite blade can be optimized by altering the order of stacking sequences, the orientation of fibers, and the location of stacks [130–132]. The authors investigated the performance of the wind turbine blade using profiles NACA 0015, DU 06-W-200, and SG6040. Wang *et al.* [133] developed a novel mathematical model to calculate the cross-sectional properties of wind turbine blades based on classical lamination theory (CLT). The results showed a good

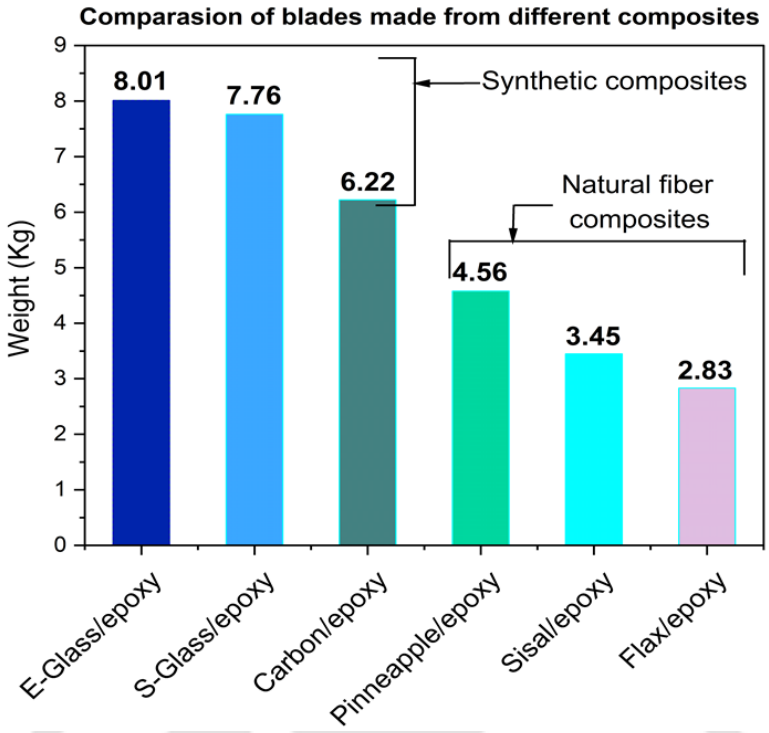

Figure 2.2: Comparison of weight of blades composed of different composites [129].

agreement with the experimental and numerical data and it is found to be more accurate than the existing codes. Further, Wang *et al.* [134] presented a structural optimization technique for wind turbine composite blades using a parametric finite element analysis (FEA) and genetic algorithm (GA) model using blade profiles NACA 0018, and NACA 0040. The results of the study demonstrated that the mass of the optimized blade is reduced to 17.40%, which indicates that the optimization model effectively reduces the mass of the blade. Similarly, Barnes and Morozov [135] explored the effects of varying different aspects of the internal structural of a wind turbine blade design with different structural configurations. The authors suggested that a wide range of loading conditions must be considered as the optimized design results varied greatly between different designs. Guo *et al.* [136] performed the finite element (FE) analysis of the VAWT straight blade using NACA 0018 blade profile. They analyzed the effect of pitch on blade deformation and found that the blade deformation and the stresses in the supporting arms

deteriorated significantly as the blades are folded in the negative direction. Lin *et al.* [137] performed the strength laminated composite VAWT blade. The blade suffered from maximum stresses in the upper support when the azimuth angle is between (60-90) degrees. Brown and Brooks [138] presented a finite element methodology to predict the structural response of the thermoplastic composite blade.

2.6 Dynamic behavior of composite blades

The dynamic characteristics are closely related to the composite mechanical properties and can significantly affect its performance. Blades of a vertical axis wind turbine (VAWT) system are the most complex and susceptible vibration components contributing to over 41% of total failures [139]. They are well-suited in-built environments where the nature of wind loading is dynamic. The complexities of aerodynamics around the VAWT blade pose a great challenge to its structural integrity. The aerodynamic shape determines the power efficiency of the turbine whereas the blade structure ensures whether it can resist the aerodynamic forces and loads during operation [140]. The aerodynamics mainly concerns the outer shape of the blade whereas structural improvements are often made through the use of appropriate materials rather than changes to blade geometry. The structural dynamics of the wind turbine blade are another major issue to ensure reliability of the system. Natural frequencies, displacement mode shapes, damping ratios, and bending stiffness are directly related to dynamic loading. These vibrations are caused by the interactions between the inertial and the elastic forces, characterized by the geometry and material properties of the system during structural deformation [141]. Analyzing natural frequencies and mode shapes is needed to avoid structural resonance and vibrational instabilities.

Reducing vibrations of VAWT has been an active area of research for the last decade, especially with the advancements in blade materials. Numerical and experimental approaches are discussed to identify the vibrational frequencies and mode shapes of the VAWT blade. Maalawi and Negm [142] developed an optimization technique to study the behavior and variation of natural frequencies of the wind turbine blade structure. Non-linear-based solutions are adapted to solve the optimization problem. They reported that higher frequencies are favorable for reducing both the steady state and transient responses of the structure after being excited. Verkinderen and Imam [143] developed a simplified analytical model to identify the vibrational frequencies of the H-Darieus VAWT system. Alaimo *et al.* [144] carried out the dynamic experimental test on the two-blade configuration to determine their dynamic response in terms of natural frequencies and their respective mode shapes. Similarly, Wang *et al.* [134] performed the modal analysis of a non-rotating blade. The FEA model exhibited good agreement with a difference of 2.63% compared to the pre-existing composite blade. Wang *et al.* [145] experimentally studied the dynamic response of a rooftop VAWT. Mabrouk *et al.* [146] studied the effect of rotational speed on the dynamic behavior of the VAWT. Recently, Tong and his colleagues [147] performed a detailed free and forced vibration analysis on two different types of H-Darrieus VAWT. The difference in natural frequencies of both models is found in the range of (3.12-3.67)%. From the above literature, it is evident that studies related to the dynamic behavior of VAWT blades are quite limited. Additionally, the vibration of the blade can be reduced by optimizing the blade design and material properties. Dey *et al.* [148] performed the free vibration analysis of a composite cantilever plate to study the effect of ply angle orientation, elastic modulus, and mass density. The results of the study revealed that small changes in composite such as fiber angle orientation, and differences

in the bonding of layers can significantly affect the modal vibrations of a composite.

2.7 Fluid-structure interaction of wind turbine

Fluid-structure interaction (FSI) plays an important role in ensuring the structural performance and reliability of VAWT particularly concerning dynamic behavior when the blades interact with the fluid. FSI simulations which are computationally expensive in many applications, have increased in popularity in recent years as available computing power has decreased in cost. During operation, the turbine blades/ entire structure interacts with the fluid causing aeroelastic instabilities such as edgewise deflection, and futter. This behavior leads to catastrophic failure of the blades as well as the entire wind system [149]. It involves both aerodynamic and structural loading to exhibit the aerodynamic and structural responses. There are several analytical and numerical coupling methods to investigate the FSI behaviour of vertical axis axis wind turbine blade. The BEM (Blade element momentum) is mostly adopted for the evaluation of aerodynamic forces in FSI modelling for its higher level of accuracy [150]. The performance of the turbine blades mainly depends on flow field and wake characteristics. The BEM method does not take into account the flow field characteristics and wake effect around the blades which acts as a barrier for studying further optimized blade design [151]. In that case, computational fluid dynamics (CFD) is another powerfool computing technique which is capable of representating the complex three-dimensional (3D) realistic fluid characteristics more accurately than BEM method. However, compared to BEM, the computational cost of CFD is more [152]. Similarly the structural modelling of FSI involes various models. The finite element analysis (FEA) model gives high level of accuracy and flexibility for defining material thickness in case of composites compared to one-dimensional (1D)

beam elements [134, 153]. Bazilevs *et al.* [154] presented an FSI modeling of a 3D VAWT using computational fluid dynamics. The aerodynamic results demonstrated good agreement with the field test data of the turbine. However, the turbine suffered from start-up issues at low rotational speed. MacPhee and Beyene [155] studied the flow conditions of a morphing VAWT blade using the finite volume FSI modeling. Results demonstrated that the flexible blade design have higher efficiency and self starting ability than the standard VAWT. Arora *et al.* [156] performed the FSI analysis of VAWT blade. The first phase of the study estimated the wind pressure on the blades using standard CFD tool, ANSYS Fluent. In the second stage, the aerodynamic pressure is imported to study the structural performance of the hollow composite blades. The blades are modelled with different thickness to reduce the effect of stress due to centrifugal forces and found that the maximum stress and deflection within the allowable safe limit. Marzec *et al.* [157] carried out the topological optimisation of H-rotor wind blade under realistic loading condition using one-way FSI simulation. It is found that the the deformation and stresses significantly reduced and over 60% mass reduction of the optimised blade is also observed. Madapur *et al.* [158] investigated the FSI simulation of VAWT using one way approach and found that the induced stresses and deformation are below the ultimate values ensuring safe working of the turbine.

2.8 Summary

After reviewing the literature, it is evident that bamboo has the potential to replace the existing materials. These composites are low cost, affordable, and most importantly biodegradable. Bamboo fibers are plant-based fibers and the composites fabricated using these fibers causes less manufacturing wastes compared to the conventional composites. It

is also important to note that the bio-based materials offer environmental benefits, such as reduced carbon footprint and biodegradability. However, in contrast to biodegradability or disposal challenges, these composites possess better biodegradability when the bamboo fibers are bonded with bio-based polymers. The utilization and production of small wind blades using bamboo material could be a source of income for the rural people and they could also generate their electricity using these domestic turbines to cut down the cost of grid-connected electricity. The strength of evaluation of these species needs to be performed to utilize these bamboos most effectively. Further, in bamboo-based polymer composites, bamboo is utilized in the form of single fibers which lowers the strength of the overall composite. The strength of composites using bamboo laminae/strips directly extracted from the bulk bamboo needs to be investigated. For Darrieus a wide range of investigation have been performed considering NACA symmetrical airfoils. The NACA 0015 showed the best performance compared to the other symmetrical profiles. Since blades are the key components of the whole turbine system, they need to be structural safe for smooth functioning. The structural strength of a blade plays very important role when the is utilized in urban environment with turbulence nature. Centrifugal and fatigue the are most dominating cause of blade failure in such environment. Most of the structural investigation on VAWT blades have been conducted on the symmteric profiles, However, the asymmetrical profiles with better aerodynamic performance also needs to be investigated.

2.9 Technical Gaps

After a detailed literature survey, the following research gaps are identified:

- The mechanical characterization of the Bamboo species such as Bambusa Tulda,

Bambusa Balcooa and Bambusa Nutan from the northeastern region of India (Assam) is not yet explored. The mechanical properties of bamboo can vary significantly between species and regions due to factors such as climate, soil conditions, and other environmental factors.

- Fatigue characterization is crucial, especially in applications where materials are subjected to cyclic loading or repetitive stress, such as wind turbine blades, structural elements, or other dynamic applications. There is limited data available on the fatigue life of bamboo composites.
- The structural behavior of bamboo-based straight vertical axis wind turbine blade have not yet been investigated.
- The wind turbine blades are subjected to continuous dynamic loads. There is no literature available on the study focusing the natural frequencies and mode shapes of bamboo based blades.

2.9.1 Research Objectives

Based on the literature survey, the primary objective of the research work is to develop Bio-composite blades for straight Darrieus wind turbines.

To accomplish the proposed major objective, the following sub-objectives are framed for the present research work:

- To select North-East bamboo species and conducting its mechanical characterization.
- To develope bamboo-based epoxy composite laminates and testing for static strength, flexure, impact and fatigue loading .

- To perform the static analysis of the bamboo composite blade considering both symmetric and non-symmetric airfoil using CAE.

- To perform the dynamic analysis of modelled bamboo composite blade for the symmetric and the non-symmetric airfoil.

- To perform Fluid-Structure Interaction (FSI) of the blade with the non-symmetric airfoil and fabricating blades using bamboo epoxy and fabrication of bamboo epoxy blade.

2.10 Motivation

Bamboo composites are emerging as promising materials for wind turbine blade applications due to several motivating factors. Firstly, in a world with an increasing focus on renewable energy sources, the utilization of bamboo in composites presents an opportunity to enhance the efficiency and environmental sustainability of wind energy generation. Bamboo composites align with global sustainability efforts, as bamboo is a rapidly renewable resource that can replace less sustainable materials like glass/carbon fibers, contributing to eco-friendly alternatives. As a renewable resource, bamboo can be harvested and replenished more quickly than other traditional materials. Bamboo also possesses an exceptional strength-to-weight ratio making it lighter in weight. Additionally, the abundance of bamboo in many regions enables the possibility of localized power generation, reducing the transportation cost and carbon emissions associated with manufacturing techniques. In conclusion, the motivation behind the research of developing bamboo composites for wind turbine application lies in the combination of strength, sustainability challenges, drive innovations, and positive impact on the environment and

society, making it an attractive choice for the renewable energy industry.

2.10.1 Organization of the Thesis

The complete research work presented in the thesis has been organized into seven chapters. The following is a brief outline of the each chapter's content.

- Chapter one presents an introduction to the wind energy, blade waste and its disposal problems, historical development and classification of wind turbines, development bio-composites for turbine blade. The anatomical features of bamboo, its distribution, extraction methods and its different applications are also discussed and presented.

- In Chapter two, a thorough review of the literature regarding the evolution of bio-composites for wind turbine blade, mechanical characterization of bamboo composites, and the structural performance of blades is presented. On the basis of in depth literature survey, research gaps are identified and, research objectives are proposed.

- Chapter three presents the mechanical and physical characterization of untreated, treated and bamboo composites. The comparative chart of the specific strength of the developed bamboo composites and other existing materials is also presented in this chapter.

- In Chapter four, the static strength analysis of the straight blade modelled using bamboo-based composites is presented.

- In Chapter five, the free and forced vibration of the modelled bamboo composite blade is summarised. The effect of different boundary condition on the natural frequencies of the straight blade is also presented.

- In Chapter six, the Fluid Structure Interaction (FSI) of the three dimensional wind turbine comprising of bamboo composite blade is presented. Fabrication of the prototype blade is also presented in this chapter.

- Finally, Chapter seven summarizes the major conclusions and suggestions for future research.

Chapter 3

Mechanical properties of Assam's bamboo-epoxy composite laminates – An experimental investigation

3.1 Introduction

The dominance of contemporary composite materials has reached heights as well worth weight-saving materials. Bamboo is one of the rapidly growing crops which is as stronger as timber and can be utilized in developing semi-replaceable industrial products. Bamboo composites are eco-friendly materials involved by combining bamboo fibers with resin or polymer matrices to enhance their individual material properties. The investigation of the mechanical properties of bamboo composites has become crucial as it helps to understand the durability and resilience of these composites over time. In this Chapter, the mechanical properties of three bamboo species collected from the North-Eastern region, "Assam" are studied. Firstly, the bamboo samples are extracted from the outer bulk bamboo and surface treated. The developed composite laminates are then characterized by tensile, compression, three-point bending, and impact loading. The Fourier transform infrared spectroscopic (FTIR) and Field emission scanning electron microscopy (FESEM) analysis is carried out to have a better understanding of the chemical composition, and surface morphology. The mechanical strength of these highly-cellulosic fiber composites conducted through various experiments are validated with theoretical equations. Further,

the fatigue behavior is also studied to determine the fatigue life of bamboo-epoxy composites under different stress ratio which will help in the development of design guidelines and standards for utilizing bamboo composites in load bearing structures.

3.2 Materials and methods

3.2.1 Raw materials

In this study, three commercial species of bamboo grown in the (NE) region (Bambusa Balcooa, Bambusa Tulda, and Bambusa Nutan) are collected from the local market of Assam, Guwahati. The maturity of the bamboo species is about (3-4) years. Sodium Hydroxide (98%) and Sodium Sulfite (98%) are used for delignification process. The polymer-based matrix material used in this study is Epoxy (Type- LY556, along with hardener HY-951). Bamboo fibers in the form of laminae/strips are used as the reinforcing material. The bamboo/epoxy composites are fabricated using the hand layup process. Further, deionized water is used as the solvent.

3.2.2 Experimental procedure

Culm length (300–350) *mm* is selected and the nodes are removed. The cylindrical culms are split into four sections using the splitter machine. Bamboo billets are procured maintaining an average thickness of (10±1.5) *mm* and length of (300±10) *mm* as shown in Fig. 3.1(a). and Fig. 3.1(b). In a study, authors investigated that external bamboo strips with thicknesses ranging between (1.2 to 2.5) *mm* demonstrated better mechanical strength performance [159].

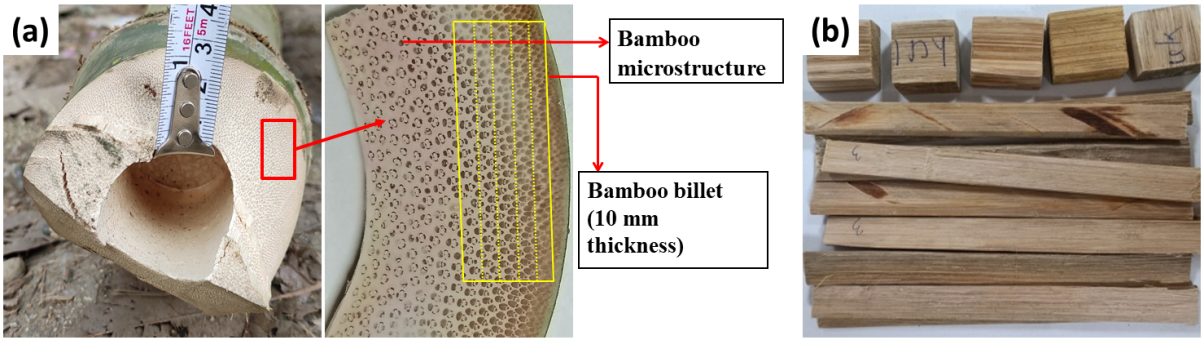

Figure 3.1: (a) cross-section of bamboo culm (b) rectangular bamboo strips.

A general flow process diagram for the sample preparation is shown in Fig. 3.2. In the present study, the composite laminates are prepared using hand-layup as shown in Fig. 3.3. It is a simple, cost-effective process compared to other manufacturing techniques such as molding, VARTM. process. Firstly, the strips are surface treated with sodium

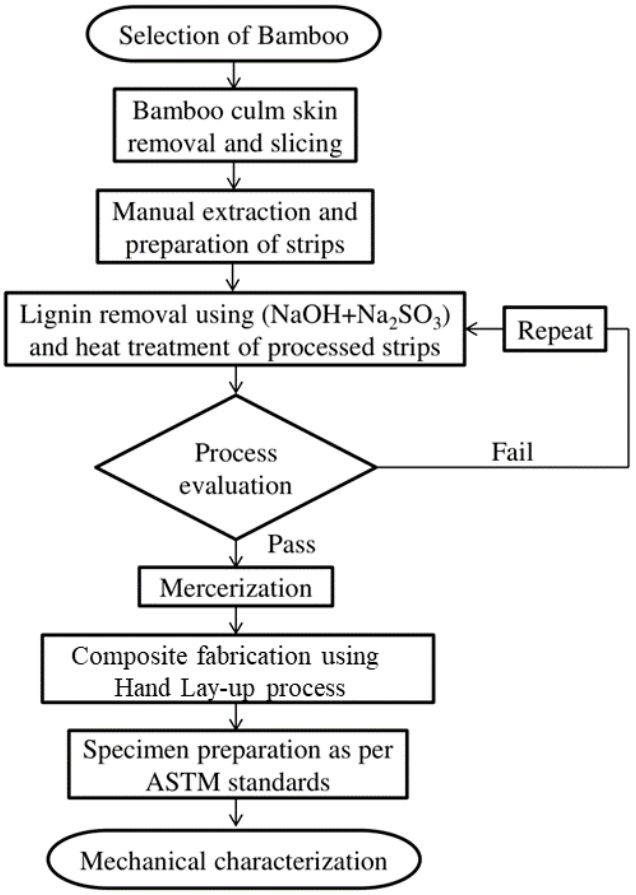

Figure 3.2: Flow chart of sample preparation.

hydroxide (2.5 *mole/L*) and sodium sulfite (0.4 *mole/L*) and heat-treated to 80°C for

8 *hours* to remove lignin and other substrates. At this temperature, single fiber pull out, and tearing is observed disturbing the fiber matrix for further process. The deligification process is achieved at an optimum temperature of 60°C as higher temperature can destroy the interconnection link between bamboo fibers and parenchyma cells. This is because the fiber density and cells strongly depend on lignin. Thus, the heat treatment parameters are reduced to 60°C for 6 *hours*. After treatment, the strips are washed thoroughly to remove the excess chemicals and dried at room temperature. Thereafter, the remaining substrates are removed by soaking the treated strips in NaOH solution (6% w/v) for 3 *hours* as reported by Asim *et al.* [160]. These dried strips are manually laid into a metallic mold (Fig. 3.3). The bamboo strips are arranged according to the design specifications ensuring proper fiber orientation and resin distribution. The strips are impregnated with epoxy resin and hardener at a ratio of 10:1. Throughout the process, attention is given to removing air bubbles and achieving uniform thickness. After the resin infusion process, the composite is compacted with a cover plate to remove the excess resin.

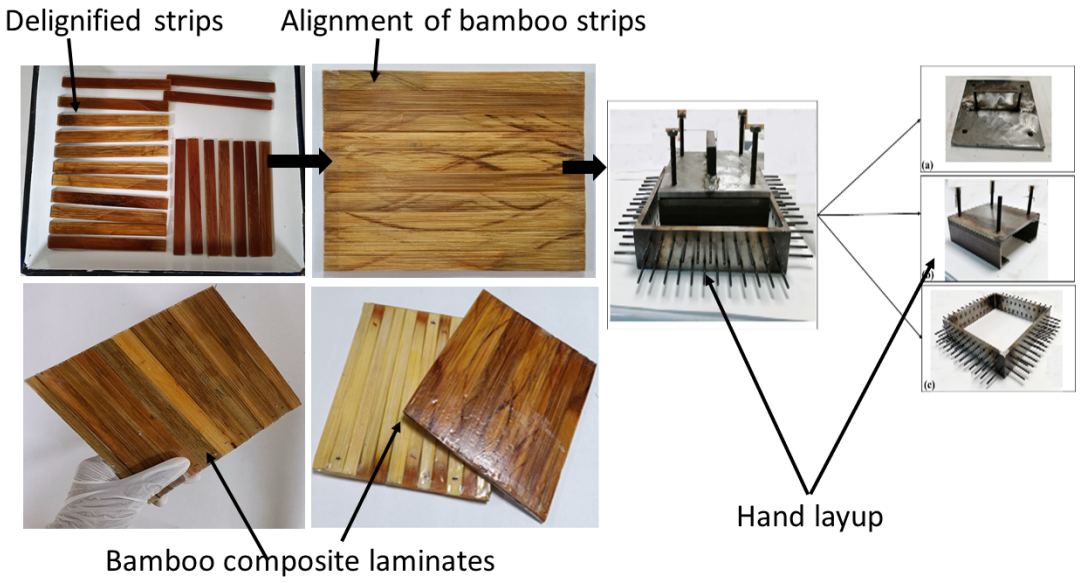

Figure 3.3: Developed bamboo-epoxy composite laminates.

3.2.3 Mechanical characterization

The FTIR analysis is conducted to differentiate the change in the chemical composition after alkaline treatment. Each spectrum consisted of 32 scans for each sample in the spectral range of (400-4000) cm^{-1} with a resolution of 4 cm^{-1}. In the ongoing delignification process, the percentage weight reduction (wt%) of the samples is recorded at every 1 *hour* interval. The delignified bamboo samples are taken out from the water, dried, and weighed. Similarly, the weight gain of the epoxy infiltrated bamboo specimens after immersion in water till the nth hour is calculated by Eq. (3.1):

$$(M_n - M_0) * 100\%/M_0 \tag{3.1}$$

where M_n and M_0 denotes the initial and final value of the specimens after nth hour. The morphology and structure evaluation of the prepared samples are examined using Sigma Field Emission microscopy (Make: Zeiss, Germany). Generally, cellulosic fibers are less or non-conductive [161]. To increase the conductivity, the samples are uniformly gold coated for 30 *seconds*. To determine the resistance of the samples against different moisture content, the weight of the specimen before and after immersion in distilled water for 24 *hours* is measured. Total of 9 samples are prepared with dimensions (100 *mm* in length, 6 *mm* wide, and 2 *mm* thick). The width and thickness of each specimen before and after water immersion is measured using a digital vernier caliper. The weight of the specimens is calculated every 2 *hours*. Water absorption, width expansion, and thickness swelling are calculated by Eq. (3.2):

$$(W_n - W_0) * 100\%/W_0 \tag{3.2}$$

where W_n and W_0 denotes the initial and final value of the specimens after nth hour. The developed composite laminates are cut in the longitudinal and transverse direction as shown in Fig. 3.4(a). These composite strips are tested for their mechanical strength such as tensile, flexural, compression, and impact using standard test machines. The tensile test specimens are prepared as per ASTM-D-638-3 with dimensions of 160 *mm* in length, 14 *mm* width, and 3 *mm* thickness. The flexural test samples are prepared as per ASTM-D-790-3 with dimensions of 130 *mm* in length, 14 *mm* width, and 3 *mm* thickness. Similarly, the compression test specimens are cut as per ASTM-D-3410. The tests are carried at a crosshead speed of 1.5 *mm/min*. The tensile and flexural test fixtures with the bamboo samples are presented in Fig. 3.4(b) and Fig. 3.4(c). Two different load cells are used i.e. 100 *kN* for the longitudinal samples and 1 *kN* for the samples cut in the transverse direction. The gauge length of the samples is taken as 50 *mm*. The charpy impact test of the un-notched samples is carried out at 120° clockwise using a manual "Pendulum Charpy Tester" capacity at room temperature.

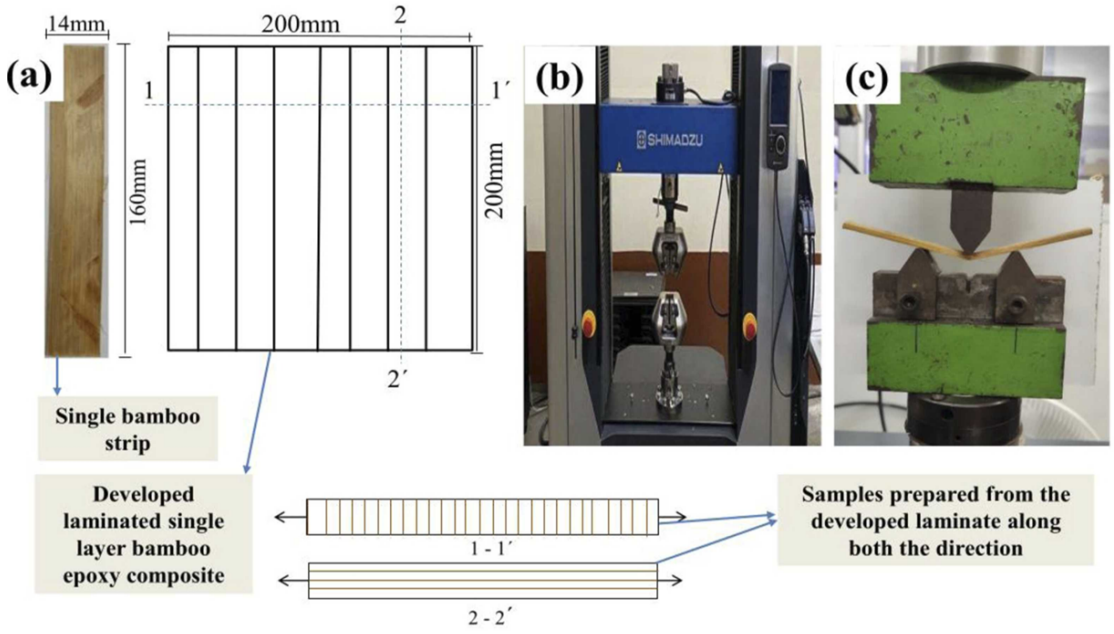

Figure 3.4: (a) single-layer laminates from single bamboo strip (b) tensile fixture (c) bending fixture.

3.3 Theoretical calculation

The elastic properties and strength of the unidirectional bamboo laminates are estimated from the fiber and matrix properties using the rule of mixture. The proposed rule for elastic properties in laminate is given by the following expression [162] -

$$E_c = E_f V_f + E_m V_m \tag{3.3}$$

$$\sigma_l = \sigma_f V_f + \sigma_m (1 - V_f) \tag{3.4}$$

$$\sigma_t = \sigma_m \left(1 - \left(\frac{4 * V_f}{\pi} \right)^{0.5} \right) \tag{3.5}$$

where E_c is Young's modulus of the composite laminate along the fiber direction, E_f is Young's modulus of the bamboo fiber, E_m is Young's modulus of the polymer matrix, V_f is the fiber volume fraction and V_m is the matrix volume fraction, σ_f is the average tensile strength of bamboo fiber, σ_m is the average tensile strength of the polymer matrix, and σ_l is the average tensile strength of the bamboo composite laminate in the fiber direction, σ_t is the average transverse tensile strength of the laminate.

3.4 Results and discussion

3.4.1 Fabrication and physical properties evaluation

In this study, the fabrication process comprises a two-step procedure. Firstly, the bamboo strips are delignified through the alkaline solution, and then the epoxy resin is impregnated into the bamboo surface through hand layup technique. In the initial step toward

the lignin removal process, Fig. 3.5 shows the comparison of solution color in every two-hour interval from the soaking period. With the increase in immersion time, a change in solution color from pale yellow to deep brown is observed as shown in Fig. 3.5(a) and Fig. 3.5(c). Cellulose and hemicellulose are simple structures with colorless substrates compared to lignin. The deep solution color signifies the removal of lignin from the bamboo sample which facilitates the infiltration of resin into the fibers as compared to virgin bamboo [163].

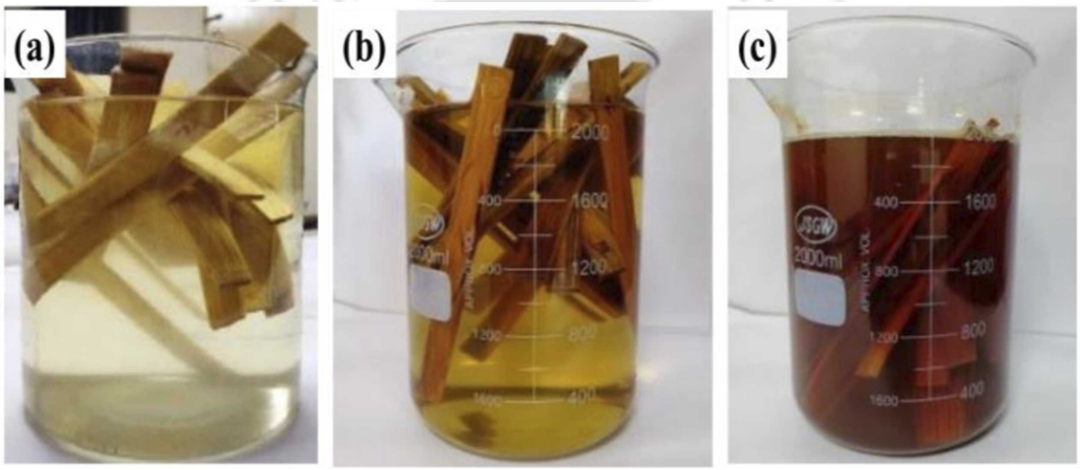

Figure 3.5: Illustration of change in solution color after delignification of bamboo samples.

The removal of lignin from the bamboo samples is also quantified using the weight reduction formula, as shown in Fig. 3.6. During the heat-treated delignification process, other substrates along with the lignin-carbohydrate complex (LCC) are eliminated swiftly in the first hour, with approximate mass loss of 37% for B.Tulda, 33% for B.Balcooa, and 31% for B.Nutan. Observations are noted every 1 *hour* and are observed that after the 6^{th} *hour*, the graph becomes stable as the mass-loss rate gradually is slower. Total mass loss after six *hours* of soaking has attained 56% for B.Tulda, 56.60% for B.Balcooa, and 49% for B.Nutan. After this process, the untreated, delignified, and composite samples are submerged in water for a week. Water absorption results are almost crucial as the water-

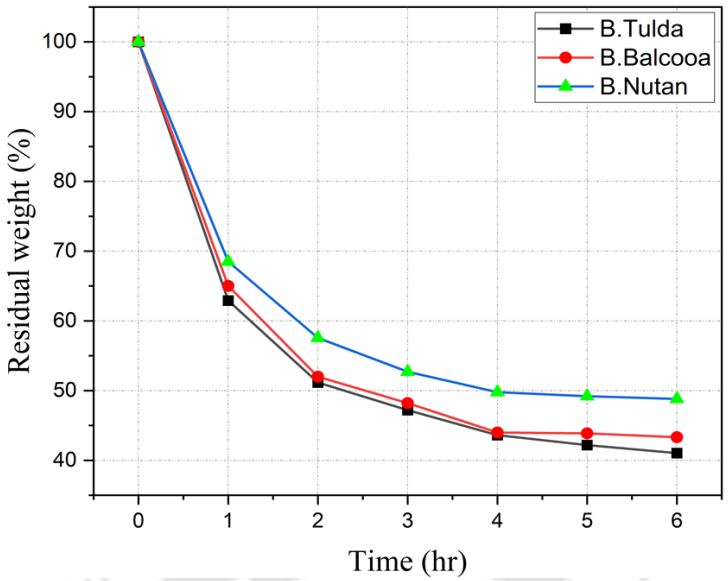

Figure 3.6: Mass loss w.r.t. soaking time during the delignification process.

resistant ability affects the physical and mechanical properties. After every 24 *hours*, the samples are taken out and weighed to examine their rate of water absorption and dimensional stability as shown in Fig. 3.7. Subsequent weight gain in the raw bamboo samples is observed subjected to one-week water immersion. Among the three species, B.Nutan has a higher water absorption capability and acquired the highest weight gain of 73%.

Bamboo structure resembles a sponge with lignin and cellulose-containing high hydroxyl (–OH) group that could interact with water molecules [164]. As shown in Fig. 3.7(a), the delignified bamboo samples absorbed the highest water with increasing immersion time due to their loose open pores to a weight gain of up to 225%. The epoxy infiltrated bamboo composites showed slight variation over increased soaking time compared to the untreated and alkali treated fibers. The reason behind this is the presence of hydrophobic nature of epoxy resin which provided good interfacial resistance against moisture. A similar pattern is observed in the case of thickness swelling and width expansion as shown in Fig. 3.7(b) and Fig. 3.7(c). It is observed that the swelling

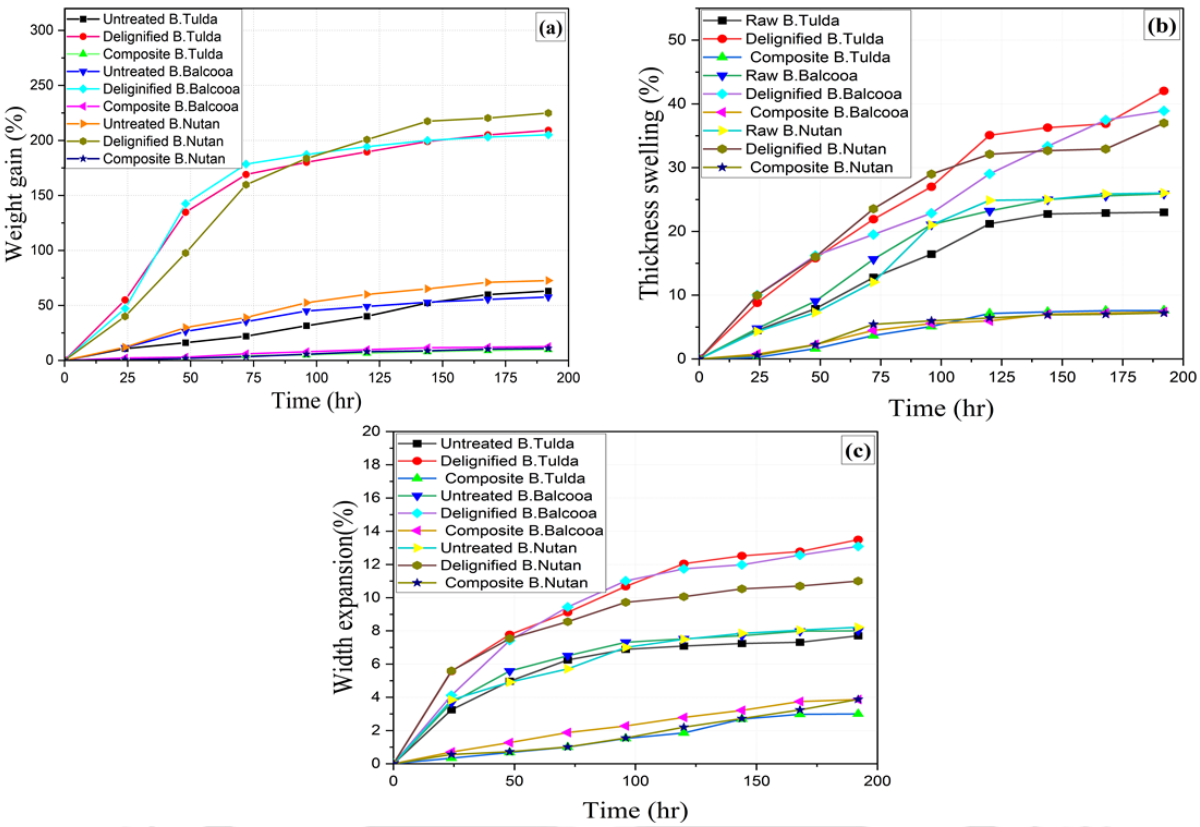

Figure 3.7: Illustration of change over increased soaking time for different bamboo samples (a) weight gain (b) thickness swelling (c) width expansion.

rate of fibers is comparatively higher with increasing moisture content than those of cell bundles. Significant shrinkage is observed once the fibers are dried. The outer green layer with highest fiber content swelled dramatically leading to fracture compared to the inner one. In this present study, untreated bamboo samples started swelling (both with thickness and width) gradually with an increment of 26% and 8% which is found to be the highest for B.Nutan. But in the case of delignified bamboo after the sixth day, misalignment of fibers and cracks are formed to final crumple of the structure. In contrast to the above two samples, stable behavior against moisture attack is noticed after the penetration of epoxy resin into porous laminae. This behavior indicated that infiltration of epoxy resin into bamboo fiber surface significantly improved the fiber-matrix interfacial adhesion reducing its negative traits due to moisture.

3.4.2 Microstructure characterization

The treatment of bamboo fibers with diluted alkaline solution leads to partial removal of organic substituents from the fiber surface resulting in their morphological and chemical changes [51]. Fig. 3.8 shows the FTIR spectra of untreated and alkali-treated bamboo samples of the selected three bamboo species to further justify the removal of lignin. Almost a similar number of peaks are observed in the entire spectral range between (3500-500) cm^{-1} for the three species of bamboo. The characteristic band in the range from (3700-3300) cm^{-1} represents the stretching vibration of strong hydroxyl groups (-OH) whereas the band ranging from (1600-1450) cm^{-1} represents C-H deformation and aromatic skeleton vibration of lignin [165]. A significant change is observed between the spectra range of (1536-1476) cm^{-1} for the untreated and treated samples. This

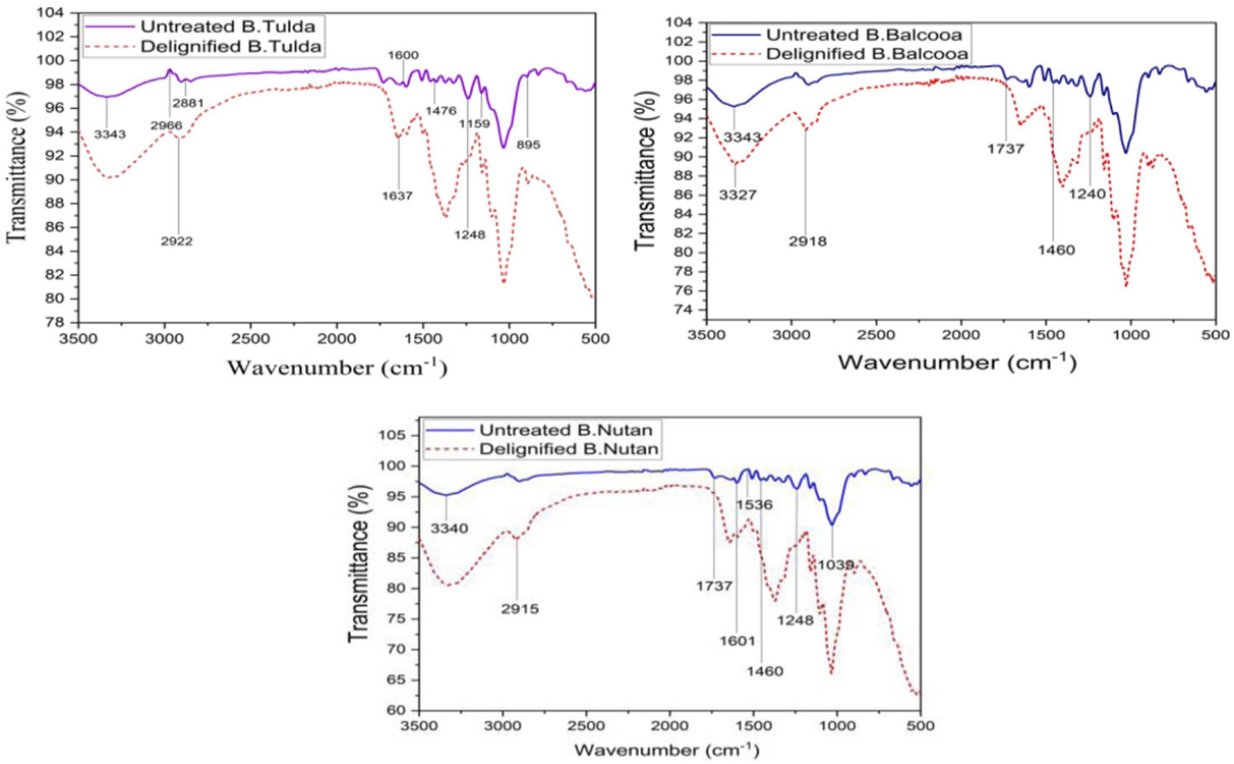

Figure 3.8: FTIR spectra for untreated and delignified bamboo of the selected bamboo species.

could justify the delignification process from the bamboo surface. On a similar note, the spectra band in the range from (3100-2700) cm^{-1} represents the (C-H) stretching aliphatic group. The characteristic bands at 2922 cm^{-1}, 2918 cm^{-1}, and 2915 cm^{-1} represent the elimination of hemicellulose [91]. Further details of the infrared spectra bands and their assignments of bamboo are reported by Cai *et al.* [166]. The peak of 1248 cm^{-1} is due to the Guaiacyl ring breathing with CO-stretching, lignin, and hemicellulose, 1151 cm^{-1} represents C-O-C, carbohydrate [167]. A slight change in these spectra for the samples after delignification is observed. Thus, the hydrophilic nature is disturbed, and the bamboo fibers are strongly attached to the matrix material. The bands at 3343 cm^{-1}, 3340 cm^{-1}, 2881 cm^{-1}, 1159 cm^{-1}, and 895 cm^{-1} can be assigned to the –OH, C-O, and C-H respectively [104]. However, these characteristics of lignin bands seem to be absent in the delignified bamboo samples resembling a substantial removal of lignin.

Bamboo is a heterogeneous orthotropic material. The surface morphologies of the untreated, alkali-treated, and bamboo composite samples perpendicular to the growth direction and parallel to the growth direction are studied by scanning electron microscope. The FESEM photographs of untreated bamboo are taken perpendicular to the growth direction and display a porous structure comprising vessels, parenchyma cells, and lignocellulosic fiber bundles as shown in Fig. 3.9(a) whereas, along the growth direction, Fig. 3.9(b) depicted the deposition of lignin and other organic particles packed with the rigid vascular fiber bundles. Cellulosic fiber bundles, parenchyma cells, and vessels are connected by a low strong natural polymer matrix of hemicellulose and lignin. However, certain inherent defects such as some intercellular spaces between fibers are also noticed in the original structure as shown in Fig. 3.9(b) which is in line with the study reported by Li *et al.* [168]. It can be seen that the rigid structure became loose and the fiber

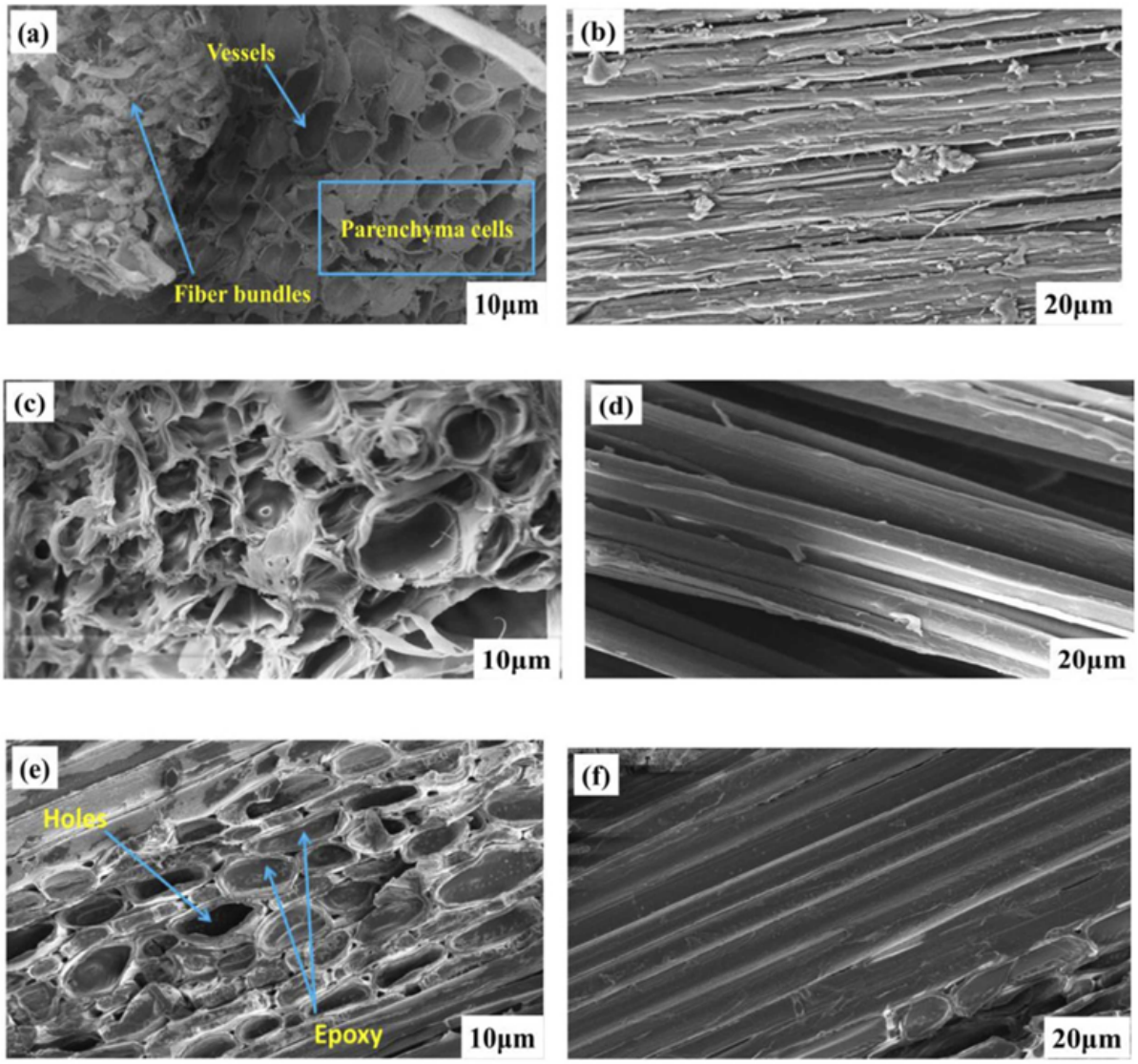

Figure 3.9: Digital FESEM photographs (a) untreated bamboo perpendicular to the growth direction (b) untreated bamboo along the growth direction (c) treated bamboo perpendicular to the growth direction (d) treated bamboo along the growth direction (e) bamboo-epoxy composite perpendicular to the growth direction (f) bamboo-epoxy composite along the growth direction.

bundles are distorted after the delignification. Organic compounds, hemicellulose, and lignin are removed to some extent in the entire process confirmed through FTIR analysis, resulting in tiny pores and gaps between the fibers as shown in Fig. 3.9(c). In cellulosic substances, the shape and size of the pores significantly depend on the process of delignification which affects the impregnation of resin into the structure, decreasing the overall properties of the composite [169]. Surface impurities are removed compared to untreated

bamboo enhancing fineness and uniformity in fibers as shown in Fig. 3.9(d). After the infiltration of epoxy, the gaps are thoroughly filled after the infiltration of epoxy resin between the fiber bundles distorting the round shape of the bundles. The fibers seemed to be tightly packed together forming a continuous solid structure with higher strength and better interfacial bonding as shown in Fig. 3.9(e). However, improper impregnation of resin identified with few holes in the composite sample. Studies from earlier investigations reported that certain parameters such as temperature, pressure, and viscosity could enhance the infiltration of resin into the porous microstructure [170, 171]. Moreover, the fiber surface appears to be slightly rough due to the deposition of epoxy resin as shown in Fig. 3.9(f). This rough surface results in strong fiber-matrix bonding reducing the effect of slippage.

3.4.3 Experimental results

The prepared specimens are tested with the help of a static tensile machine. Three species are selected and grouped under three categories (untreated, treated, and composites). Fig. 3.10(a), Fig. 3.10(b), and Fig. 3.10(c) are the obtained stress-strain curves for the three species of bamboo composite. Five samples for each category are tested and the average value is recorded for the three bamboo composites as shown in Fig. 3.10(d). Compared to the other two species, B.Tulda composites demonstrated higher tensile strength. It is seen from the stress-strain curves that the value of stress increases quasi-linearly as the value of strain increases to its maximum and a sudden rupture is observed when the stress reaches its maximum value. This behavior of fracture is attributed to the britle nature of bamboo fiber, which is quite similar to other lignocellulose fibers. The tensile strength of B.Tulda composite is (259.00±41.10) MPa, B.Balcooa composite is

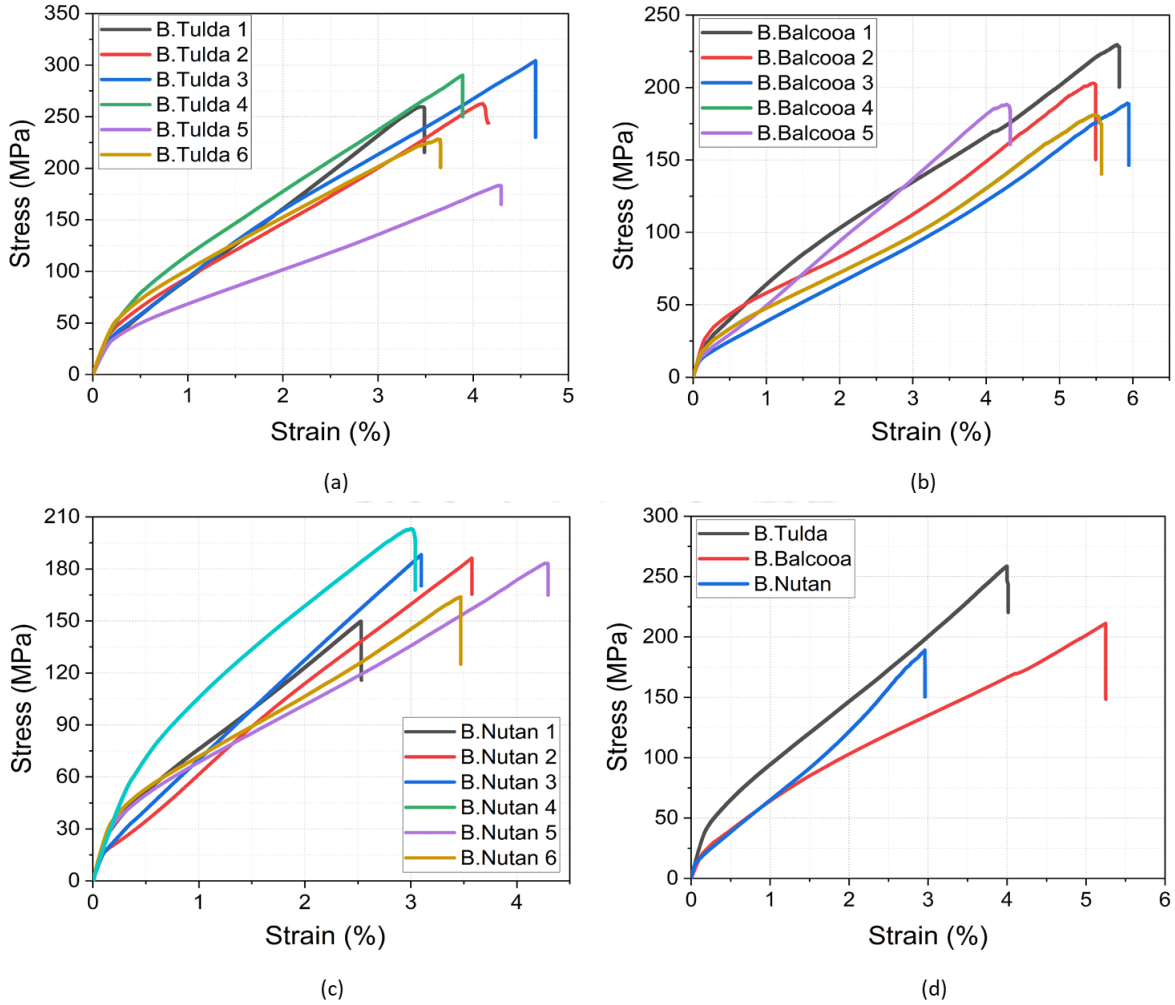

Figure 3.10: Stress-strain curve (a) B.Tulda composites, (b) B.Balcooa composites, (c) B.Nutan composites and (d) comparative stress-strain curve.

(200.12±25.62) *MPa*, and B.Nutan composite is (188.52±39.45) *MPa*.

The mechanical properties of bamboo composites compression, flexural, and toughness are also tested as these properties are of crucial importance in the construction and building domain [172]. The mechanical strength of the different bamboo species in its three different forms are displayed in Fig. 3.11(a). Among the other two species, B.Tulda showed the highest mechanical performance in terms of strength and stiffness. The tensile strength of untreated B.Tulda is 195.36 *MPa* whereas B.Tulda composite is 259 *MPa*, which is 133% of that of untreated, 222% of that of the treated (116.65 *MPa*), and 253% from neat epoxy (73.30 *MPa*). The modulus of elasticity (MOE) and modulus of rupture

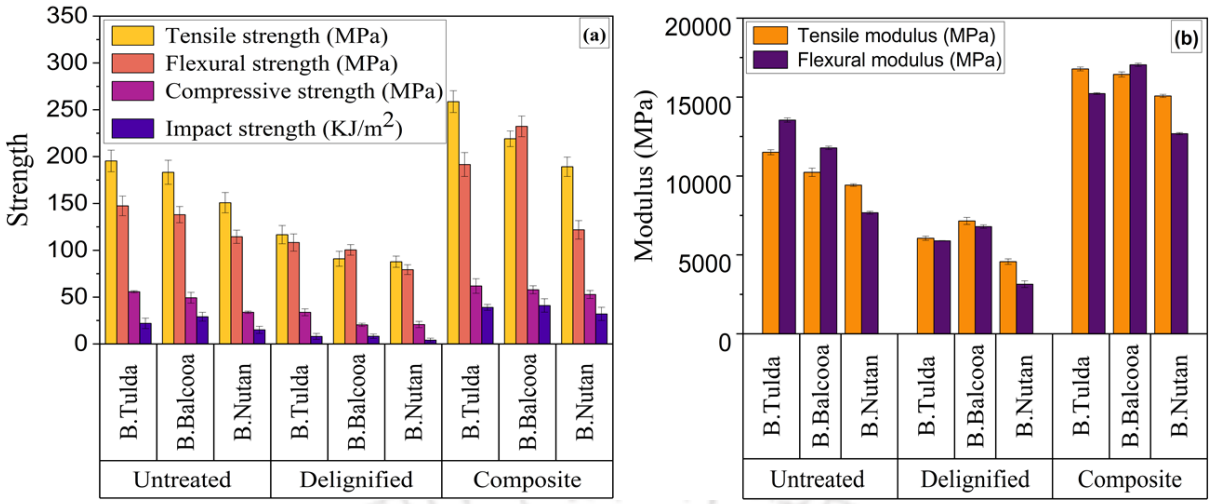

Figure 3.11: Mechanical properties of different species of bamboo under various categories (a) strength (b) modulus.

(MOR) of the bamboo samples are represented in Fig. 3.11(b). The values are higher for B.Tulda. Untreated samples reached up to modulus of 11 *GPa* and 13.20 *GPa* whereas surface modification composites achieved higher modulus of 16.78 *GPa* and 15.90 *GPa* which is 52.50% and 20.45% of untreated. Out of all samples, composite B.Balcooa achieved the highest flexural modulus. However, the alkali-treated samples demonstrated a significant reduction in strength and modulus. This is because after the chemical treatment the compact vascular bundles start swelling (FESEM images). This also leads to larger gap formation with less tight bonding between fiber bundles damaging the internal fiber bond [163]. The sudden drop in the tensile strength of the alkali treated samples is due to the absence of lignin which is dissolved during the delignification process. Similar results are obtained from bending analysis. Flexural properties reflect the synergic of two strengths (tensile and compressive) whereas the modulus indicates the resistance against bending deformation [173]. Compression and charpy impact tests are also performed to examine the fracture and ductility of the material. The highest compressive strength is recorded for the B.Tulda composite which is about 61.85 *MPa*. As reported by Xu *et al.* [167], the most crucial parameter responsible for the compressive properties of fiber

composites is the strong interfacial bond between the fiber and the matrix. Further, the composites demonstrated better fracture toughness than the original bamboo samples which means the former absorbed more energy before fracture failure than the original bamboo samples. Composites showed toughness of 39 kJ/m^2 for B.Balcooa, 35 kJ/m^2 for B.Tulda, and 27 kJ/m^2 for B.Nutan which is almost 34%, 59%, and 50% that of untreated.

The density of bamboo strips is measured by taking the ratio of the mass of the three specimens to their volume and is tabulated in Table. 3.1. After the chemical treatment, due to mass loss the density decreased from 0.76 g/cm^3 to 0.26 g/cm^3 for B.Tulda, 0.60 g/cm^3 to 0.30 g/cm^3 for B.Balcooa and 0.52 g/cm^3 to 0.15 g/cm^3 for B.Nutan. The percentage weight of the fiber content in the composite is determined by weighing the ratio of the initial weight of the treated bamboo samples to the resultant composites. The density of B.Tulda composite is 1.12 g/cm^3. The FESEM images are post-processed using ImageJ software and the approximate fiber content in the composite is estimated in the range of (53-56)%. The bamboo-epoxy composites showed slightly higher strength as compared to untreated and treated samples. From the FESEM images, it can be confirmed that the fibers are strongly packed with each other due to the presence of epoxy which provides a solid structure with higher strength. The delignification step

Table 3.1: Density of bamboo and bamboo epoxy composites.

	Density(g/cm^3)		
	B. Tulda	B. Balcooa	B. Nutan
Untreated	0.76±0.04	0.60±0.05	0.52±0.11
Alkali treated	0.26±0.03	0.30±0.02	0.15±0.05
Composites	1.12±0.12	1.08±0.09	0.96±0.07

is necessary as it cleans the surface impurities improving the mechanical properties of the composite. Further, increases composite resistance against environmental moisture attacks and fungal degradation with an increase in its life span. The tensile behavior of the prepared bamboo composites in the transverse direction is also studied. Low tensile strain rate of 0.1 *mm/min* is selected to minimize the chance of dynamic effect during the test. Fig. 3.12 depicts the stress-strain curve for the bamboo composites in the transverse direction. The curve showed similar brittle behavior as shown in Fig. 3.10. The failure initiated at the joints/interface of the composite in the transverse direction.

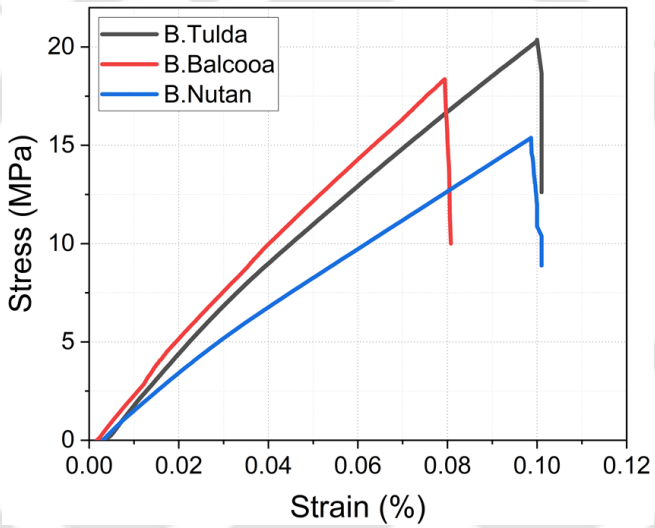

Figure 3.12: Tensile stress-strain of the bamboo composites in transverse direction.

The sustainable strength is the strength of the resin as there is no reinforcing effect in that direction. In a study by Mylsamy and Rajendran [174], the authors also revealed that the tensile properties of composite mainly depend on the orientation of the fibers and fiber-matrix adhesion i.e. the fibers should be placed along the direction of their loading capacity to avail its highest tensile strength. The mechanical strength of bamboo-epoxy laminates and several other bamboo boards/ply are presented in Table. 3.2.

Table 3.2: Comparison of the mechanical properties of bamboo laminate with other engineered bamboo boards.

Material	Reference	Tensile (MPa)	Modulus (GPa)	Flexural (MPa)	Compressive (MPa)
Bamboo-epoxy composites	Present investigation	259	16.78	212	61.85
Laminated bamboo	[175]	90.00	19	77–83	77
Bamboo laminates	[176]	169-205	14.3-16	168-128	55-88
Bamboo composite board	[177]	-	-	-	47.17
PDMS-bamboo composite	[178]	130.10	7.60	-	78.20
Laminated bamboo lumber (LBL)	[179]	112.56	9.90	118	50.57

The tensile strength of the developed composites in this study is found to be significantly higher than the composites in the previously reported studies [180–182]. The tensile and flexural strength of the bamboo-epoxy laminates is higher when compared with the other engineered bamboo boards. The tensile modulus is higher than other bamboo boards but is found to be slightly lower than the laminated bamboo. The compressive strength of the bamboo-epoxy laminates is lower than other engineering bamboo, however, is slightly higher than bamboo composite board and laminated bamboo lumber (LBL). It is found to be worth mentioning that the mechanical properties of bamboo composites in the present study are comparatively higher than other bamboo composites reported in the literature. The specific strength and elastic modulus of the developed composites are compared with some practically used materials in industrial applications as shown in Fig. 3.13. It is observed that the specific strength of the B.Tulda compos-

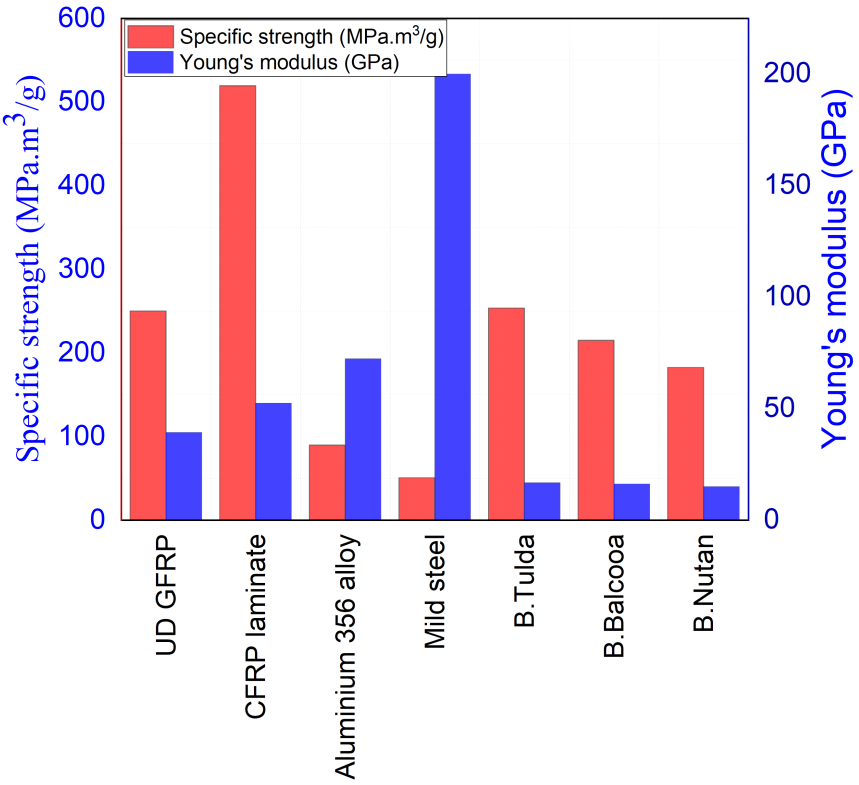

Figure 3.13: Specific strength and young's modulus of existing materials and developed bamboo-epoxy composite laminates.

ite is 245 $MPa.m^3/g$ with 54% fiber fraction is half that of the carbon fiber-reinforced polymer (CFRP) composites which is 554 $MPa.m^3/g$ [183], and much lower than that of Aluminum 356 alloy [184], and mild steel [185]. However, the strength of the B.Tulda composite is almost comparable to that of bi-axial (0-90) glass fiber-reinforced polymer (GFRP) composite i.e. 239.77 $MPa.m^3/g$ (Awad *et al.*) [186]. The young's modulus of the bamboo composites such as B.Tulda is 16.78 GPa, B.Balcooa is 16.43 GPa, and B.Nutan is 15.07 GPa which is lower compared to mild steel (200 GPa), aluminum (72 GPa) and CFRP (52 GPa). This indicates that these composites have better strength with low rigidity. Moreover, the density of B.Tulda composites is 1.09 g/cm^3, B.Balcooa is 0.96 g/cm^3, and B.Nutan is 0.88 g/cm^3 which is much lower than density of mild steel and aluminum alloy i.e. 7.90 g/cm^3, and 2.67 g/cm^3. Thus, with the specific amount of strength, these bio-composites are highly superior in strength and can be used as

a replacement in small semi-structural applications like panels, batten columns, etc. It should also be noted these substitutes are environment friendly with very less/no residual waste during the manufacturing process.

3.4.4 Validation

The elastic properties of the three species of the bamboo composite are calculated based on the experimental results for the material properties using the rule of mixture law. The theoretically measured values can provide a reasonable prediction of the behavior of the composite strength compared to the experimental results. Results of both experimental and theoretical calculations are listed in Table. 3.3. The theoretical values for tensile strength and modulus are found to be closer to the measured values with a relative percentage error of less than 15%. However, the strength of the composite laminates in the transverse direction differed slightly from the theoretical values which are due to the improper infiltration of epoxy into the pores. The tensile strength of the composite is mainly due to the strong interfacial bonding of fiber-matrix adhesion. Holes are noticed

Table 3.3: Comparison of the mechanical properties of developed laminates.

Theoritical properties				% Error with experimental results		
	B.Tulda	B.Balcooa	B.Nutan	B.Tulda	B.Balcooa	B.Nutan
Longitudinal tensile strength (MPa)	260.32	218.18	200.00	1.24	1.29	5.44
Transverse tensile strength (MPa)	14.05	11.41	13.09	9.07	6.70	7.66
Young's modulus in longitudinal direction (GPa)	17.12	16.96	17.12	1.98	3.12	11.90

in the microstructure of the samples from FESEM images which ultimately results in poor interface adhesion with the fibers. Moreover, for natural fiber-related plants, the physical and mechanical properties gradually vary in every direction. This change in attributes may also be one of the factors that reduce the accuracy of the rule of the mixture model predicted values compared to the experimental values.

3.4.5 Fatigue life assessment

The fatigue behavior of the B. Tulda specimen are studied under tensile loading conditions. Smooth rectangular samples with dimensions 250 *mm* in length, 25 *mm* width, and 5 *mm* thickness are prepared from the outer region of the bamboo culm. The specimens are prepared as per the ASTM-3479 [187] with a gauge length of 100 *mm*. The ends of the composite samples are bonded with a metal sheet to avoid material slippage. The fatigue test is carried out on raw bamboo and bamboo composite specimens. Two types of bamboo composite specimens are prepared, one from high fiber density and the other from low fiber density as shown in Fig. 3.14. The raw and bamboo composite specimens are loaded in an Instron servo-hydraulic system with a load cell of 100 *kN*. The maximum UTS of the raw bamboo sample is 152.16 *MPa*, and that of the composite samples is

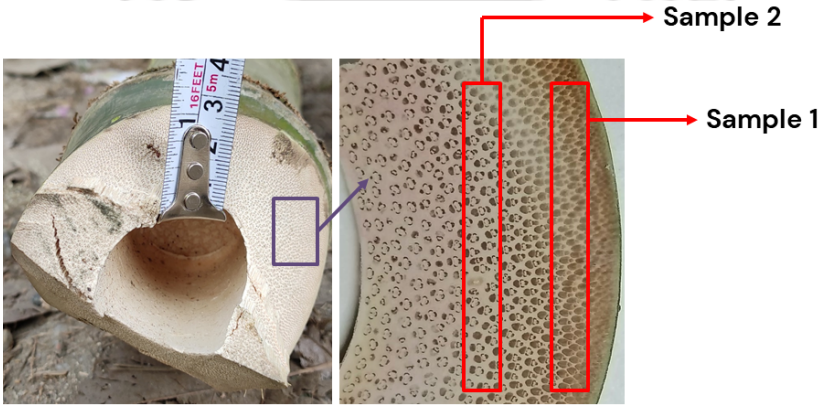

Figure 3.14: Extracted sample 1 and sample 2 bamboo strips.

221.07 *MPa* for sample 1 and 183.34 *MPa* for sample 2. The stress-strain curve of the prepared specimens is shown in Fig. 3.15. The composite sample from the higher fiber density has high tensile strength as already explained in Section 3.2. The fatigue test is performed by varying the maximum stress limit starting from 95% of UTS to 45% of UTS at every 5% interval from the experiment conducted in static tensile mode. Constant load amplitude is applied in the form of a sinusoidal wave at a loading frequency of 10 H_Z to minimize the impact of self-heating. The minimum stress ratio is kept constant at 0.2.

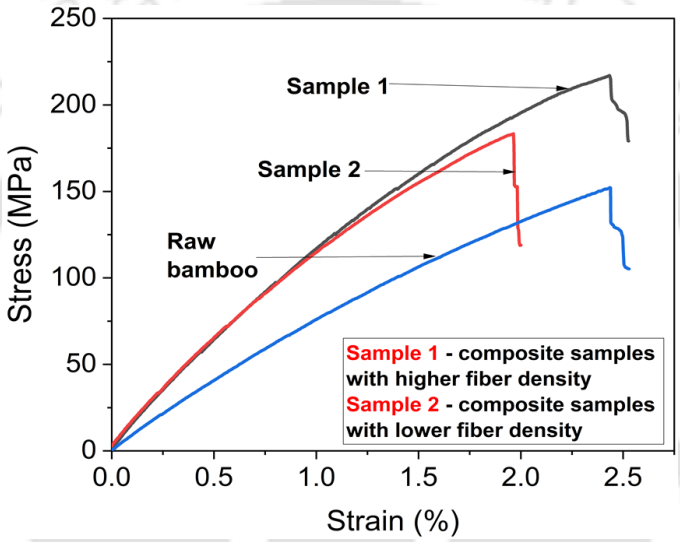

Figure 3.15: Extracted sample 1 and sample 2 bamboo strips.

The tensile stress-life (S-N) curve obtained for the three types of bamboo specimens is presented in Fig. 3.16(a) and Fig. 3.16(b). The failure point of the specimens is defined when the samples are visibly fractured till the sudden load drop under the specific loading condition. Even though the care has been taken in sample extraction, there is significant varying of fatigue strength seen in the bamboo species. This may be expected due to the natural variation of material properties of bamboo [188]. Thus three samples in each set is tested and the average value is considered. From Fig. 3.16, it is observed that the composite with high fiber density has a high fatigue limit of 108 *MPa* which is 50% of UTS compared to less fiber density which achieved a fatigue limit of 85 *MPa* i.e. 45%

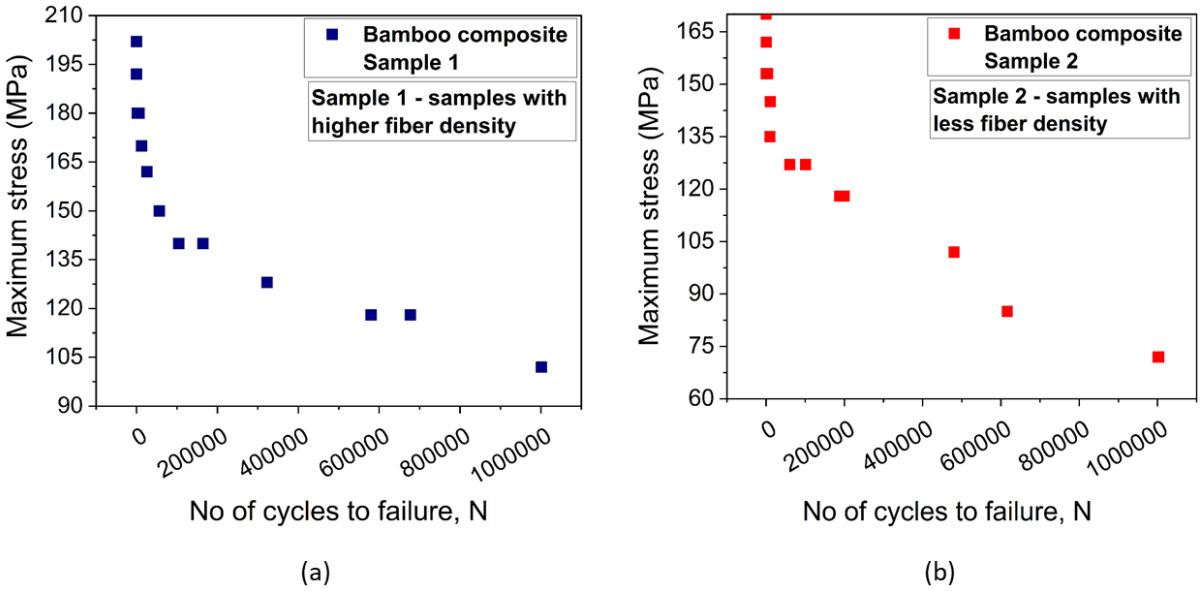

Figure 3.16: Maximum stress vs cycles to failure of composites (a) sample 1 (b) sample 2.

of UTS. The samples achieving maximum fatigue limit of UTS prior to 1,000,000 cycles (considered as run-out) is marked as the transition point, i.e. below this value the samples will not undergo failure at the early stage [108, 109]. The comparative S-N curve of all the specimens is presented in Fig. 3.17, which shows good gradual decrease in fatigue life cycle with decreasing max stress levels. Most of the samples failed at 90% to 60%

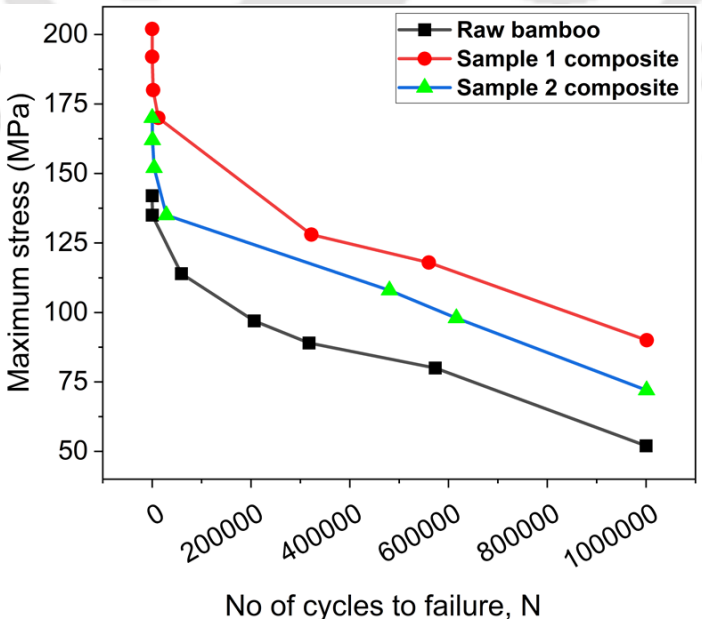

Figure 3.17: Comparison plot of max. stress vs cycles to failure.

of UTS, however the samples below 45% of the UTS did not failed even after 4,00,000 cycles. Similar trend in the S-N curve of natural composites has been reported by Ali *et al.* [110], Keogh *et al.* [108], Shah *et al.* [189] in which the the samples below 40% of static strength survived more than 10^5 cycles, which is similar to most of the engineering materials.

3.5 Summary

The current findings infer that the developed composite using highly cellulosic bamboo strips and epoxy resin posses good mechanical strength and stiffness than the other species reported in the literature. Two step-wise fabrication processes are incorporated such as delignification of the bamboo samples followed by infiltration of epoxy resin into the porous highly aligned fibrous structure. The bamboo-epoxy composites demonstrated a significant increase in strength, modulus, and toughness compared to the untreated and delignified samples which enabled effective force transfer from the base matrix to the bamboo fibers. Among the three selected bamboo species, Bambusa Tulda showed highest strength and stiffness. The experimental results are validated with the theoritical results and an error between (1-10)% is reported. Apart from these, the developed Bambusa Tulda composites possess high fatigue life which is equivalent to many engineering materials. These composites are further pollution-free and less expensive than GFRP, and CFRP. The GFRP can be semi-replaced by these bamboo laminates in many industrial/ structural applications.

Chapter 4

Investigation of bamboo-based vertical axis wind turbine blade under static loading

4.1 Introduction

Fiber-reinforced polymer composites such as glass and carbon fibers are extensively used as wind turbine blades followed by a major challenge of recycling and waste disposal etc. The primary aim of this study is to investigate the suitability of bamboo-epoxy composite blades for vertical-axis wind turbine under static loading condition. The utilization of bamboo as a structural material offers several benefits, including its renewable nature, low environmental impact, and favorable mechanical properties. The study aims to replicate its strength, and light-weight characteristics in synthetic composites used for wind turbine blades. The two different profiles from the NACA family i.e. NACA 0015 and NACA 4415 has been chosen for study. The static structural analysis of blades is performed using various cross-ply and angle-ply layups. The effect of shear webs is also analyzed. Additionally, the stress and deflection of the bamboo composite blades are compared with conventional blade materials. This innovative approach will help in contributing to the sustainablity practices by reducing the dependency on conventional materials such as glass/carbon fibers.

4.2 Governing equations

The aerodynamic characteristics of the straight Darrieus wind turbines are quite complex even though it is the simplest design of VAWT. These turbines are easy to manufacture and give a performance that is comparable with HAWT, with almost 40% extraction of wind energy [190]. The blades of the straight Darrieus wind turbine rotate due to the lift force produced by the incoming wind flow. The longer blades of straight Darrieus wind turbine are subjected to a large value of centrifugal force leading to blade failure. Even the small turbines are potentially dangerous as blades are allowed to spin freely due to the absence of a stall. This phenomenon creates explosive centrifugal forces within moments [191]. High rotational speeds generate large centrifugal forces and pulsating torque which stands in support of the blade aerodynamics, but at the same time, the probability of structural failure increases.

4.2.1 Essential design parameters of straight Darrieus wind turbine

VAWT blades need to be designed for both ultimate loads based on static strength and fatigue loads based on fatigue strength. Straight Darrieus wind turbines are fatigue-critical machines, the design of the blades is significantly dictated by fatigue considerations. For small-scale wind turbines, some design parameters i.e. choice of the airfoil, supporting strut configuration, shape, solidity, and material are more sensitive and critical than others. In this section, a complete design methodology for the selection of blade geometry, profiles, and dimensions is described when designing it for the required power output. The expression for essential parameters required for the design of VAWT is illustrated

below -

Number of blades - The torque ripple can be reduced in the case of the Darrieus rotor by taking three or more blades. For small-scale domestic use, VAWT normally contains three blades which is an optimum number of blades. It is denoted by n.

Tip speed ratio (λ) - It is defined as the ratio of turbine rotational speed of the tip of the blade to actual wind velocity. It calculates the tangential speed of the turbine blade speed concerning the free wind speed. Mathematically it is denoted as -

$$\lambda_{max} = \frac{\omega r}{V} \tag{4.1}$$

where ω is the rotational velocity of the turbine, r is the radius of the wind turbine, and V is the free wind speed velocity in m/sec.

Solidity (σ) - It is defined as the blade surface area to the rotor swept area and is mathematically expressed as follows -

$$\sigma = \frac{nc}{D} \tag{4.2}$$

where n is the number of blades, c is the chord length of the blade, and D is the diameter of the turbine.

Aspect ratio – It is defined as the height of the rotor to the diameter of the rotor.

$$AR = \frac{H}{D} \tag{4.3}$$

where H is the span height of the rotor blade.

Lift coefficient – The lift coefficient is expressed in as follows -

$$C_L = \frac{F_L}{0.5\rho c V^2} \tag{4.4}$$

where F_L is the lift force of the turbine blade, ρ is the density of the fluid.

Drag coefficient – The drag coefficient is expressed in as follows -

$$C_D = \frac{F_D}{0.5\rho c V^2} \tag{4.5}$$

where F_D is the lift force of the turbine blade.

Power coefficient – It represents the fraction of the extracted power from the total power of the airflow, which runs through the projected area of the turbine in the flow direction. It is represented by the following equation -

$$C_P = \frac{\omega T_{turbine}}{0.5\rho A V^3} \tag{4.6}$$

where A is the swept area, T is the torque produced during rotation. According to Betz's law, the wind turbine has a maximum C_P limit. No turbine in the wind can capture more than 16/27 (59.30%) of kinetic energy. The fraction 16/27 (0.593) is known as Betz's coefficient.

4.2.2 Aerodynamics of straight Darrieus wind turbine

The pressure generated on the blade surface due to wind is divided into two major components- lift and drag. The velocity components and force diagram of of VAWT blade is presented in Fig. 4.1. A higher lift force will mean a lower value of drag and vice-

versa. The performance of the airfoil mainly depends on the lift coefficient (C_L) and drag coefficient (C_D). As the wind passes over the airfoil, a relative velocity W is generated which is due to a vector variation between the absolute wind speed velocity $(V\alpha)$ and peripheral blade speed (u). The generation of the relative velocity (W) component is due to the variation of the chordal velocity vector (V_C) of the blade concerning the wind direction (V). The angle between the velocity components W and V_C is the angle of attack, AoA (α). According to the flow aerodynamics, a drag force (F_D) in the direction of the free stream and a lift force, (F_L) normal to the free stream is generated. These forces are variable and dependent on the AoA of the fluid flow. By resolving these drag and lift forces, the normal force (F_N) and the tangential force (F_T) are obtained.

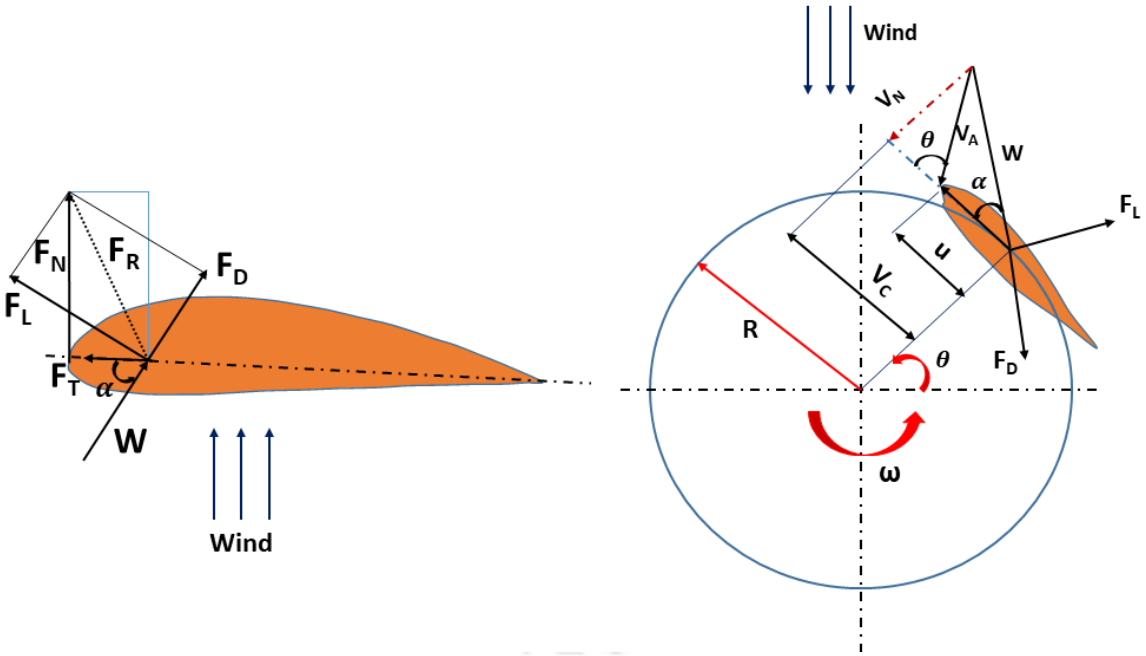

Figure 4.1: Flow velocities and force diagram of straight Darrieus airfoil.

The variation of the local angle of attack

The flow velocities of a straight Darrieus wind turbine in both the upstream and downstream surfaces of the blade are not constant. The velocity components on the airfoil due

to airflow in the axial direction are shown in Fig. 4.1. The velocity components are resolved into chordal velocity *(V_C)*, and normal velocity *(V_n)* respectively. The expressions for the chordal and normal velocity are as follows -

$$V_C = R\omega + V_A Cos\theta \tag{4.7}$$

$$V_N = V_A Sin\theta \tag{4.8}$$

V_A is the airflow through the rotor in the axial direction, ω is the rotational velocity, R is the radius of the turbine, and θ is the azimuth angle.

Variation of pitch angle (θ) and angle of attack (α)

During the complete 360° rotation of the turbine blade, the wind hits the blade profile at different angles. The relation between the angle of attack, azimuth angle, and tip speed ratio as shown in Fig. 4.1 is expressed as -

$$\alpha = tan^{-1}\frac{V_C}{V_N} \tag{4.9}$$

$$\alpha = tan^{-1}\frac{Sin\theta}{TSR + Cos\theta} \tag{4.10}$$

Variation of local relative flow velocity, W

From Fig. 4.1, the relative velocity W is expressed as -

$$W = \sqrt{(V_C)^2 + (V_N)^2} \tag{4.11}$$

Substituting the values of V_C and V_N in Eq. 4.12,

$$W = \sqrt{(V_A Sin\theta)^2 + (R\omega + V_A Cos\theta)^2} \tag{4.12}$$

Variation of normal and axial forces

The direction of lift *(L)* and drag *(D)* forces during the rotation are resolved into axial *(F_A)* and normal *(F_N)* force coefficients. The expression for F_A and F_N is given by-

$$F_A = LSin\alpha - DCos\alpha \tag{4.13}$$

$$F_N = LCos\alpha - DSin\alpha \tag{4.14}$$

The axial force coefficient *(C_A)*, and tangential force coefficient *(C_N)* are expressed as –

$$C_A = F_A \frac{1}{2} \rho c H W^2 \tag{4.15}$$

$$C_N = F_N \frac{1}{2} \rho c H W^2 \tag{4.16}$$

where c is the chord of the airfoil, H is the span length of the rotor blades, and ρ is the density of the fluid flow.

Calculation of total power output

The total power of the turbine is expressed as follows -

$$P_{out} = Q \times \omega \tag{4.17}$$

Where Q is the total torque, and ω is the turbine rotational velocity.

4.3 Modelling of blade in CAE

4.3.1 Geometric and design parameters of the wind turbine blade

The majority of research on the aerodynamic performance of Darrieus VAWT blade focussed on 4-digit symmetric airfoils [119]. Based on the power performance, two different airfoils i.e. symmteric and non-symmteric profiles from the NACA family is considered. The NACA 0015 and NACA 4415 airfoils are modelled to study the structural behavior under static wind loads. A 3D straight Darrieus wind turbine composite blade is modelled using mechanical APDL as shown in Fig. 4.2(a) by Hameed and Afaq [192].

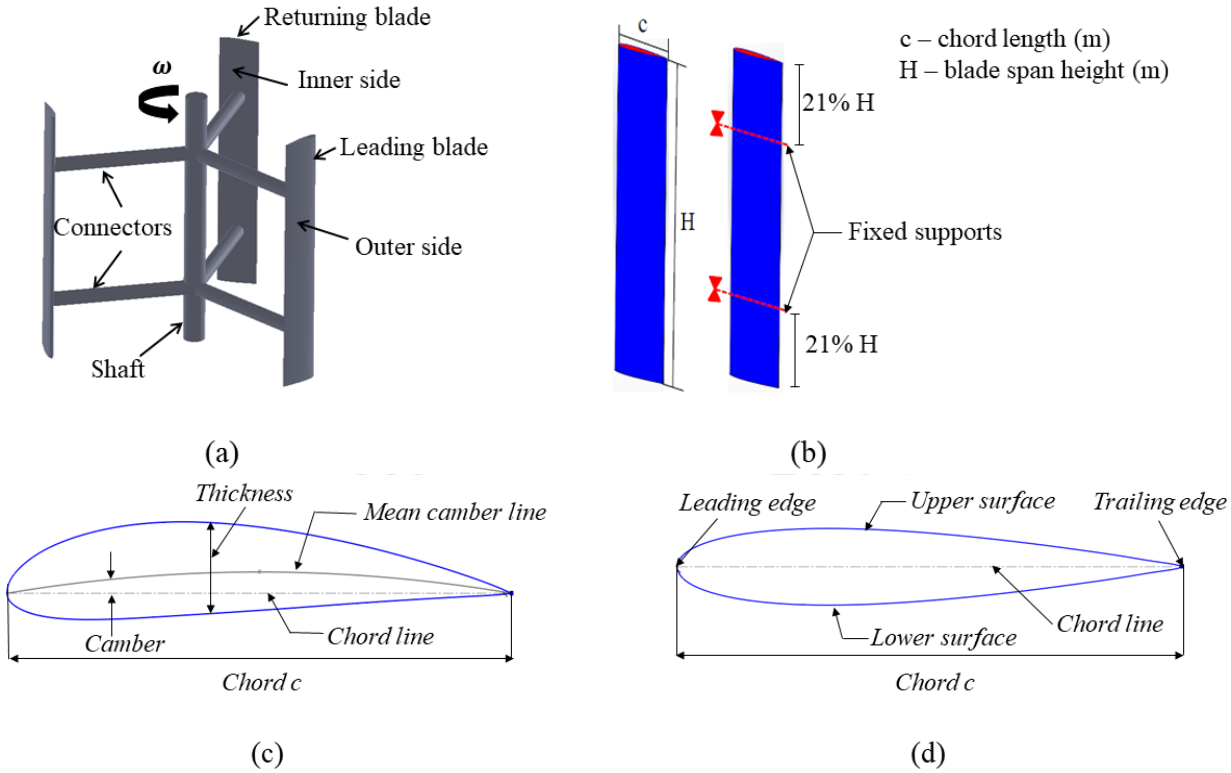

Figure 4.2: Geometry of blade profiles (a) Darrieus VAWT model as presented in [192]) (b) blade model for present simulation (c) cross-section of the symmetric blade (d) cross-section of the non-symmetric blade.

The blades are stationary and non-rotating at zero pitch angle. These blades are connected to the main rotating shaft with the help of six radial supporting arms. However, a simplified physical model with one blade at zero pitch angle is modelled for the current case. The 3D model of the blade with chord length, span height, and two boundary conditions [193] constrained at equidistance from the two ends (i.e. 21% from each end) is shown in Fig. 4.2(b). The 2D cross-section of the two airfoils is shown in Fig. 4.2(c) and Fig. 4.2(d). Table. 4.1 outlines the descriptive geometrical details of the 1 kW VAWT for the two blade profiles. A wind speed of 8 m/sec is selected for the calculation of the aerodynamic forces. For the wind speed of (3-15) m/sec, the design parameters of Darrieus turbines such as the TSR lies in between (2.5-4.5) reported by Atlaschian and Metzger [194], and solidity, σ lies in the range of (0.09-0.36) reported by Rezaeiha *et*

Table 4.1: Design variables description.

Rotor type	H-rotor
Blade shape	Straight
Blade profile	Symmetric- NACA0015, asymmetrical NACA 4415
Number of blades	3
Diameter, D (mm)	2670
Blade span height, H (mm)	2670
Chord length, c (mm)	214
Wind velocity, V (m/s)	8
Tip Speed Ratio, TSR	3
Solidity	0.24
Targeted power, P (kW)	1

al. [195]. The value of the power coefficient (C_P) against TSR =3, and $\sigma = 0.24$ is approximately 0.445. The diameter of the turbine is calculated from the correlation, $P = 0.5 C_P \rho V^3 D^2$. For 1 kW output power and air density of 1.23 Kg/m^3, the diameter of the turbine is 2.67 m. Moreover, the blade aspect ratio plays an important role in the overall performance. The performance of the turbine is reduced when the aspect ratio is reduced. Straight-bladed vertical axis blades should use long and thin blades with a high aspect ratio in the range of $10 \geq H/c \geq 20$ [196]. Thus, a high aspect ratio of 12.5 is considered. Using these design parameters, the symmetric and non-symmetric blades are designed to take the maximum aerodynamic forces.

4.3.2 Evaluation of effective composite material properties

Experimental determination of the composite mechanical properties is a challenging task, particularly when the longitudinal and transverse shear modulus is concerned. This is because the properties of composite materials are inherited from the constituent materials and are dependent on various factors such as the manufacturing process, material properties, geometric configurations, etc. resulting in uncertainties at various scales. Several analytical and numerical models have been proposed for predicting the mechanical properties of these materials [197]. The rule of mixture (ROM) is the simplest mathematical correlation used widely. However, for natural fiber-reinforced composites, ROM is less preferred due to the vast variation in the physical and mechanical properties of natural fibers. Homogenization is a common technique to design components with composite materials. This process homogenizes the elastic stiffness properties between scales which provides an estimate of the effective elastic characteristics [198]. There are several homogenization methods such as Chamis' micromechanical model, and Mori-Tanaka's

asymptotic mean-field homogenization techniques [199], but none of these methods are capable of accommodating the effect of geometrical variations of the constituent materials. Thus, a finite element-based numerical model known as representative volume element (RVE) is widely used to predict the effective elastic properties of composite materials. Though this technique is more accurate, it is computationally more expensive and takes a large amount of computational time [200]. To overcome certain computational difficulties, researchers have simplified the RVE to unit cell (UC) fiber arrangements such as hexagonal, square, and random as shown in Fig. 4.3(a).

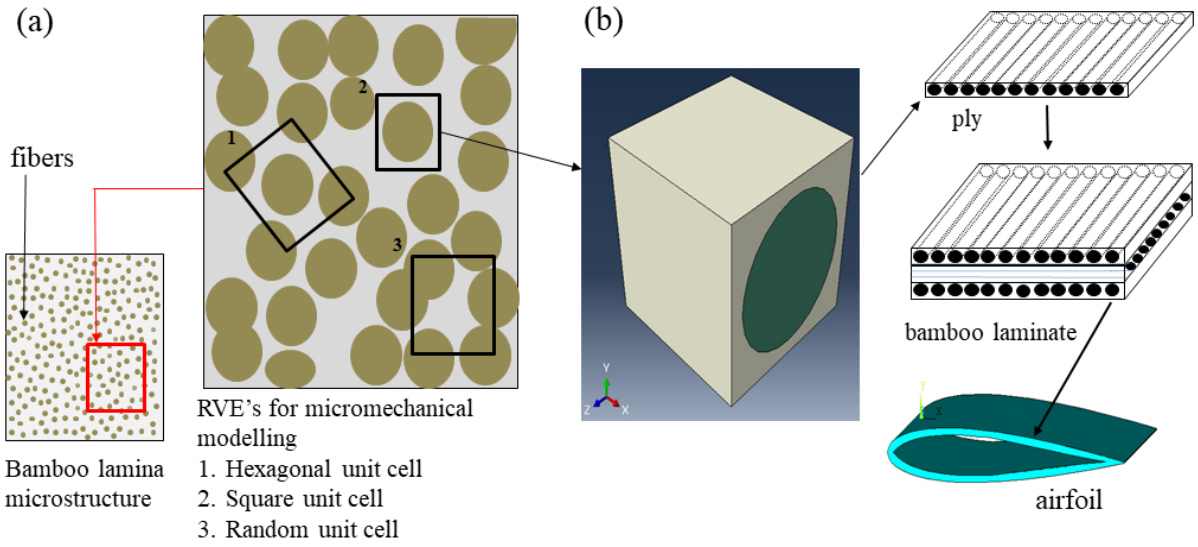

Figure 4.3: (a) Illustration of various micromechanical RVE's model for unidirectional bamboo lamina (b) present case RVE with square UC representating fiber orientation in modelling of composite structure.

In the present case, the composite elastic constants are established from an RVE micromechanical FE analysis with a square unit cell (UC) model as shown in Fig. 4.3(b). RVE homogenization is the process of numerically imposing uniform strains to evaluate the effective elastic properties of a composite model. Fig. 4.4 shows the displacement boundary conditions applied to the RVE model to evaluate the elastic properties of the composite. RVEs are visualized as a periodic array to demonstrate composite materials.

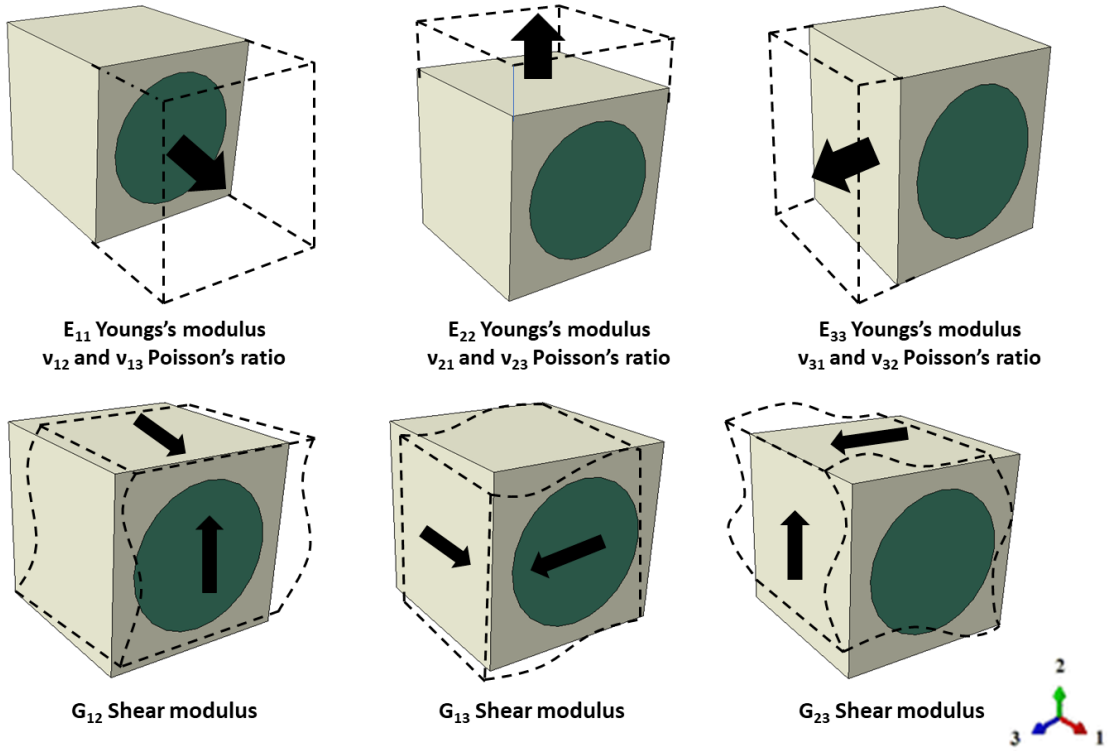

Figure 4.4: Schematic presentation of displacement boundary conditions required to evaluate the composite's elastic properties.

Due to its periodicity or repeating microstructure, periodic boundary conditions (PBC) are applied to the modelled RVE. The PBCs are imposed on all edges (i.e. node to node periodic conditions) of the RVE model. The boundary condition used in the model is expressed by the Eq. (4.18)-

$$u_i^{j+} - u_i^{j-} = \varepsilon_{ik}(v_i^{j+} - v_i^{j-}) = \varepsilon_{ik}\Delta v_k^j \tag{4.18}$$

where u_i is the displacement in the periodic function from one RVE to another RVE. j^+ and j^- denotes the parallel opposite RVE faces. $\Delta v_k{}^j$ denotes the tensor strain of the corresponding RVEs. Since the composite is modelled as a homogeneous orthotropic medium the fibers and matrix are assumed to share ideal bonds. Thus, when similar stress

and strain conditions are applied to the RVE model the overall stiffness is expressed as-

$$[\overline{\sigma}_{IJ}] = [C_{IJ}][\overline{\varepsilon}_{IJ}] \tag{4.19}$$

where $\overline{\sigma}_{IJ}$ and $\overline{\varepsilon}_{IJ}$ are the average normal stresses and strains in the x, y, and z direction and $[C_{IJ}]$ is the stiffness matrix of the material respectively. For transversely isotropic materials, the following elastic constants are related due to isotropy in the plane normal to the fiber direction i.e $E_{22} = E_{33}$, $G_{12} = G_{13}$, $\nu_{12} = \nu_{13}$. The values of average stresses and strains are represented by the following set of equations in Eq. 4.20 and Eq. 4.21.

$$[\overline{\sigma}_{IJ}] = \frac{1}{V} \int_0^v \sigma_{IJ}(x, y, z) dV \tag{4.20}$$

$$[\overline{\varepsilon}_{IJ}] = \frac{1}{V} \int_0^v \varepsilon_{IJ}(x, y, z) dV \tag{4.21}$$

A square UC is considered in this case with a volume fiber (V_f) content of 54% and the same is utilized in the form of ply for the airfoil analysis as shown in Fig. 4.3(b). The elastic properties of the composite with specific fiber volume (V_f) are determined using an ABAQUS plugin EasyPBC. Easy PBC is developed to automatically find and generate the required displacement boundary conditions, constraint equations, node sets, and post-processing calculations to evaluate the effective material properties within the graphical user interface of ABACUS CAE. The ABACUS plugin runs in two phases to evaluate the homogenized elastic properties. In the first phase, the RVE geometrical dimensions are defined and all necessary boundary conditions are applied. The post-processing phase is mainly responsible for performing the stress-strain calculations to estimate the elastic properties. A detailed explanation for identifying the material elastic

properties is provided by Omairey *et al.* [199]. In the current study, the blade is designed with bamboo composite material. The elastic properties of the constituent materials such as bamboo fiber is 12.26 *GPa*, and epoxy resin is 3.5 *GPa*. With the help of these properties and appropriate boundary conditions, the elastic properties of the bamboo-epoxy composite are evaluated using the RVE model and presented in Table 4.2.

Table 4.2: Material properties of bamboo-epoxy composite.

E_x (GPa)	$E_y = E_z$ (GPa)	$\nu_{xy} = \nu_{xz}$	ν_{yz}	G_{xy}=G_{xz} (GPa)	G_{yz} (GPa)	Density, ρ Kg/m^{-3}
22.37	10.00	0.35	0.25	4.10	3.10	1120

4.4 Loading details and boundary condition

The composite blade is modelled in ANSYS software. The optimal range of wall thickness of 4 *mm* is selected for the FE analysis as in Ref. [130]. The airfoil is set at zero angles of incidence in a fluid flow and is allowed to complete one rotation cycle. The values of the angle of attack *(α)* with the varying pitching angle *(θ)* is determined using the correlation given in section 4.2.1. During complete 360° rotation, the lift and drag coefficients for both the airfoils with each angle of attack *(α)* are evaluated using a small commercial software "DESFOIL". The lift and drag coefficients with varying angles of attack and pitching angle are presented in Table 4.3. The mathematical correlations of aerodynamic forces such as lift, drag, normal, and centrifugal are given in Ref. [192]. Using these correlations, a MATLAB code is written to obtain the value of maximum forces during the complete 360° rotation. The obtained maximum force for the symmetric profile is 3000.21 *N* and the non-symmetric profile is 4253.00 *N* presented in Table 4.4 and Table 4.5. The detail

of the FE model is presented in Fig. 4.5.

Table 4.3: Variation of aerodynamic lift and drag coefficients during one rotation cycle.

Pitch angle (θ)	Angle of attack (α)	NACA 0015		NACA 4415	
		C_L	C_D	C_L	C_D
0°	0.00	0.00	0.00	0.46	0.009
45°	10.80	0.94	0.02	1.33	0.015
90°	18.43	1.18	0.04	1.52	0.050
135°	17.14	1.12	0.03	1.50	0.030
180°	0.00	0.00	0.01	0.47	0.009
225°	-17.14	-1.12	0.03	-0.45	0.010
270°	-18.43	-1.18	0.04	-0.27	0.146
315°	-10.80	-0.94	0.02	-0.48	0.020
360°	0.00	0.00	0.00	0.46	0.009

Table 4.4: Total forces acting on the symmetric blade.

Wall thickness (mm)	Cross-sectional area, A (mm^2)	Mass of bamboo-epoxy, Kg	Magitude of total forces (normal force + centrifugal force), N
5	1.93×10^6	5.98	4321.99
4	1.56×10^6	4.84	3000.21
3	1.20×10^6	3.85	2844.47
2	0.82×10^6	2.55	1999.98
1	0.42×10^6	1.32	1420.85

Table 4.5: Total forces acting on the non-symmetric blade.

Wall thickness (mm)	Cross-sectional area, A (mm^2)	Mass of bamboo-epoxy, Kg	Magitude of total forces (normal force + centrifugal force), N
4	1.54×10^6	4.28	4253.30

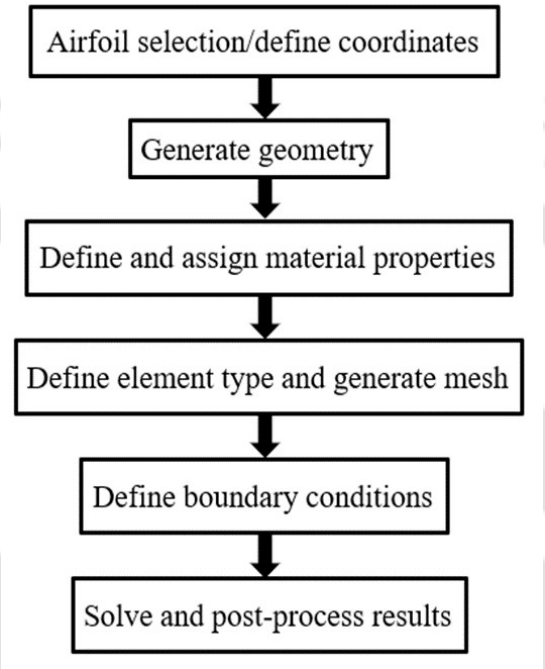

Figure 4.5: Flow chart of FEA blade analysis.

The blade is modelled as 2D orthotropic material and meshed with SHELL 181 element type. SHELL 181 element can be used for both linear and nonlinear structural applications. This element has four nodes with six degrees of freedom (DOF) at each node, which includes three translational DOFs and three rotational DOFs. This element is suitable for layered applications that involve modelling composite shells or sandwich structures where the material properties can vary across the thickness of the structure. Although the blade model appears to be a shell as shown in Fig. 4.6, it has skin thickness which is specified in its real constants. For larger blades, the computational time is re-

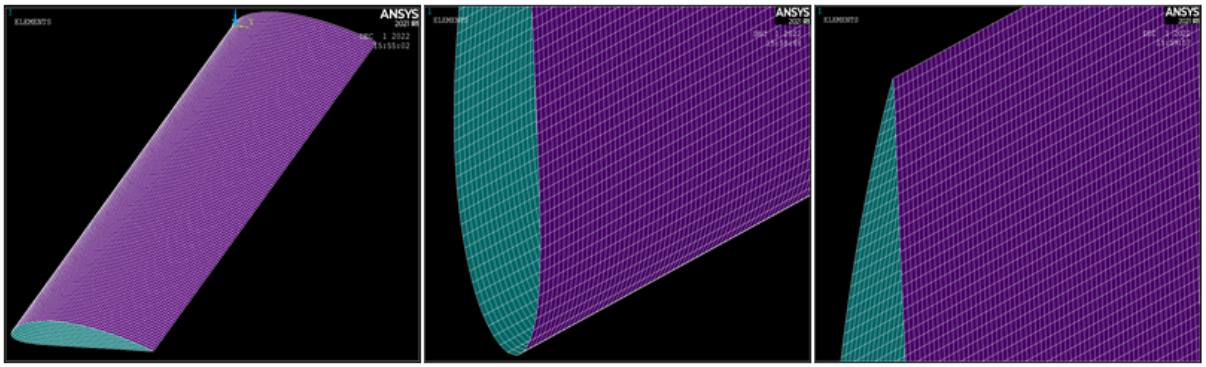

Figure 4.6: VAWT blade with meshed SHELL 181 elements.

duced to half by applying a symmetric boundary condition at the mid-plane of the blade as explained by Hand *et al.* [131]. In the present case, the complete blade is analyzed. Two fixed boundary conditions are applied at the blade-strut connectors at an equidistance of 21% from each end (i.e. 560 *mm*) to achieve a minimum bending stress as shown in Fig. 4.2(b) [193]. The total force is applied on the blade surface facing windward at a distance of one-fourth of the chord. The mesh convergence of the FE blade model is performed to ensure the accuracy and reliability of the numerical solution. The entire blade is meshed with structured mesh with 64 divisions along its length and 50 divisions along the chord. It is noticed that as the number of nodes is increased, the value of stress

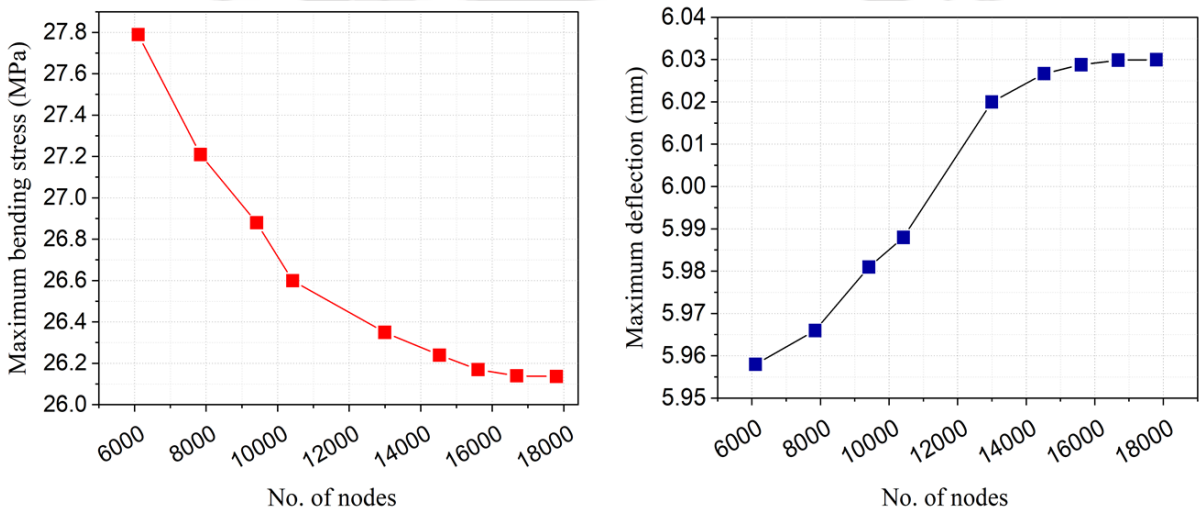

Figure 4.7: Convergence of results by improving mesh quality – FEM model.

and deflection starts reducing as shown in Fig. 4.7. It is observed that the results gets converged at the fine mesh size of 150×74 divisions. For the number of nodes equal to 17792, the difference from the previous stress and deflection value is less than 10^{-4}, which is considered as the convergence criteria.

4.5 Numerical results and discussions

4.5.1 Validation of FEA model - Glass-epoxy blade validation

A two-dimensional blade with skin thickness of 4 *mm* is considered for the FE model validation. The modelled blade is meshed with SHELL 181 elements. The material properties of the glass-epoxy blade described by Hameed *et al.* [130], are applied to the current blade for model validation. As the cross-sectional area of the blade is uniform, a total normal force of 7341.17 *N* is applied along the blade span. Since the aerodynamic shape of the blade is the same, the aerodynamic forces are also the same for model validation.

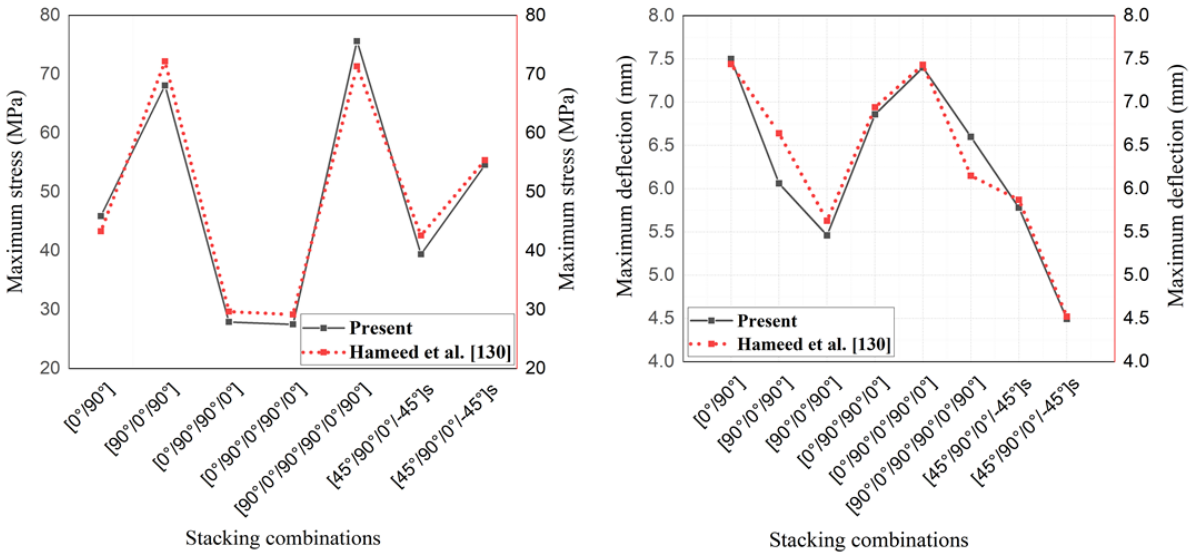

Figure 4.8: Validation of glass-epoxy blade results using SHELL 99 and SHELL 181 element type.

The evaluation of the aerodynamic forces is presented in detail by Hameed and Afaq [192]. Various stacking combinations such as cross-ply and angle-ply are evaluated. The values of stresses and deflections on the blade are presented in Table 4.6. The present results are obtained by using SHELL 181 whereas Hameed *et al.* [130] used SHELL 99 element. There is not much difference between the two SHELL elements. The percentage error for each case of stresses and deflection has been obtained and found within the acceptable range below 10%. However, the slight difference observed is due to

Table 4.6: Validation of glass-epoxy blade with element type SHELL 99 and SHELL 181.

Ply angle orientation	Thickness of each Layer(mm)	Max. Stress (MPa) Shell 99	Max. Deflection (mm) Shell 99	Max. Stress (MPa) Shell 181	Max. Deflection (mm) Shell 181	% error	
		Hameed *et al.* [130]		(Validation)		Stress	Deflection
[0°/90°]	2.00	45.90	7.50	43.33	7.44	5.59	0.80
[90°/0°/90°]	1.30	68.10	6.06	72.17	6.64	5.63	8.73
[0°/90°/90°/0°]	1.00	27.90	6.86	29.66	6.94	5.93	1.15
[0°/90°/0°/90°/0°]	0.80	27.50	7.40	29.16	7.43	5.69	0.40
[90°/0°/90°/90°/0°/90°]	0.67	75.60	6.60	71.33	6.15	5.65	6.82
$[45°/90°/0°/-45°]_S$	0.50	39.40	5.78	42.60	5.87	7.51	1.53
$[45°/90°/0°/-45°]_S$	45°-1.30 90°-1.56 0°-0.26 -45°-1.30	54.60	4.49	55.40	4.52	1.44	0.66

the difference in SHELL element type and mesh size. The values of stress and deflection are plotted in Fig. 4.8 and found in good agreement. This validation will help to freeze the process parameters during FE modelling. In the next section, the bamboo-composite blade is discussed.

4.5.2 Bamboo-epoxy blade analysis

The bamboo composite blade with a 4 *mm* wall thickness is analyzed in this section. Different stacking sequences i.e. placing different plies same or different fiber orientations are analyzed with different stacking angles such as 0°,45°,90°. Six stacking combinations are studied as shown in Fig. 4.9. Four cross-ply combinations and two angle ply combination are selected.

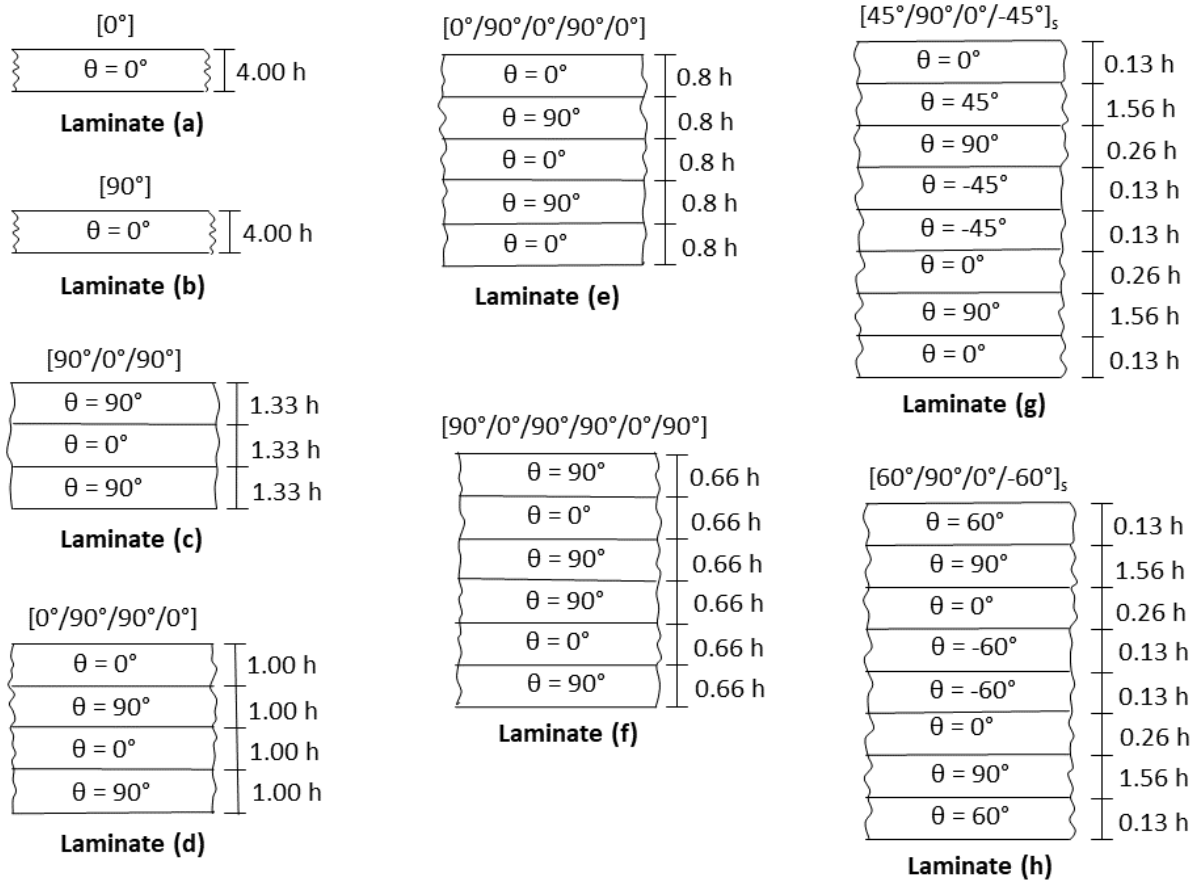

Figure 4.9: Schematic presentation of different laminates for the straight blade.

Table 4.7 presents the maximum and minimum stress and deflection of NACA 0015 and NACA 4415 blades. Maximum stress and deflection in the former one are less compared to the non-symmetrical blade. This is because the NACA 0015 profile has sym-

Table 4.7: Maximum and minimum stresses and deflections of the bamboo-epoxy blade for different ply angles.

Ply angle orientation	Thickness of each Layer(mm)	Bamboo-epoxy(Present study)			
		NACA 0015		NACA 4415	
		Bending stress, σ_x (MPa)	Deflection, (mm)	Bending stress, σ_x (MPa)	Deflection (mm)
Laminate (a)	4.00	23.29	9.86	31.08	11.47
Laminate (b)	4.00	23.65	4.34	38.36	5.78
Laminate (c)	1.30	27.61	5.12	44.96	6.93
Laminate (d)	1.00	13.98	5.46	21.02	7.38
Laminate (e)	0.80	14.66	5.78	22.10	7.85
Laminate (f)	0.67	30.31	5.21	46.51	6.69
Laminate (g)	45°-1.30	18.35	4.45	23.89	6.23
	90°-1.56				
	0°-0.26				
	-45°-1.30				
Laminate(h)	60°-1.30	20.86	4.39	30.92	6.15
	90°-1.56				
	0°-0.26				
	-60°-1.30				

metric upper and lower surfaces due to which the loads are equally distributed over the entire blade structure. Ply angle 90° resists the longitudinal stresses along the x-axis (tensile/compressive) whereas, 0° provides the maximum transverse material modulus and withstands the transverse loading along the y-direction. The composite shear modulus is maximum at 45° laminate direction, thus ply angle of 45° is introduced to support the shear stresses. It is observed that for a single unidirectional ply [0°] / [90°], deflection values are almost 50% higher compared to the other stacking combinations.

The stacking sequence has a significant impact on the performance of blades. It is reported that maximum angle-ply laminate makes the structure ductile [201]. From Table 4.7, it is observed that the deflection decreases with an increase in the number of 90° ply but the stresses fluctuate. However, the purpose of the study is to achieve optimum value of stress and deflection under safe limits. From cross-ply combination, laminate (d) has the lowest stress value for both symmetric as well as non-symmetric blades. It is observed that for laminate (c) and laminate (f), the stresses are maximum for both types of profiles i.e. NACA 0015, and NACA 4415. Here, two angle-ply laminates namely, laminate (g) and laminate (h) with different thickness for each ply is considered for the study. It is observed that the composite blade with laminate (g) has the minimum stress value however, the deflection is slightly higher than the laminate (h).

Since bamboo is a low-density material, the stresses on the blades are comparatively less than glass-epoxy as shown in Table 4.6, and Table 4.7. However, the value of deflection is found to be higher for the non-symmetrical blade as shown in Table 4.7. The distribution of von-mises stresses on the blade for both profiles is depicted in the contour plot in Fig. 4.10, and Fig. 4.11. The ultimate strength of bamboo composite under tensile load and bending load is 259 *MPa* and 212 *MPa* respectively from the experimental in-

vestigation in section 3.4.3. According to design standards, the material safety factor for composite blades is 2.20 [133]. The allowable safe stress of the bamboo-epoxy material is obtained as 96.14 *MPa*.

The maximum stress in the blade occurred at the position of the applied loads (i.e. c/4 location). The value of maximum stress and deflection is obtained by selecting all the nodes on a path along c/4 as shown in Fig. 4.12. The variation of bending stresses for all the stacking combinations along the loading path is presented in Fig. 4.13(a) for the symmetric blade, and Fig. 4.14(a) for the non-symmetric blade respectively. It is observed that maximum stress occurred at the blade-strut connectors for both blades. The value of maximum bending stresses is found in the range of (12–16) *MPa*. These values are significantly lower than the unidirectional strength of bamboo-epoxy compos-

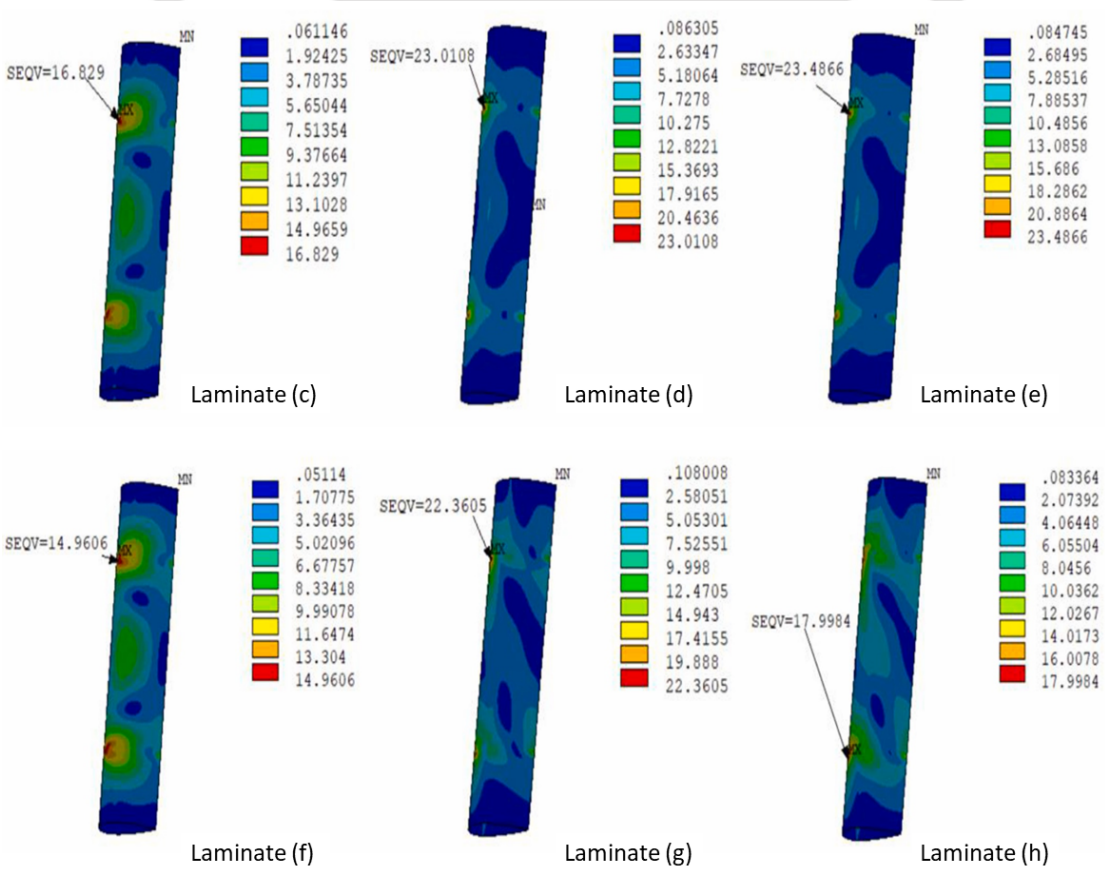

Figure 4.10: Stress contour for the symmetric blade with different stacking combinations.

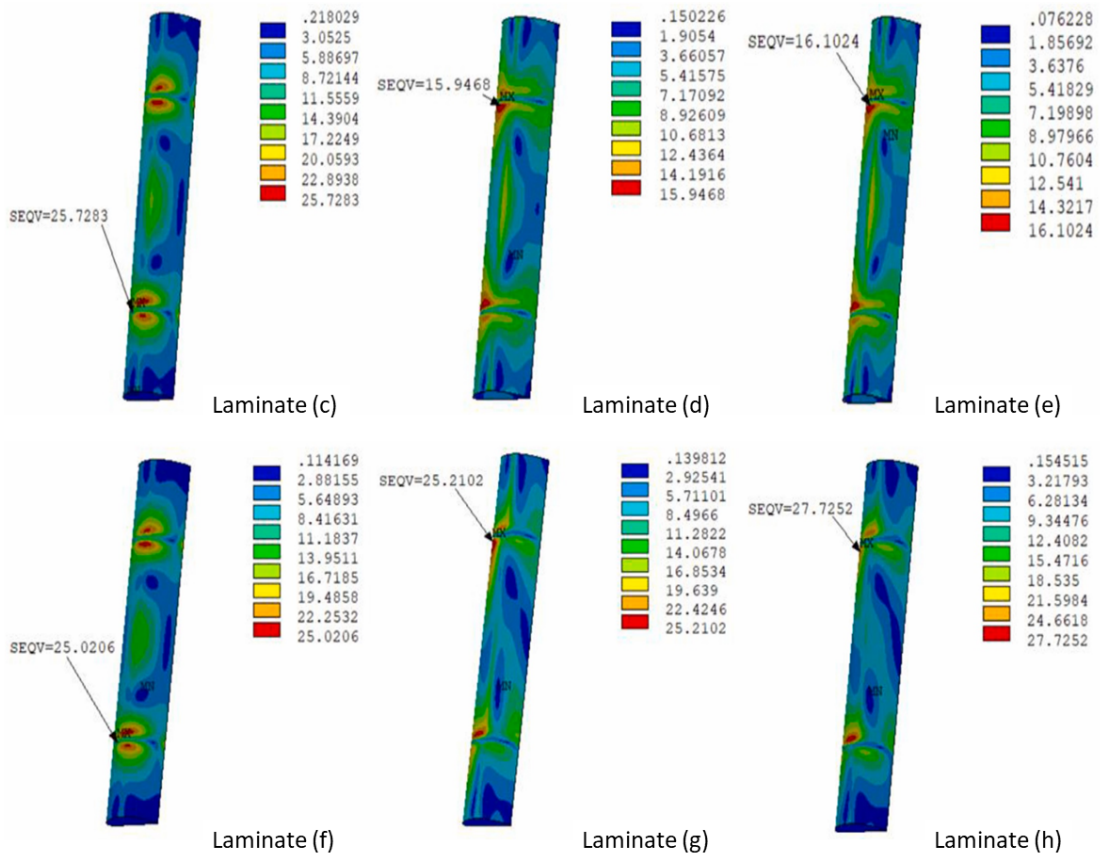

Figure 4.11: Stress contour for the non-symmetric blade with different stacking combinations.

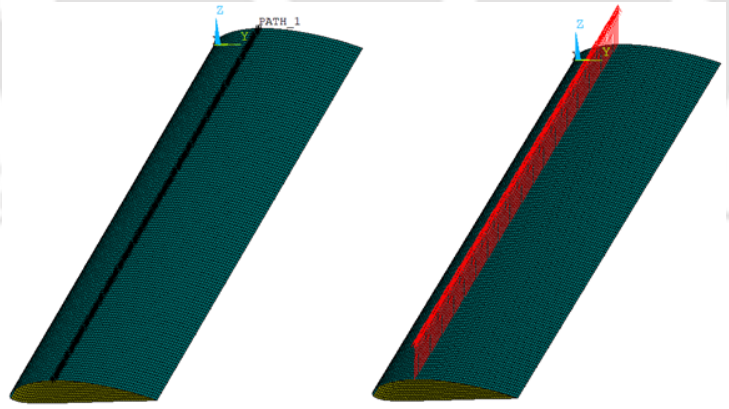

Figure 4.12: Application of load along path quarter chord location of VAWT blade.

ite i.e. 96.14 *MPa* which indicates safe blade design. Deflection over the path is also plotted for all the configurations as shown in Fig. 4.13(b), and Fig. 4.14(b). It is observed that the cross-ply layup [0°/90°/0°/90°/0°] has the highest deflection and the angle-ply $[60°/90°/0°/\text{-}60°]_S$ has the lowest deflection for both NACA 0015 and NACA 4415 airfoils.

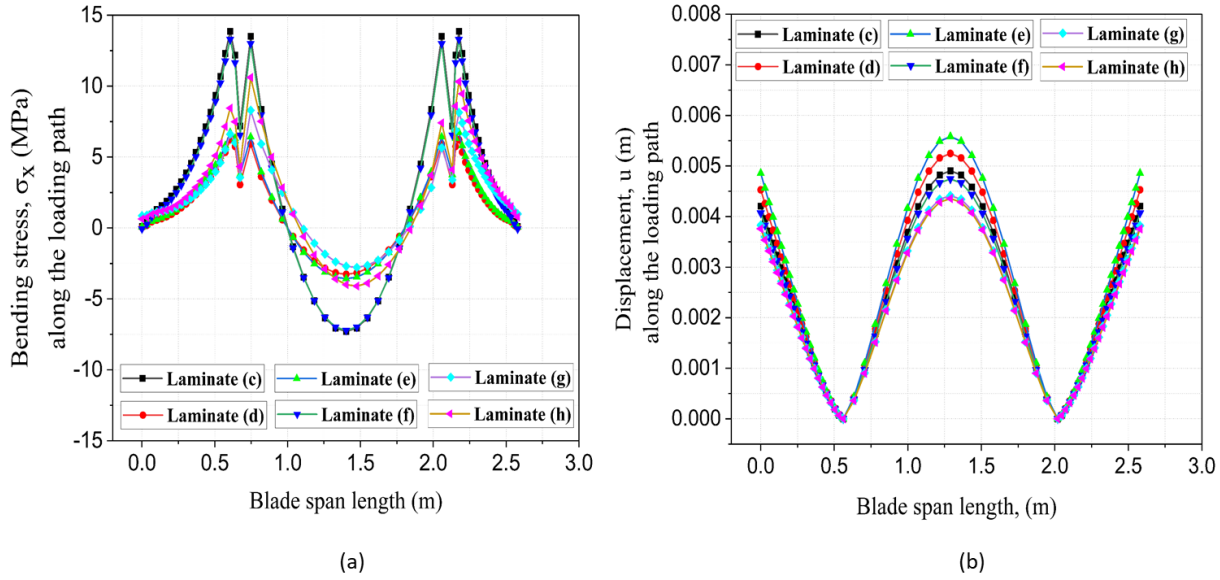

Figure 4.13: Variation of bending stresses and deflection along the loading path for the symmetric profile.

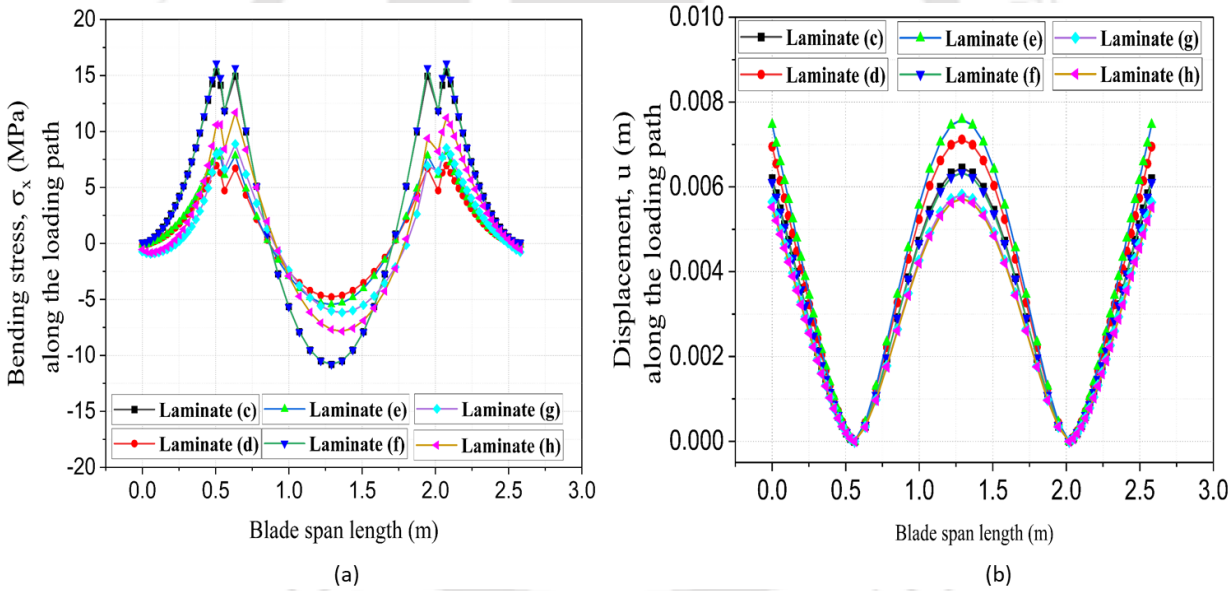

Figure 4.14: Variation of bending stresses and deflection along the loading path for the non-symmetric profile.

The obtained deflection of NACA 0015 airfoil for angle-ply layup $[45°/90°/0°/\text{-}45°]_S$ is 4.45 *mm* which is less by 1.11% for the glass-epoxy blade [130] and 8.44% for the aluminum blade [192]. However, for non-symmetrical blade, the value of deflection is higher i.e. 6.23 *mm*. In the next section, the non-symmetric blade with shear webs is analyzed for further investigation.

4.5.3 Bamboo blade analysis using shear web

A shear web is a structural component that resists the torsional loads without significantly increasing the overall mass of the structure. Typically, it is utilized to stiffen the structure and prevent significant deflection. In the present case, the effect of shear webs (single, double, triple) on the stress and deflection of the non-symmetric NACA 4415 is studied. The two shear webs at placed at the critical location of 15%, and 50% of the blade chord length as reported by Belfkira *et al.* [202]. Double webs can increase resistance to torsion, shear, and buckling deformation of the blade. The third shear web is placed at a distance of 25% from the blade chord. The two major angle-ply configurations $[45°/90°/0°/\text{-}45°]_S$, and $[60°/90°/0°/\text{-}60°]_S$ termed as laminate (g) and laminate (h) are selected for the shear web design analysis.

Table 4.8: Comparison of stress and deflection of non-symmetric blade for different shear webs.

Ply angle orientation	No. of shear webs	NACA 4415 airfoil	
		Stress (MPa)	Deflection (mm)
Laminate (g)	Shear web 1	19.02	5.10
Laminate (h)		24.56	5.01
Laminate (g)	Shear web 2	15.84	4.45
Laminate (h)		20.47	4.35
Laminate (g)	Shear web 3	15.91	4.42
Laminate (h)		19.53	4.31

The FE model of the blade structure with shear webs is shown in Fig. 4.15(a), Fig. 4.15(b), and Fig. 4.15(c). From Table 4.8, it is observed that by using a single shear web at a distance of a quarter chord length of the blade, the deflection signifi-

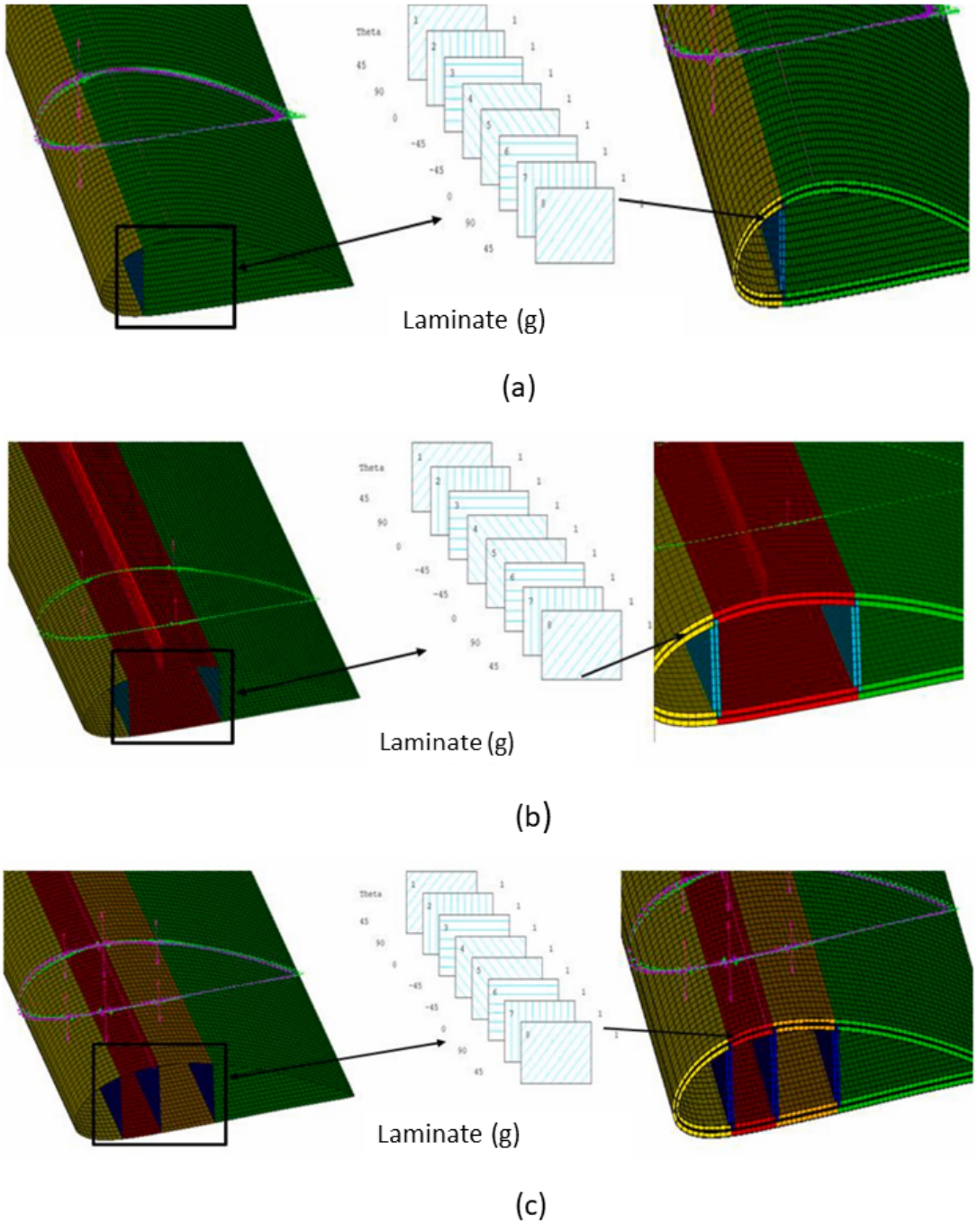

Figure 4.15: Blade structure with (a) single shear web (b) double shear webs, and (c) three shear webs.

cantly dropped down from 6.23 *mm* to 5.10 *mm*. For double-shear webs, the deflection value further dropped from 5.10 *mm* to 4.45 *mm*. However, there is not much difference observed in the values for using three shear webs. The variation of blade displacement and bending stress along the loading path for the three cases of the two-angle layups

are plotted in Fig. 4.16. The variation of stress is similar for all the cases as shown in Fig. 4.16(a), and Fig. 4.16(c). From Fig. 4.16(b), and Fig. 4.16(d) it is observed that the value of deflection of the blade with shear web two and three are close to each other, which proves that adding an extra shear web does not improve the deflection. The deflection of the blade is smaller near the blade strut connectors and maximum at the ends. The maximum bending stress and deflection of the bamboo-epoxy NACA 4415 profile with the double-shear web are 15.84 MPa and 4.45 mm for layup $[45°/90°/0°/\text{-}45°]_S$, and 20.47 MPa and 4.35 mm for layup $[60°/90°/0°/\text{-}60°]_S$.

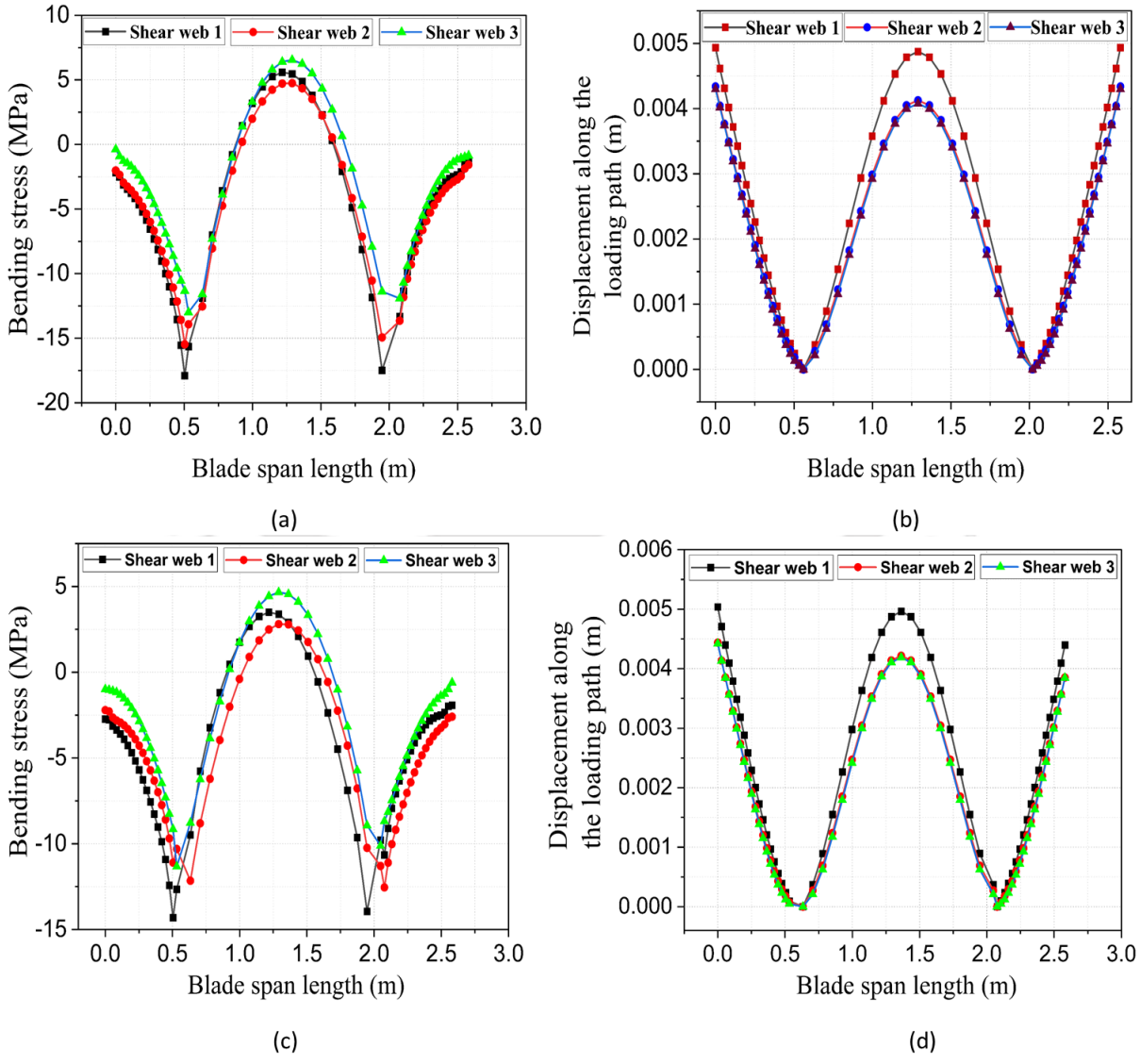

Figure 4.16: Variation of maximum bending stresses and displacement of the NACA 4415 profile with (a), (b) $[60°/90°/0°/\text{-}60°]_S$, and (c), (d) $[45°/90°/0°/\text{-}45°]_S$.

Moreover, it is observed that by adding a third shear web there is not much difference in deflection and stress whereas it will put an additional weight on the entire structure. The stress contour plots of the blade structure with a double shear web are depicted in Fig. 4.17. The same loading path as that of the non-symmetric blade without a shear web is considered for this case. The value of stress for the two-angle layups is observed to be maximum at the point of strut connectors. The stacking layup $[45°/90°/0°/\text{-}45°]_S$ has lower stress than layup $[60°/90°/0°/\text{-}60°]_S$. Further, Cox and Echtermeyer [203] have observed that the composite laminate with $\pm 45°$ plies has more resistance to shear buckling and torsional stiffness. Thus, based on the numerical results angle-ply layup $[45°/90°/0°/\text{-}45°]_S$ i.e. laminate (g) can be recommended for wind turbine blade design.

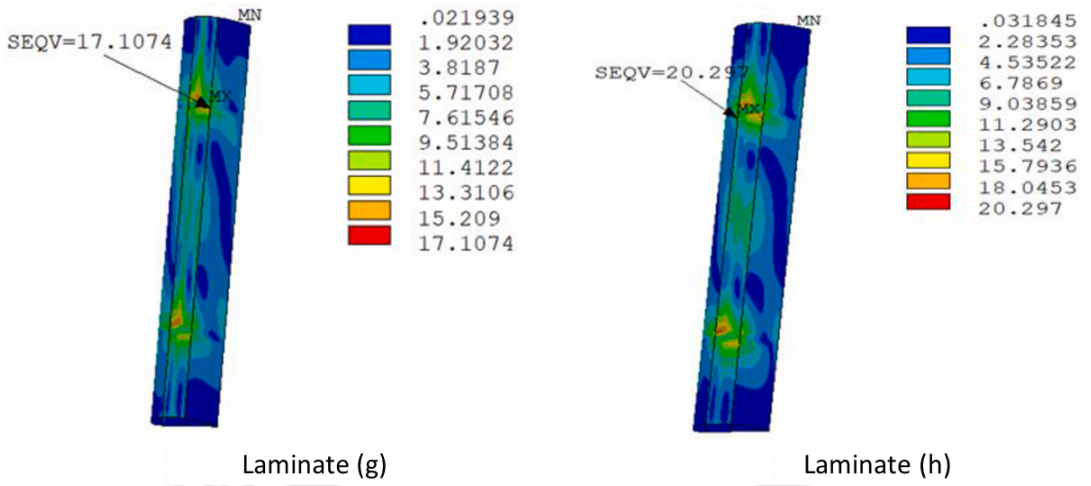

Figure 4.17: Stress contour of the blade with double shear web for laminate (g) and laminate (h).

The stress and deflection of the bamboo-epoxy composite blade with and without shear webs are presented in Table 4.9. The present results are compared with the existing results of glass-epoxy blade and aluminum blade from the published literature. The percentage (%) difference in the value of stress and deflection w.r.t to the bamboo-epoxy blade is also calculated and presented in Table 4.9. The stress and deflection value of the bamboo-epoxy composite blade without shear web is 23.89 MPa and 6.23 mm which

Table 4.9: Comparison of stress and deflection of non-symmetric bamboo-epoxy blade with glass-epoxy and aluminum blade.

Material	Stress *MPa*	Deflection *mm*	%Difference	
			Stress *MPa*	Deflection *mm*
Bamboo-epoxy blade without shear web	23.89	6.23	-	-
Bamboo-epoxy blade with double shear web	15.84	4.45	-	-
Glass-epoxy blade [130]	54.60	4.49	# 56.24% ↓	# 38.44% ↑
			@ 70.98% ↓	@ 1.11% ↓
Aluminum blade [192]	74.90	4.86	# 68.10% ↓	# 28.19% ↑
			@ 78.85% ↓	@ 8.43% ↓

Note: # % difference w.r.t without shear web bamboo-epoxy composite, @ % difference w.r.t with shear web bamboo-epoxy composite.

is observed to be decreased by 56.24% (stress) and increased by 38.44% (deflection) respectively in comparison with the glass-epoxy blade. Similarly, the aluminum blade has 68.10% higher stress than the bamboo-epoxy blade without shear webs and reduced deflection by 28.19%. It can be seen from the table that the percentage difference further decreases when the conventional blade materials are compared with the bamboo-epoxy blade with double shear web. From the above results, it is observed that adding shear webs in the case of bamboo composite blade will reduce the blade displacement. Based on the numerical results it can be recommended that bamboo-epoxy composites can be used for small-scale wind turbine blades for power generation.

4.6 Summary

The static structural analysis of bamboo-based composite straight blades is successfully performed using various cross-ply and angle-ply layups. Compared to the symmetric

profile, the non-symmetric profile experienced maximum stress and deflection under the same loading conditions. Structural components in the form of shear webs are also introduced to the blade cross-section to reduce the deflection of the non-symmetrical profile. The effect of the number of shear webs on the value of deflection is studied and found that the blade with two shear webs showed the minimum values of stress and deflection. The values of deflection and stresses did not showed much significant difference on addition of a third shear web. Through the structural analysis, it is recommended that the designed blade with natural bamboo composite is acceptable for structural safety. The maximum stress and deflection for the bamboo-epoxy blade are also compared with glass-epoxy and aluminum blade for the same wall thickness. Based on the present analysis, it is recommended that the natural bamboo-epoxy composite can be used for wind turbine blades. Moreover, the production of blades using natural composites will reduce waste composite disposal.

Chapter 5

Free and forced vibration analysis of bamboo-based composite vertical axis wind turbine blade

5.1 Introduction

Wind turbine blades experience both free and forced vibrations during their operations. Free vibration occurs when the blades are subjected to an external force such as wind, turbulence whereas during rotation the blades experience cyclic loading which causes forced vibration. These vibrations lead to excessive deflection of the blades to ultimate failure. To reduce these deflections, light weight and high strength composites are utilized in the blade structure. The scope of natural fiber composites are increasing because of their sustainability and better mechanical properties. In this chapter, the free and forced vibration of bamboo-epoxy composite blade is studied. The blade's vibrational behavior, natural frequencies, mode shapes, and dynamic characteristics are investigated through finite element modal analysis. The effect of boundary conditions is also studied. The forced vibration analysis of the blade along with the effect of damping is also considered. Further, the natural frequencies of these composite blades are compared with the frequencies of carbon and graphite epoxy blades.

5.2 Governing equations

Numerical modal analysis is a powerful technique to ensure the safety and reliability of structures subjected to dynamic loading. The FEM represents the VAWT blade as a series of interconnected nodes and elements where each element has a mass, stiffness, and damping associated with it. By calculating the eigen values and eigen vectors of the FEM, the software determines the natural frequencies, mode shapes, and damping ratios of the blade. The general equation of motion of a system is defined as

$$[M]\{\Delta^2(u,t)\} + [C]\{\Delta(u,t)\} + [K]\{u\} = F\{u\} \tag{5.1}$$

Where M is the mass matrix of the system, C is the damping matrix, K is the stiffness matrix, u is the displacement vector representing the modal coordinates, and $F\{u\}$ is the external load vector. In this case, the impact of structural damping on the modal frequencies is neglected. The modal matrix equation of the structure with non-damping and free-vibration as represented as in [141] -

$$[M]\{\Delta^2(u,t)\} + [K]\{u\} = 0 \tag{5.2}$$

Assuming that the system delivers a simple harmonic response, the displacement vector can be written as –

$$\{u(t)\} = U * e^{i\omega t} \tag{5.3}$$

Substituting these values in Eq. 5.2, the natural frequencies and modes of the system can be derived from Eq. 5.3 as follows –

$$\left[K - \omega^2 M\right] * U = 0 \tag{5.4}$$

Here U is the complex amplitude vector that defines the spatial distribution (mode shapes) of the displacement vector u, and ω is the natural frequency of the simple harmonic motion.

5.3 Modelling of blade

In the present study, a three-dimensional H-Darrieus wind turbine composite blade is modelled. The geometric details and material properties of the modelled blades are explained in Chapter 3 in section 4.3. Symmetrical NACA 0015 and non-symmterical NACA 4415 airfoils are selected. The axis of the blade in the x-direction is the chord length, y-axis denotes the wall thickness of the blade, and z-axis is the span length of the blade as shown in Fig. 5.1. Two types of boundary conditions, most commonly occurring in the design of VAWTs are considered for the finite element analysis as shown in Fig. 5.2. In the first case, the boundary conditions at a distance of 21% and 79% of the span length i.e. both equal distance from the free ends and the second boundary condition is applied at the mid span length of the blade. By applying these boundary conditions, the modal analysis can accurately determine the vibration modes and frequencies of the blade. Once the necessary inputs are defined, the modal and harmonic analyses are performed. The results can be visualized and analyzed using post-processing software such as contour plots, animations, graphs, etc.

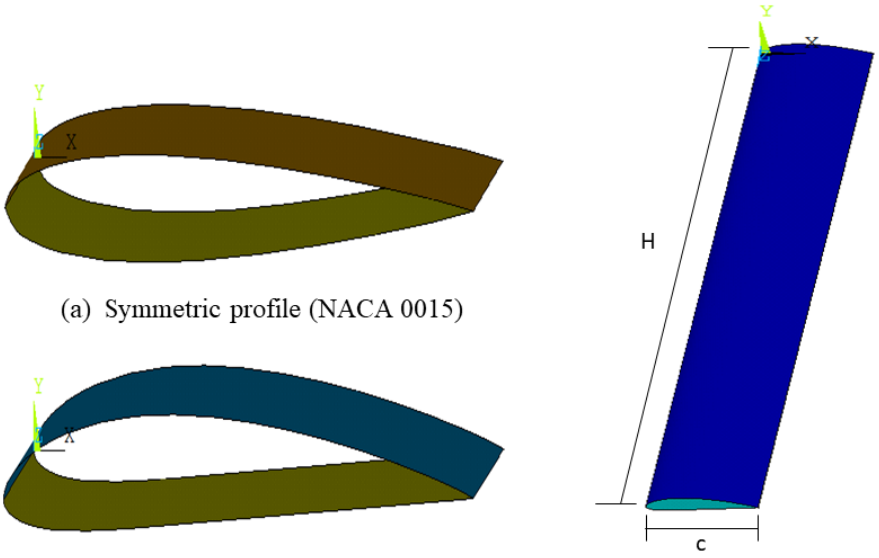

(a) Symmetric profile (NACA 0015)

(b) Non-symmetric profile (NACA 4415)

(c) 3D isometric view of the modelled VAWT blade

Figure 5.1: Schematic of VAWT blade profiles.

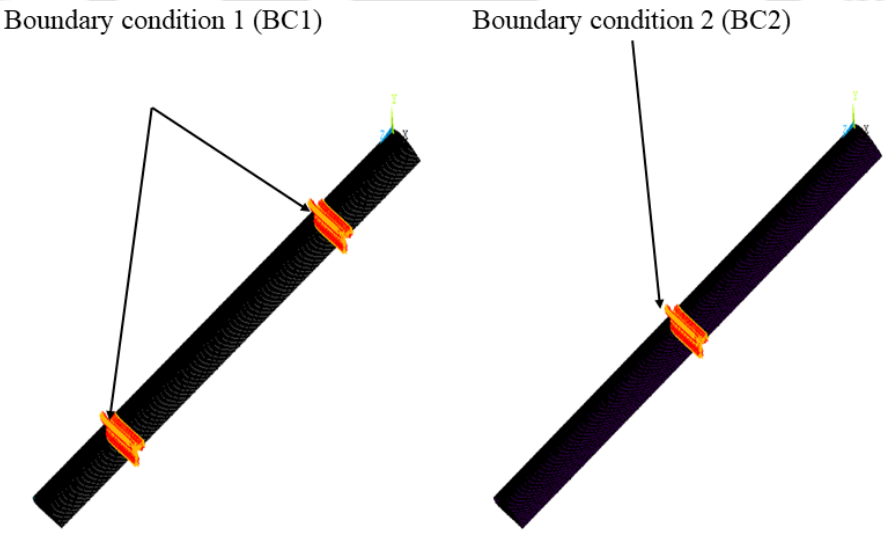

Figure 5.2: Applied boundary conditions for the VAWT blade.

5.4 Validation of the model

Based on the blade design parameters explained in section. 5.3, a laminated blade shell model is established using 4 node SHELL 181 elements in Ansys APDL interface. The blade profile including skin thickness is modelled as a 2D orthotropic material. The 2D blade is made up of an "n" number of orthotropic layers stacked in various cross-

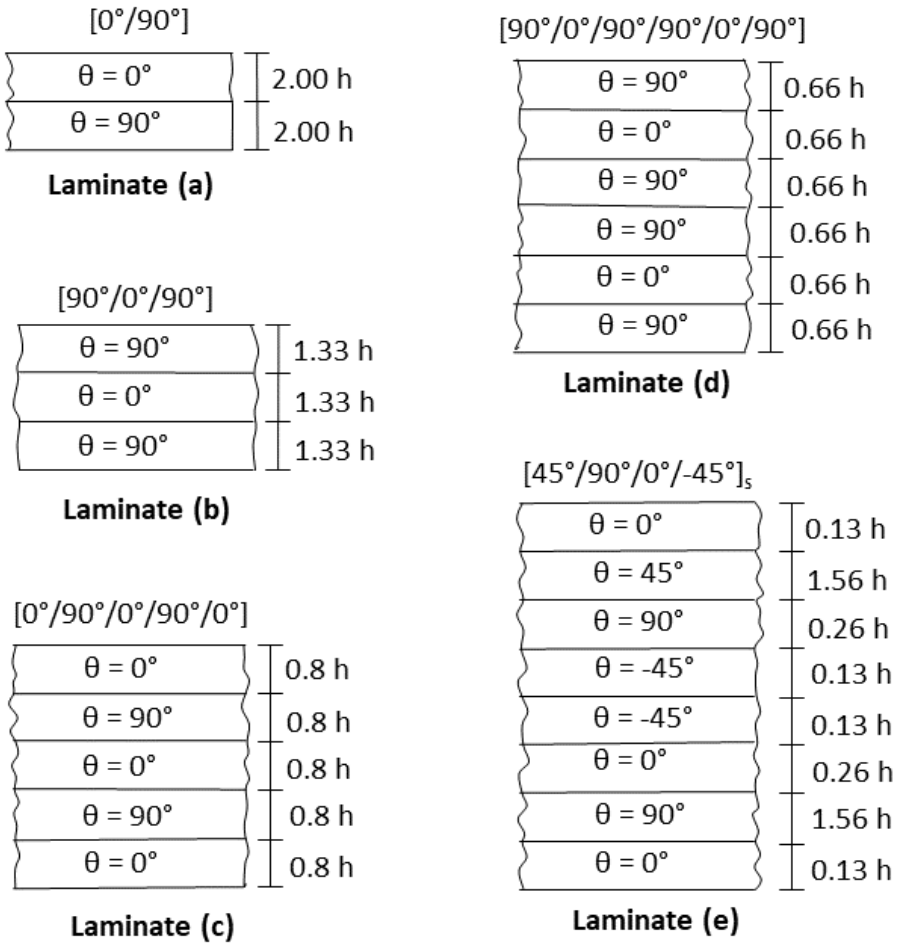

Figure 5.3: Laminates with different stacking sequences for the straight blade.

ply and angle-ply laminated stacking sequences ($\theta1/\theta2/\theta3/...$). Four different cases of fiber laminate sequences such as cross-ply [0°/90°], [90°/0°/90°], [0°/90°/0°/90°/0°], [90°/0°/90°/90°/0°/90°] and angle-ply $[45°/90°/0°/\text{-}45°]_S$ are selected for the present study. These layups are selected based on the static structural results as explained in section 4.5.2. The diagrammatic presentation of the laminate sequences for the straight VAWT blade is shown in Fig. 5.3.

To verify the convergence of the finite element analysis, the model is meshed with linear quadrilateral layered shell elements SHELL 181 for each stacking combination. Initially, the blade is meshed into 120 divisions along the span length (H), and 64 divisions along the chord (c). As the recursive deviation increases with the mesh refinement,

the convergence of the proposed FE model is verified. The convergence of the natural frequencies and the corresponding element numbers are listed in Table 5.1.

Table 5.1: Convergence of the non-dimensional frequencies of the different layups composite blade.

Laminate layups		Mesh divisions (H×c)			
		120×64	125×64	130×64	135×64
[0°/90°]	Natural frequencies (Mode 1)	34.36	34.43	34.44	34.44
[90°/0°/90°]		36.28	36.35	36.36	36.36
[0°/90°/0°/90°/0°]		32.98	33.17	33.18	33.18
$[45°/90°/0°/\text{-}45°]_S$		37.51	37.52	37.53	37.53

Model validation is an essential step to ensure the usefulness and reliability of a model for a specific application. This section presents an FE model validation of the VAWT blade by comparing the present simulations with the prior numerical study reported by Singh *et al.* [204]. The straight blade is analyzed with two different wall thicknesses i.e. 4 *mm*, and 6 *mm*. The same boundary condition is applied to the present FE model and the obtained frequencies are compared with the existing frequency values for the same performance characteristics. The blade is meshed with SHELL 181 element and the model validation is achieved. The numerical predictions on the natural frequencies of the blades with different thicknesses throughout the length are presented in Table 5.2. These values are compared with the results reported in [204]. It is observed that the natural frequencies calculated from the present FEA model show good agreement with a percentage difference below 5%.

Table 5.2: Validation of modal frequencies with different thicknesses.

Different modes		Thickness					
		Singh *et al.* [204]		Present study		% difference	
		4 *mm*	6 *mm*	4 *mm*	6 *mm*	4 *mm*	6 *mm*
1^{st}		12.48	12.55	12.57	12.60	0.72	0.40
2^{st}	Natural	66.15	68.96	66.32	70.20	0.26	1.79
3^{st}	frequencies	82.18	82.34	81.97	82.46	0.25	0.15
4^{st}		100.43	108.42	102.66	108.66	2.22	0.22
4^{st}		126.42	152.00	126.92	152.12	0.40	0.08

5.5 Results and discussion

This section discusses the dynamic responses performed on three blade profiles i.e. symmetrical, non-symmetrical, and non-symmetrical blade with double shear web. Since VAWTs have low rpm, the rotational effects of their rotating parts are neglected in this present work. The modelled blades are at zero degrees of rotation. The influence of various blade parameters such as stacking sequence, and various boundary conditions on the natural frequencies is studied. Further, the linear harmonic response of the asymmetric blade having bamboo-epoxy composite as the blade material is also carried out. The solutions are obtained using a mesh size of (130×64).

5.5.1 Free vibration results

Influence of stacking sequence and boundary conditions

In this section, the free vibration results of the three profiles are presented. The values of the modal frequencies for the selected layups for the three airfoils are presented in Table 5.3. An increase in the frequencies is observed for all the sequences by increasing the number of plies. Among the cross-ply laminates, laminate (d) has the highest values of natural frequency. The non-symmetric blade with double shear web has the better values of natural frequencies for all four modes respectively i.e. 37 H_Z (Mode 1), 53.15 H_Z (Mode 2), 72.61 H_Z (Mode 3), and 149.04 H_Z (Mode 4). A higher frequency value represents a stiffer blade which reduces the risk of dynamic instabilities and fatigue failure. From Table 5.3, it is observed that the frequency values of the non-symmetric blade without shear webs are comparatively less than the blade with shear webs. The static structural results of the bamboo-epoxy blade also reported that the non-symmetric blade profile with the double shear web delivered better structural performance with minimum values of stress and deflection. The frequency values of the angle-ply laminate are higher than those of the cross-ply laminate. It is reported that the composite laminate shear stiffness and modulus are maximum at a 45° fiber angle, which results in fiber delamination from the perspective of structural safety. Thus, it is essential to introduce 45° plies to reduce such stresses. The two types of laminates, (c), and (e) are chosen for further study.

The non-symmetric blade with shear web is analyzed to study the effect of two boundary conditions. The results of the effect of boundary conditions on the blade natural frequencies are presented in Table 5.4. It is observed that the blade with boundary condition 2 have lower frequencies than the blades with boundary condition 1. However, the

Table 5.3: Influence of stacking sequence on the natural frequencies of the bamboo-epoxy blade.

	NACA 0015		NACA 4415		NACA 4415 (shear web)	
	Mode	Frequency (H_Z)	Mode	Frequency (H_Z)	Mode	Frequency (H_Z)
Laminate (a)	1	39.08	1	33.58	1	35.75
	2	51.84	2	47.64	2	50.21
	3	62.59	3	63.36	3	68.83
	4	120.88	4	120.68	4	140.59
Laminate (b)	1	40.64	1	35.27	1	37.89
	2	53.98	2	49.90	2	53.18
	3	65.10	3	65.75	3	72.58
	4	123.17	4	122.08	4	148.74
Laminate (c)	1	37.97	1	32.45	1	34.47
	2	50.38	2	46.19	2	48.44
	3	60.95	3	61.79	3	66.47
	4	119.24	4	119.29	4	137.65
Laminate (d)	1	40.81	1	36.43	1	37.86
	2	54.20	2	51.53	2	53.15
	3	65.31	3	67.79	3	72.61
	4	124.71	4	126.82	4	149.04
Lamiante (e)	1	41.91	1	36.32	1	38.92
	2	55.65	2	51.43	2	54.73
	3	67.15	3	67.83	3	74.89
	4	127.44	4	126.37	4	153.42

VAWT blades should be constrained with two supporting struts to reduce the maximum bending deformation. The free vibration frequencies for the four different stacking layups have also been reported. The mode shapes of the first five natural frequencies for the two laminates (c), and (e) are presented in Fig. 5.4 and Fig. 5.5.

Table 5.4: Effect of boundary condition on blade's natural frequency.

	Non-symmetric blade (NACA 4415)			
	BC1		BC2	
	Mode	Frequency (H_Z)	Mode	Frequency (H_Z)
Laminate (a)	1	33.58	1	5.88
	2	47.64	2	14.47
	3	63.36	3	60.70
	4	120.68	4	69.91
Laminate (b)	1	35.27	1	6.09
	2	49.90	2	15.39
	3	65.75	3	65.07
	4	122.08	4	74.66
Laminate (c)	1	32.45	1	6.26
	2	46.19	2	13.36
	3	61.79	3	59.30
	4	119.29	4	65.86
Lamiante (e)	1	36.32	1	7.02
	2	51.43	2	15.19
	3	67.83	3	66.97
	4	126.37	4	74.11

Fig. 5.4 depicts the mode shapes of the non-symmetric shear web bamboo-epoxy blade under boundary condition 1 and Fig. 5.5 depicts the corresponding mode shapes under boundary condition 2. In both the figures, the fifth mode depicts the torsional bending of the blade whereas the first three modes show the pure bending behavior of the blade. The blade is also designed with the existing carbon-epoxy and glass-epoxy materials to study the free vibrational frequencies. The comparative chart of the free vibration

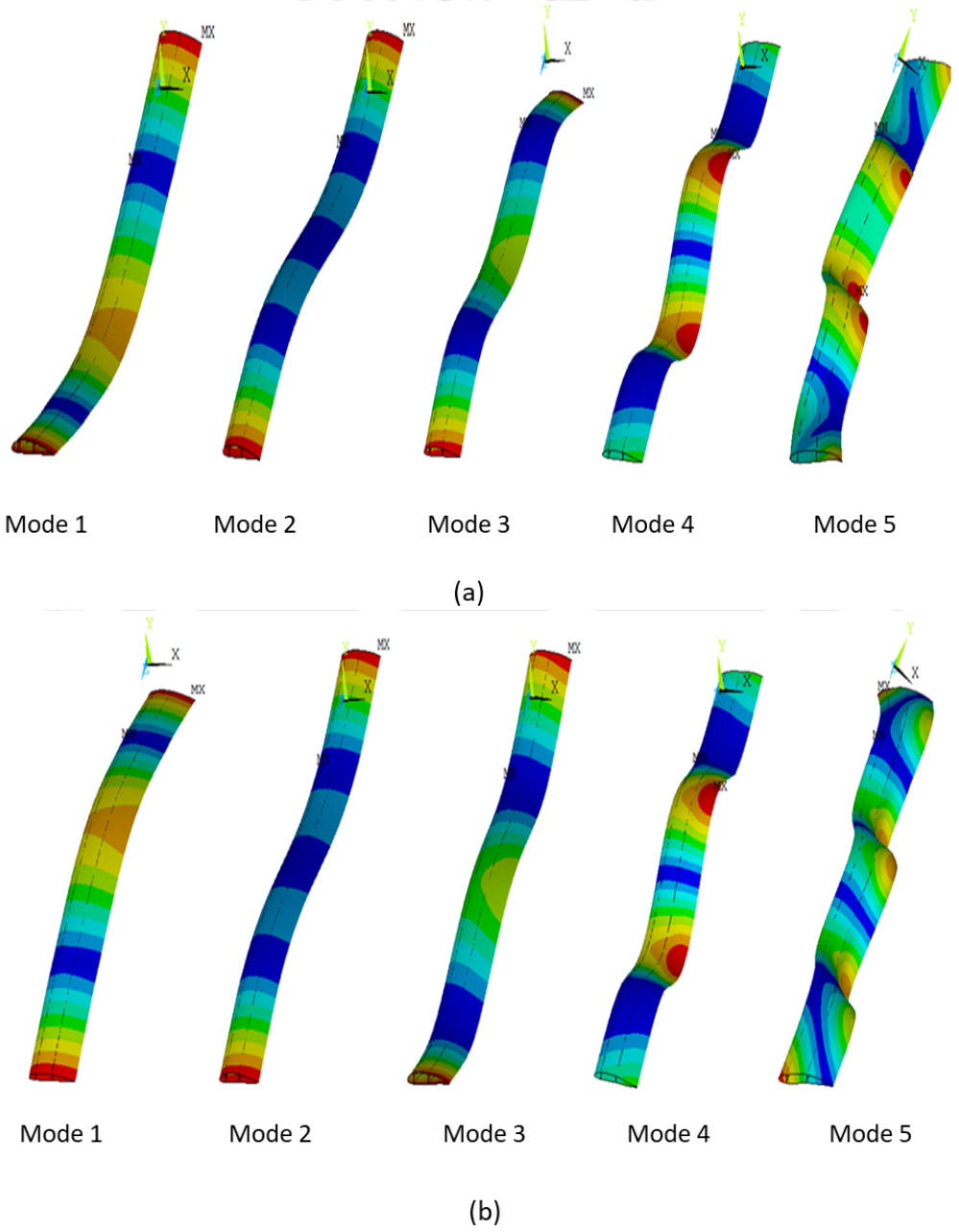

Figure 5.4: Different mode shapes (a) laminate (c), (b) laminate (e) for boundary condition 1.

results of the bamboo-epoxy blade with the wind turbine blade composed of carbon-epoxy and glass-epoxy composites is shown in Fig. 5.6. It is observed that the carbon-epoxy blade posses a higher natural frequency than the glass-epoxy and bamboo-epoxy blades. Carbon fiber composites have exceptional stiffness and lightweight properties allowing the turbine blade to withstand excessive deformation and vibration. Due to such characteristics, these composites are highly suitable for turbine application. The

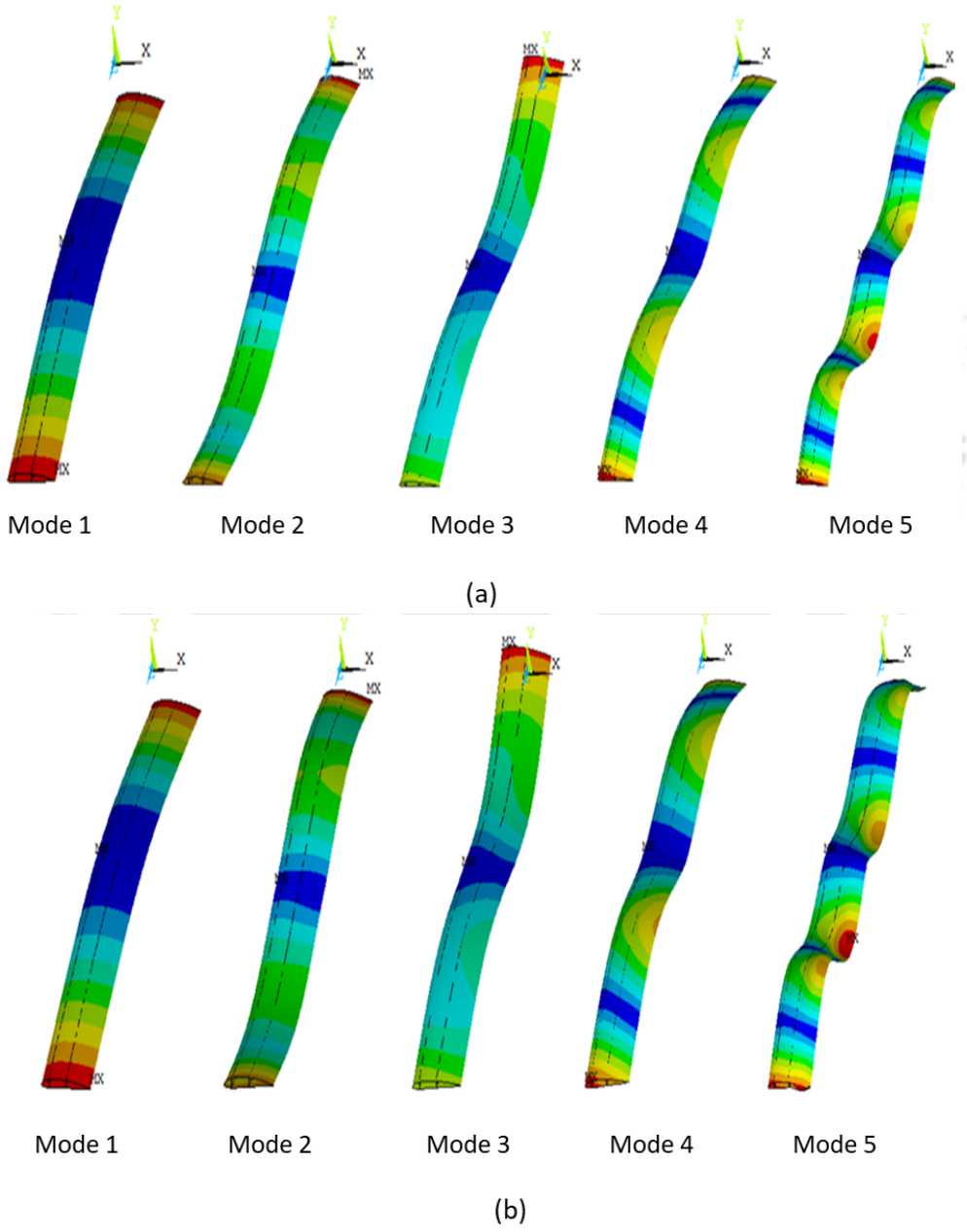

Figure 5.5: Different mode shapes (a) laminate (c), (b) laminate (e) for boundary condition 2.

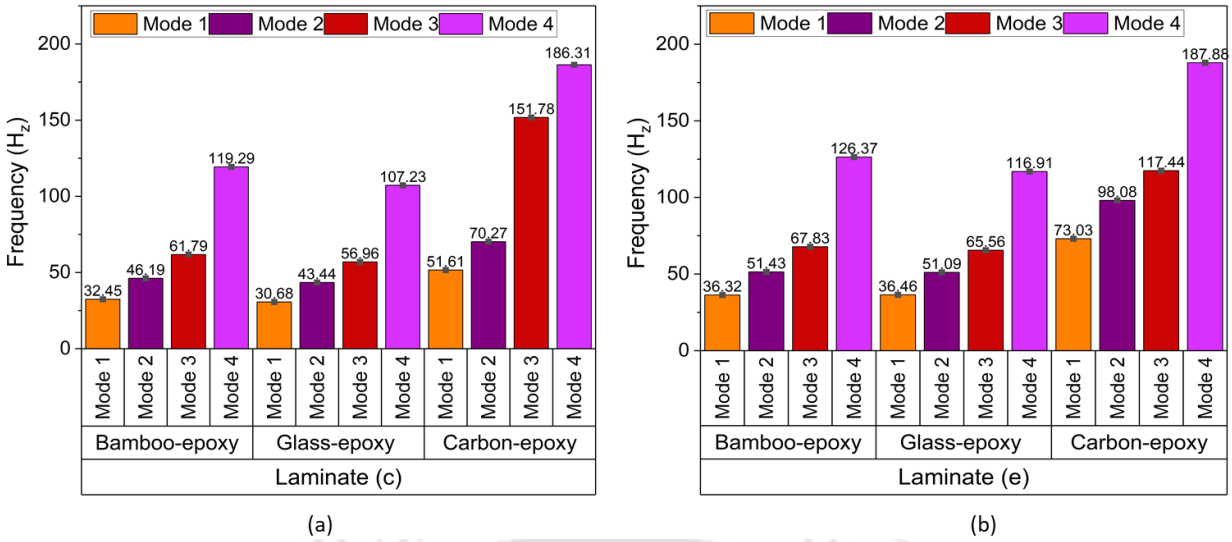

Figure 5.6: Comparison plots for natural frequencies of different composites with boundary condition 1 (a) laminate (c), (b) laminate (e).

frequency values for glass and bamboo composites on the other hand posses low frequency values compared to carbon composites. The mechanical properties of bamboo composites evaluated in the current study are almost similar to the mechanical properties of glass composites demonstrated by Hameed *et al.* [130]. It is observed that the designed blade from bamboo composites demonstrates higher values of natural frequencies as compared to glass composite blade. Considering similar strength properties, bamboo composites are lighter than glass composites due to their lower density. The bamboo composites have the potential to serve as a feasible replacement for glass-epoxy blades, offering potential advantages in terms of material properties, cost effectiveness and sustainability.

5.5.2 Harmonic vibration results

Harmonic analysis is an important technique that helps in determining the composite blade structural response under dynamic loads/ vibrations. It is generally represented by sinusoidal or harmonic functions [205, 206]. It ensures the structural integrity and performance of the turbine blade over its operational lifespan. Composite blades are

designed to withstand different types of loads including aerodynamic, gravity, and rotor-induced vibrations. Thus, it is necessary to perform harmonic analysis to have a better understanding of how these loads affect the blade structural behavior and resonance frequencies. When the excitation frequency of the blade is close to its natural frequency it causes resonance and consequently increases the fatigue stress on the blade [207]. Thus, the dynamic characteristics such as natural frequencies and their corresponding mode shapes play an important role in preventing premature fatigue, damage, and sudden catastrophic failure in the design of these structures. In this section, the harmonic analysis results of the wind turbine blade are discussed. The linear frequency response in the neighborhood of natural frequency is obtained. Laminate (c), and laminate (e) are considered for the harmonic analysis. The analysis is performed for the non-symmetric airfoil and the results are compared with an non-symmetric blade with a double shear web. The frequency response function (FRF) plot is obtained mainly based on the range of natural frequencies from 30 to 130 H_Z for the non-symmetric blade and 30 to 150 H_Z for the shear web blade with boundary condition 1. Similarly, for the blades with boundary condition 2, the set of natural frequencies of 5 to 80 H_Z and 10 to 90 H_Z are analyzed. The process is carried out with substeps of 100 for both blades.

The FRF plot will generate a graph of amplitude vs. frequency, in which frequency is plotted on the x-axis and amplitude on the y-axis. The relationship between maximum amplitude response and frequency in the y direction of the blade is plotted in Fig. 5.7 and Fig. 5.8. It is observed that the displacement peaks for the blades with boundary condition 1 are comparatively lower than that of the blades with boundary condition 2. Moreover, some minor peaks are also observed for the blade with boundary condition 2. Further, the peaks of laminate (c) comprising cross-ply layups are lower than laminate (e)

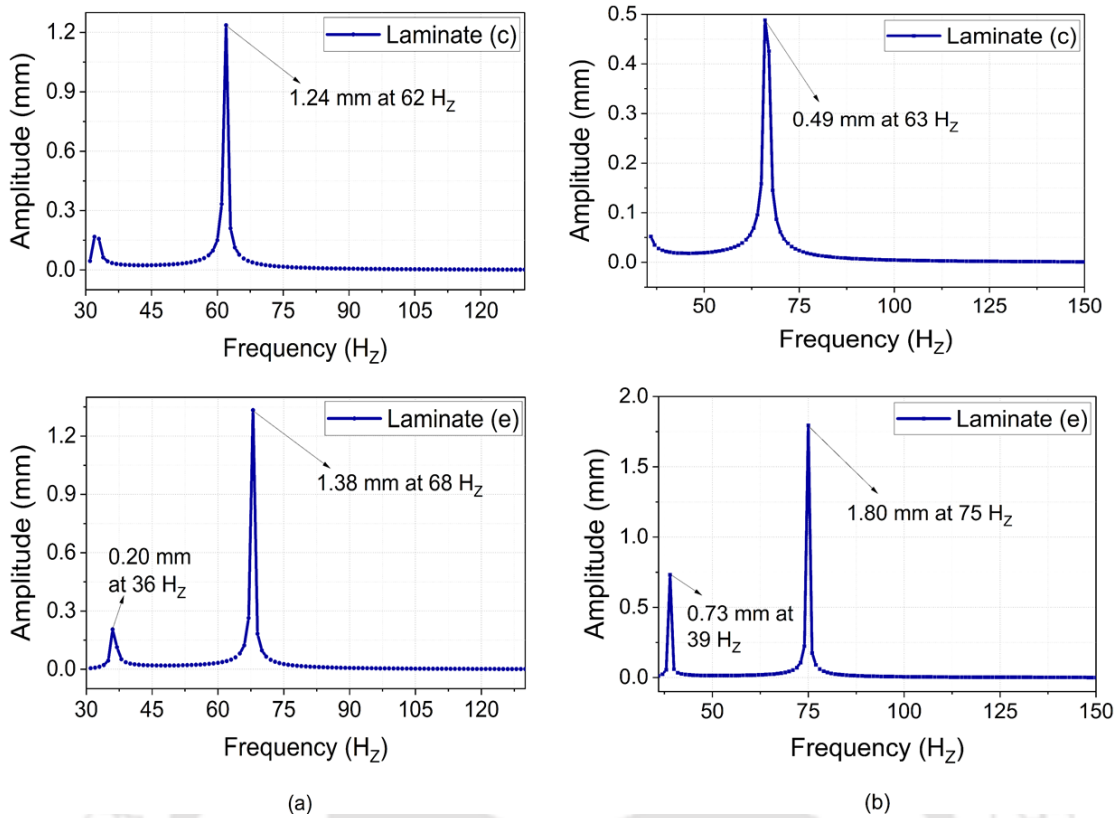

Figure 5.7: Amplitude spectra of blade deformation for different laminates with boundary condition 1 (a) non-symmetric blade without shear web (b) non-symmetric blade with double shear web.

for both blades. The maximum displacement peaks are observed at the tip of the blade and gradually decrease towards the mid-span. Fig. 5.7 presents the displacement peaks for the blade with boundary condition 1. The maximum displacement peaks for the non-symmetric blade with laminate (c) and laminate (e) are 1.24 mm at 62 H_Z and 1.38 mm at 68 H_Z. From Table 5.3, it is observed that the third-order natural frequencies of the blade for both laminates are almost equal to the exciting frequencies. Fig. 5.8 depicts the amplitude displacement peaks for the blades with boundary condition 2. Maximum peaks are observed between (13-15) H_Z which are nearly close to the range of their natural frequencies. Thus, the blades are under resonance conditions. In the next section, the effect of the damping ratio is studied.

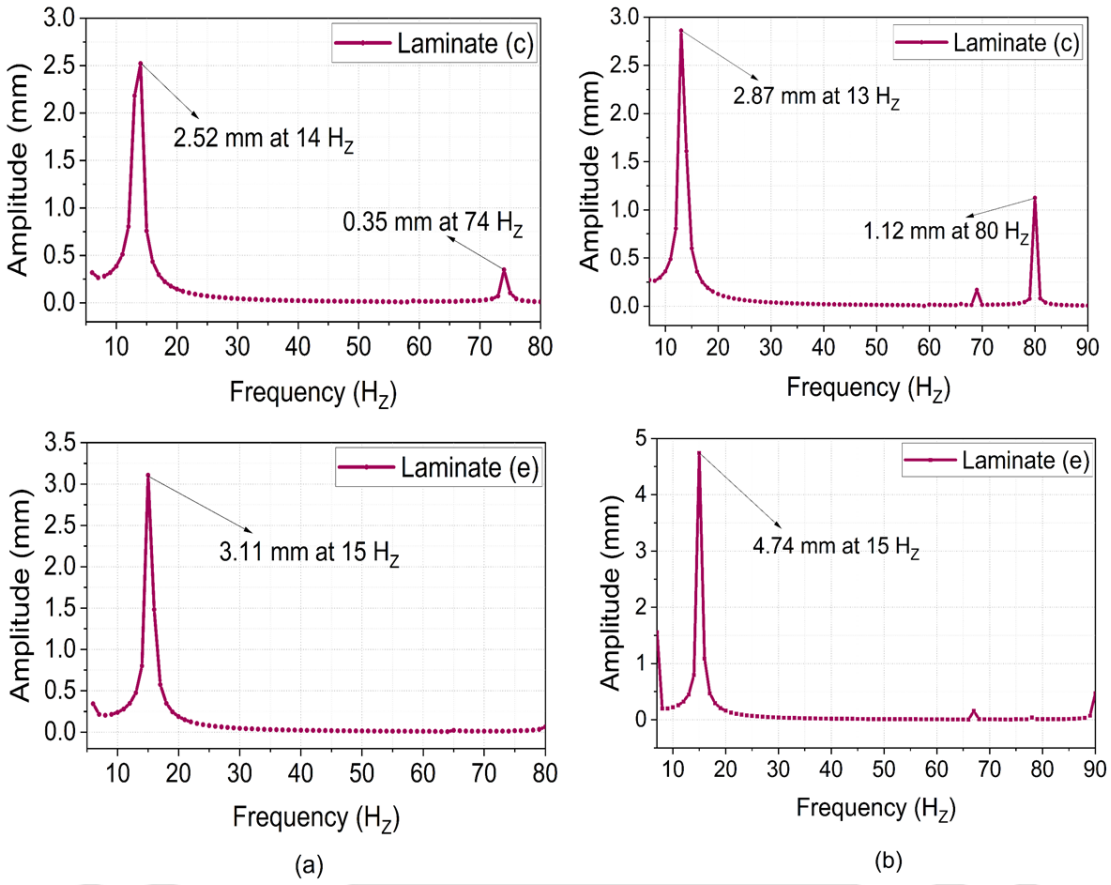

Figure 5.8: Amplitude spectra of blade deformation for different laminates with boundary condition 2 (a) non-symmetric blade without shear web (b) non-symmetric blade with double shear web.

5.5.3 Effect of damping on the harmonic response of cross-ply laminated non-symmetric blade

In most of the engineering applications, the Rayleigh damping model is widely used [208]. The damping of a structure is characterized by the damping ratio ζ. Different types of damping are associated with wind turbine blade structure i.e. structural, aerodynamic, and material damping. Although structural damping is different from material damping, they are closely related to each other [209]. Zang *et al.* [210] considered the structural damping ratio $\zeta = 0.5\%$, to study the effect of the blade structure. However, according to Popelka [211], the critical structural damping for the Darrieus wind blade is (0.1-0.4)%.

The aerodynamic damping ratio for VAWTs is reported to be in the range of (1.80-5.30)% [212]. In the present study, the aerodynamic damping is neglected as the blade is non-rotating at a zero-pitching angle. The effect of structural damping from (0.35-2)% on the natural frequencies of the VAWT blade structure is studied. The non-symmetric blade without the shear webs is considered. The effect of damping on the natural frequencies

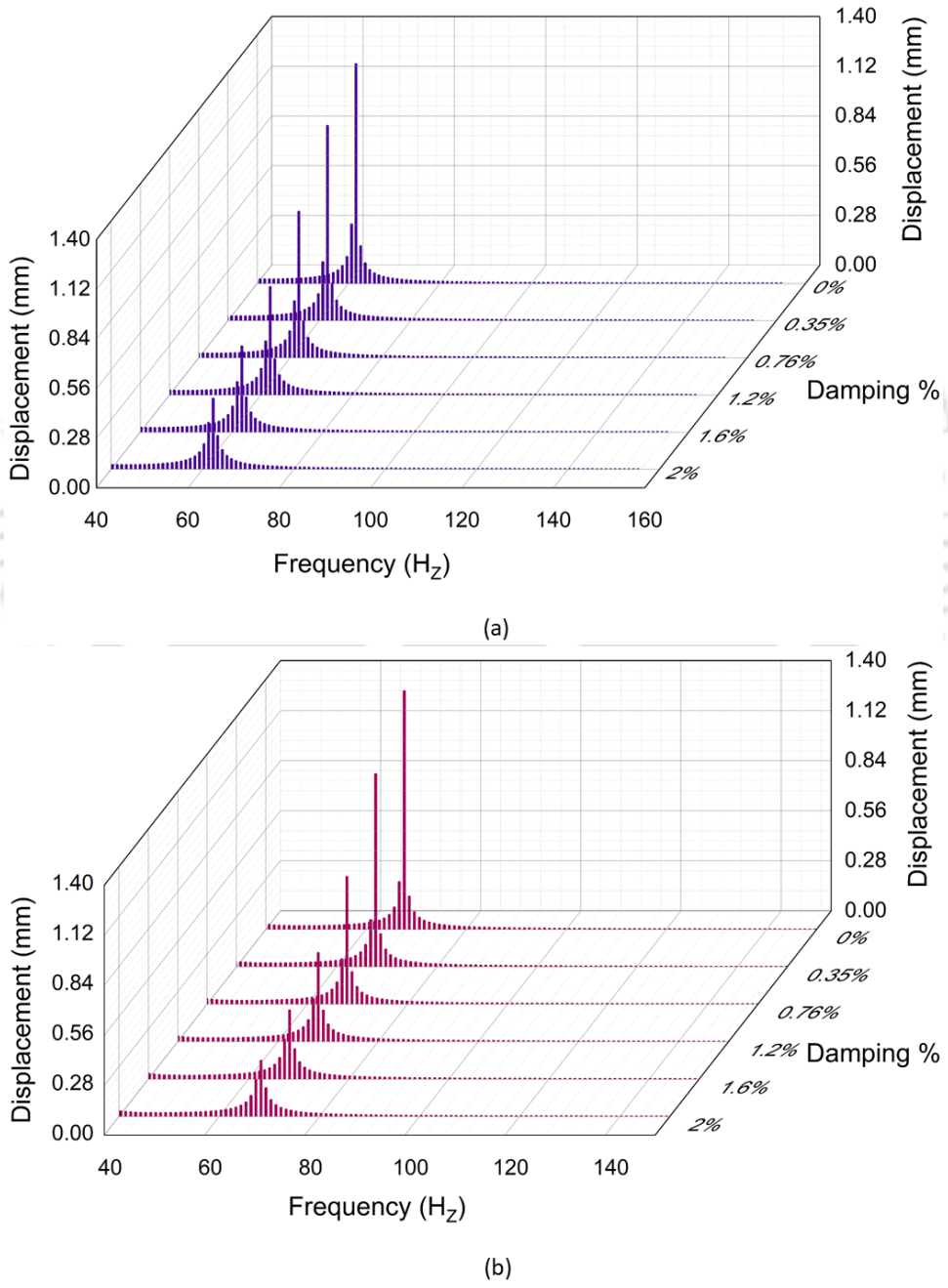

Figure 5.9: Effect of damping of the harmonic response of the blade for boundary condition 1 (a) laminate (c), and (b) laminate (e).

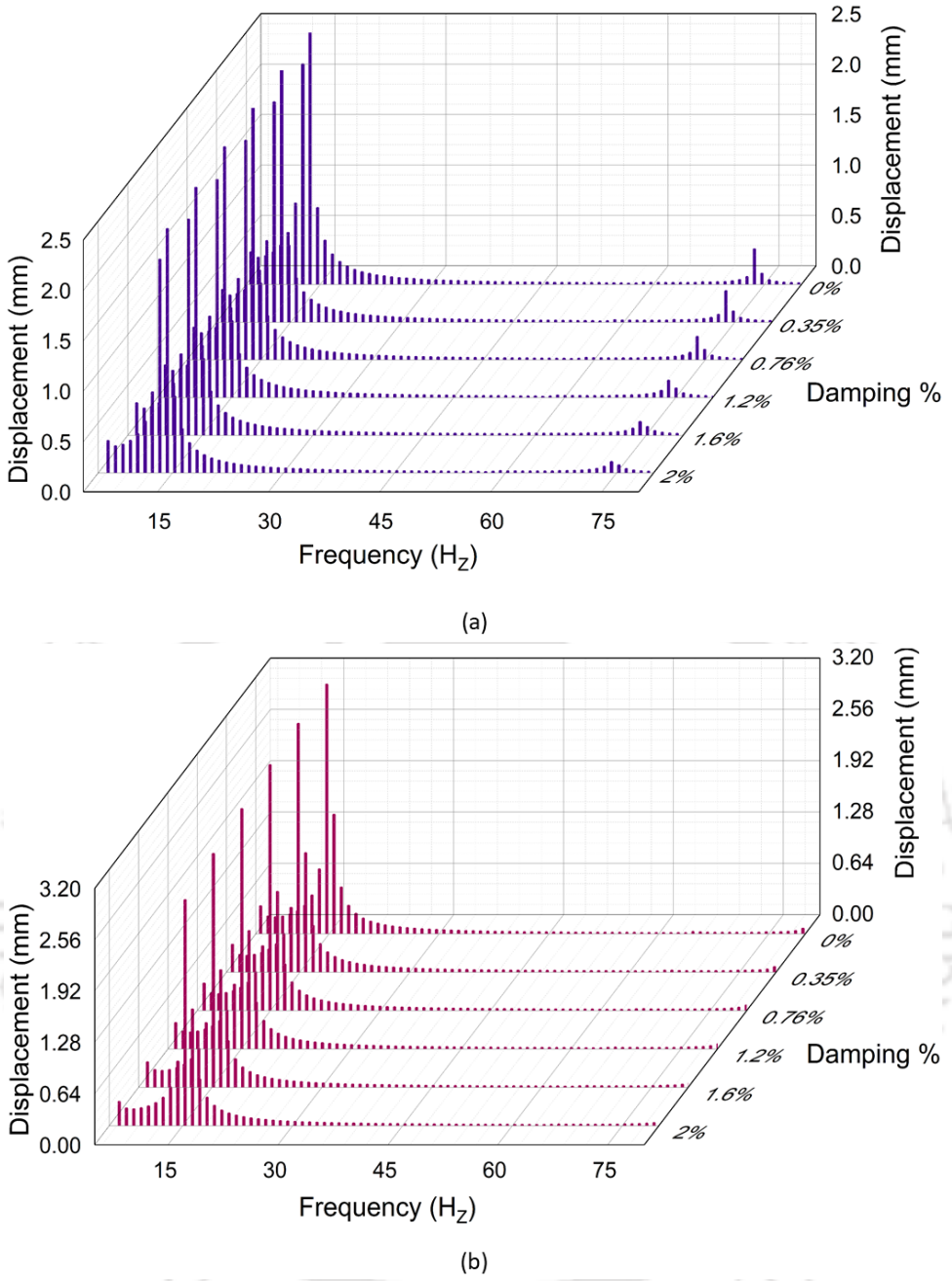

Figure 5.10: Effect of damping of the harmonic response of the blade for boundary condition 2 (a) laminate (c), and (b) laminate (e).

is presented in Fig. 5.9 and Fig. 5.10. Fig. 5.9(a) and (b) presents the damping effect on the non-symmetric blade of type 1 boundary condition for the laminate (c) and laminate (e). It is observed that the maximum amplitude for both laminates is obtained within the range of 60 H_Z to 70 H_Z. The resonance amplitude decreases at a faster rate as the damping ratio increases from 0% to 2% for the same range of natural frequency. A

similar observation is obtained for the blades with type 2 boundary conditions for the frequency range of 10 H_Z to 15 H_Z as shown in Fig. 5.10. However, some small peaks are also observed at the frequency range of 75 H_Z to 80 H_Z.

5.6 Summary

The free vibration analysis of composite blades plays a pivotal role in ensuring structural integrity, performance, and safety. The natural frequencies, mode shapes, as well as damping characteristics of the blades under different boundary conditions are successful investigated. From the free-vibrational results, it is observed that the non-symmetric blade obtained the least free-vibrational values compared to the other profiles. Four cross-ply layups and one angle-ply layup are studied and it is observed that the cross-ply layup i.e. laminate (c) has the minimum value of natural frequency. The blades are modelled with the conventional materials and the frequency results are compared with the bamboo composite blades. It is observed that the frequency values for the bamboo composites blades almost resembles that of the glass composite blades which signifies that these composites can be a suitable and sustainable replacement for the conventional materials.

Chapter 6

Fluid-structure interaction of bamboo composite straight blade and final blade fabrication

6.1 Introduction

During the operation of wind turbines, the aerodynamic loads on the blade may cause blade deflection. This deflection causes additional changes in the flow characteristics resulting in excessive load alteration. The interphase between the fluid and the structure cause reliability issues regarding aeroelastic loads such as edgewise, and flapwise instability, which can cause a disastrous effect on the blades and the turbine as a whole system. Therefore, accurate FSI modelling is essential in the design and development of wind turbines. FSI can be a one-way or two-way interaction. In two-way interaction, the aerodynamic model is solved to obtain the load data independently. The structural stresses and deflection of the model are then achieved by mapping these pressure loads as boundary conditions to the structural model. Once the convergence criteria are achieved, this deflection is imported back to the aerodynamic model, and the process is repeated. This method is computationally expensive and produces accurate results. On the other hand, in one-way interaction, the resulting aerodynamic pressure from the CFD simulation is imported to the structural model to assess the structural stresses and deflection in the same way as in two-way interaction. Compared to two-way, the computational cost for

one-way interaction is cheaper and requires less time making it suitable for initial modelling. In the present study, an FSI simulation of a three-dimensional vertical-axis wind turbine is conducted. This study presents a one-way coupled FSI model for wind turbine composite blades at full scale, taking account of detailed composite layups of the blade. The aerodynamic loads are calculated using CFD and blade structural responses are determined using FEA. The coupling strategy is based on the one-way coupling strategy, in which aerodynamic loads calculated from CFD modelling are mapped to FEA modelling as load boundary conditions.

6.2 Computational fluid dynamics (CFD) modeling

Computational fluid dynamics (CFD) is used to study the characteristics of fluid flow and pressure variation on the blade surface. It uses computer-based simulations to analyze the complex fluid flow around the VAWTs which can accurately predict the parameters such as lift, drag, torque generation etc. CFD models can also study the interactions between the rotaing blades and the surrounding air, including the phenomena such as flow seperations, stall, and turbulence which further helps in identifying the potential challenges such as structural loads, vibrations, etc. CFD is classified into finite volume method (FVM), finite difference method (FDM), and finite element method (FEM).

6.3 Description of the turbine model and the numerical domain

A 3D straight Darrieus turbine with three blades is modelled in SolidWorks software for the FSI coupling. The blades of the turbine are connected by the struts to the rotating

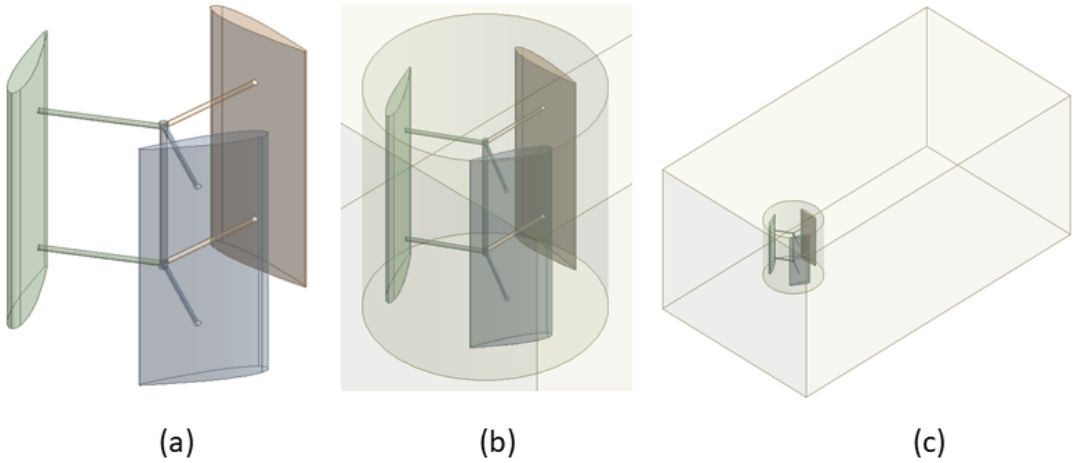

Figure 6.1: Three dimensional presentaion (a) straight Darrieus wind turbine (b) rotating doamin (c) stationary domain.

shaft as shown in Fig. 6.1. Fig. 6.1(a) depicts the 3D model of the turbine and the 3D view of the rotating and stationary domain is shown in Fig. 6.1(b), and Fig. 6.1(c). The blades are modelled using Kirchhoff-Love shells, whereas the connecting struts and main rotating shaft are modelled as beams. From section 4.5.2, it is clear that the bamboo composite blade with angle-ply $[45°/90°/0°/\text{-}45°]_S$ showcased the optimum stress and deflection values. Thus for the current study, the angle-ply layup is considered. The dimensions of the turbine is taken small to reduce the computational time. The geometric design parameters of the 3D VAWT are presented in Table 6.1.

Table 6.1: Geometric details of the straight Darrieus wind turbine.

Blade profile	Asymmetrical NACA 4415
Number of blades	3
Diameter, D (mm)	120
Blade span height, H (mm)	150
Chord length, c (mm)	60
Wind velocity, V (m/s)	8

The straight Darrieus VAWT operates in open field conditions, thus a large rectangular domain is considered to avoid flow blockage. The turbine is modelled in such a way that it has two domains i.e. stationary domain known as fluid domain through which the flow is passing and the rotating domain known as solid domain consisting of turbine blades that rotate with the passage of airflow. The rectangular domain has been partitioned with suitable dimensions in ratio between turbine diameter and the rectangular domain length. This ratio is 16D in the length of the domain and 8D in the width of the domain as shown in Fig. 6.2. The boundaries of the domain are kept at a suitable distance from the turbine to reduce the effects of boundary flow conditions such as flow blockage, and insufficient wake development. In the rotating domain, the blades connected to the struts are placed at an azimuth angle of 120° to one another. In the CFD domain, the left vertical line is defined as the velocity inlet and the right vertical line is the pressure outlet. The velocity of the flow is taken as 8 *m/sec*, the same as in Chapter 4. The hor-

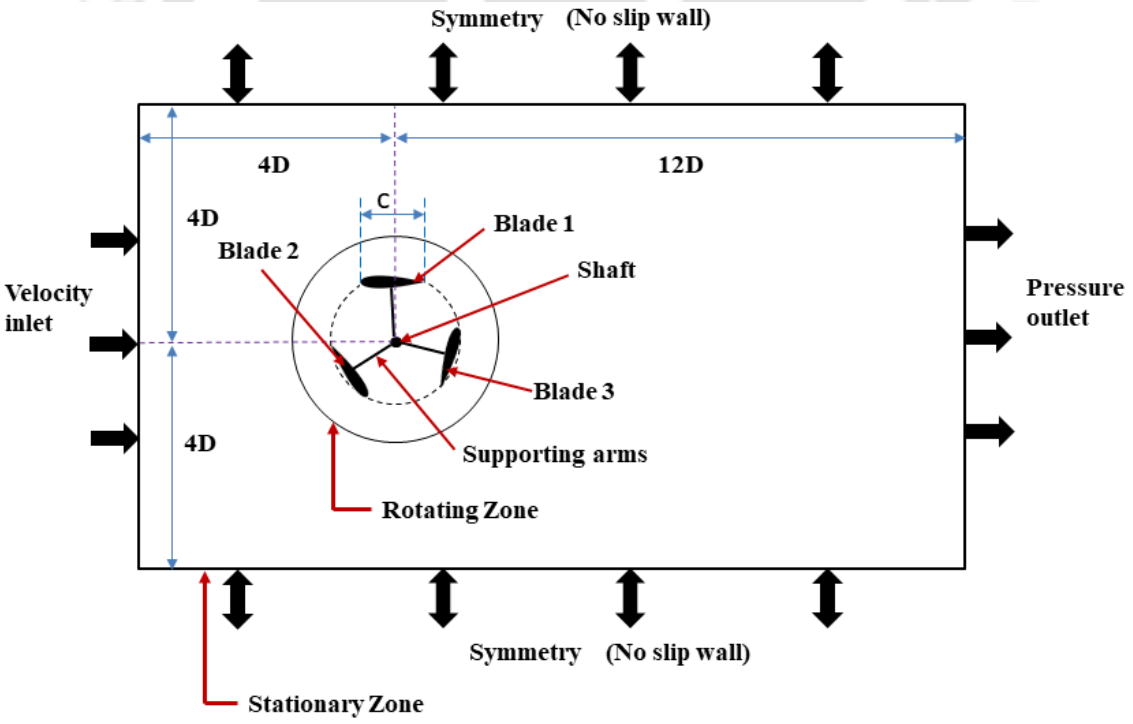

Figure 6.2: Geometrical features and boundary conditions of the CFD domain consisting of turbine with the standard blades.

izontal boundaries are defined as symmetry-type boundary conditions with no-slip walls to minimize the wall effects. The rotating domain is provided with an angular velocity of 50 *radian/sec*, with a sliding mesh interface between the rotating and stationary domain.

6.4 Turbulence model and solution method

ANSYS FLUENT has several turbulence models that are capable of handling both steady-state and unsteady-state analysis. The turbulence model used in this one-way coupling is the SST (shear stress transport) k-ω model is used to estimate the Reynold stresses. This model combines the benefits of both k-ϵ and k-ω turbulence models making it suitable to analyze both the far field flow characteristics, boundary layer separation, and vortex shedding [213, 214]. Two transport equations are required to calculate the eddy viscosity in the SST, k-ω model i.e. turbulent kinetic equation, k and turbulence dissipation/frequency rate ω.

The transport equation for turbulent kinetic energy k for the k-ω turbulence model is given as following equations below [122] -

$$\frac{\partial(\rho k)}{\partial t} + \frac{\partial(\rho U_i k)}{\partial x_i} = \frac{\partial}{\partial x_i}\left[\left(\mu + \frac{\mu_t}{\sigma k}\right) grad(k)\right] + P_k - \beta \times \rho k\omega \tag{6.1}$$

where

$$P_k = \left(2\mu_t \frac{\partial U_i}{\partial x_j} . \frac{\partial U_i}{\partial x_j} - \frac{2}{3}\rho k \frac{\partial U_i}{\partial x_j}\delta_{ij}\right) \tag{6.2}$$

The transport equation for turbulent frequency ω for the k-ω turbulence model is given as follows [122]-

$$\frac{\partial(\rho\omega)}{\partial t}+\frac{\partial(\rho U_i\omega)}{\partial x_i}=\frac{\partial}{\partial x_i}\left[\left(\mu+\frac{\mu_t}{\sigma_{\omega,1}}\right)grad(\omega)\right]+\gamma_2\left(2\rho\frac{\partial U_i}{\partial x_j}.\frac{\partial U_i}{\partial x_j}-\frac{2}{3}\rho\omega\frac{\partial U_i}{\partial x_j}\delta_{ij}\right) \\ -\beta_2\rho\omega^2+2\frac{\rho}{\sigma_{\omega,2}\omega}\frac{\partial k}{\partial x_k}\frac{\partial \omega}{\partial x_k} \tag{6.3}$$

where $\sigma_{\omega,1}$, $\sigma_{\omega,2}$, γ_2, β_2 are constant.

In the current study, the flow is modelled by RANS (Reynolds averaged Navier-Strokes) 3D CFD flow model. The RANS flow model equations are solved using a pressure-based coupled algorithm [149]. Compared to the pressure-based segregated algorithm, the pressure-based algorithm solves the pressure-based continuity and momentum equations equivalently in a closed coupled manner. This process significantly increases and improves the convergence rate. The continuity and momentum equations for the unsteady and incompressible flow are expressed as follows -

Continuity equation:

$$\frac{\partial u_i}{\partial t}+\frac{\partial u_i}{\partial x_i}=0 \tag{6.4}$$

Momentum equation:

$$\frac{\partial u_i}{\partial t}+u_i\frac{\partial u_i}{\partial x_j}=-\frac{1}{\rho}\frac{\partial P}{\partial x_i}-\frac{\partial}{\partial x_j}\left[\nu\left(\frac{\partial u_i}{\partial x_j}+\frac{\partial u_j}{\partial x_i}-\frac{2}{3}\delta_{jj}\frac{\partial u_i}{\partial x_i}\right)\right]+\frac{\partial}{\partial x_j}(-\overline{u_i'u_i'}) \tag{6.5}$$

6.5 Mesh independent study

To determine the appropriate mesh size for each component, a mesh sensitivity study is performed with varying face sizing. Unstructured tetrahedron mesh with a prismatic layer attached to the blade walls is selected as the mesh type. This mesh type is selected due to its simplicity and its ability to represent complex domains with reduced computational

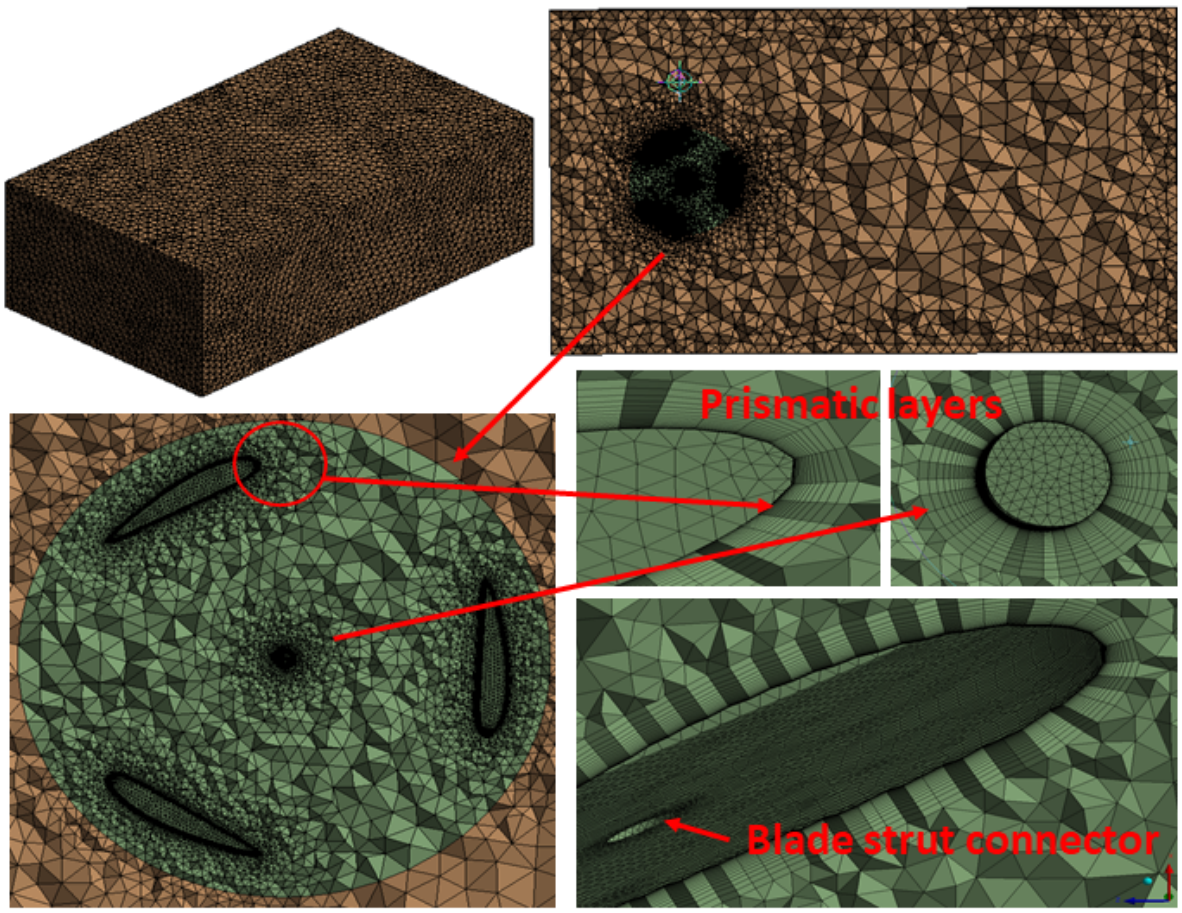

Figure 6.3: Computational grids for the CFD domain and straight Darrieus wind turbine.

time. The blade is meshed with an face sizing of 1.8 *mm* which is refined to 0.42 *mm* near the trailing edge (TE) and leading edge (LE) as shown in Fig. 6.3. The computational domain with rotating and stationary domain is mesh with 30 *mm*, and 15 *mm* mesh size as shown in Fig. 6.3.

The mesh near the blade wall is well refined to ensure the non-dimensional normal distance from the boundary wall i.e. y^+, falls under the permissible range. The wall y plus, y^+ is used to characterize the near wall behavior of the flow. The "y^+" denotes the distance from the boundary wall and "$^+$" is the normalized distance that denotes the

thickness of the each layer from boundary wall. Mathematically, it is defined as -

$$y^+ = \frac{yu_\tau}{\nu} \tag{6.6}$$

where y is the distance from the boundary wall, u_τ is the friction velocity, and ν is the kinematic viscocity of the fluid flow. It is necessary to ensure that the y^+ values are appropriate for the different turbulence models. The model such as SST k-ω, smaller y^+ values are required to resolve the near wall region for better accuracy. The prismatic boundary layers (BL) or inflation layer is applied to the blade surfaces to improve the persistency of boundary flow layer. The inflation layer is used to ensure that there are enough grids points to resolve the boundary layer separation. The "inflation growth rate" is a dimensionaless factor and is defined as the rate at which the size of the cells in the inflation layer increases from the surface of the blade. For the current SST k-ω model, 20 boundary layers are applied to the blade surfaces with an element growth rate of 1.2. The first prismatic layer thickness is 0.04 mm with small wall y^+ less than 1 and wind

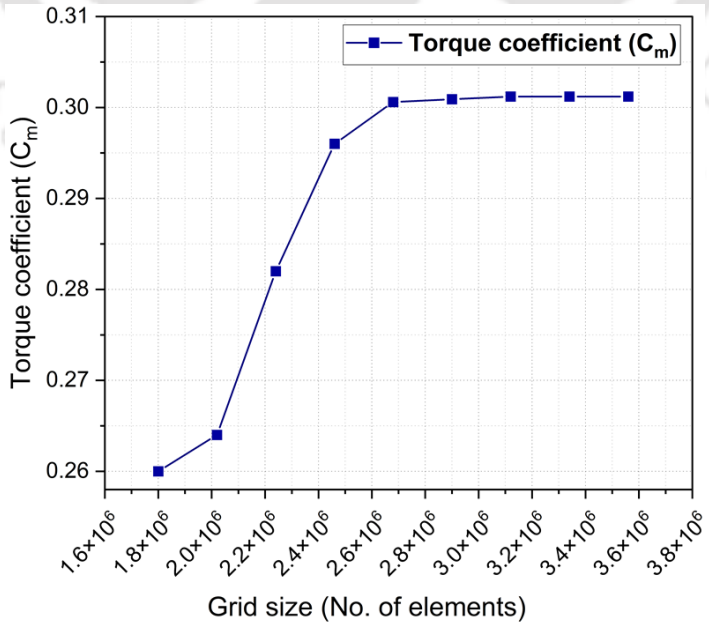

Figure 6.4: Mesh independent study.

velocity 8 *m/sec* as shown in Fig. 6.3. The quality and density of the unstructured mesh are identified with several grid sizes ranging from 1.8×10^6 to 3.8×10^6 cells as shown in Fig. 6.4. It is observed that the value of torque coefficient from grid cells of 3.0×10^6 is relatively stable with a percentage(%) deviation less than 0.86%. Therefore, the grid size of 3.0×10^6 cells is deemed as the appropriate mesh size for further analysis to decrease the computational time.

6.6 Convergence criteria

After the mesh study, the model is checked for its convergence. The convergence for each time step is achieved under two criteria i.e. residual values and variation in total mass. The residual check is the most commonly used criteria for evaluating the solution of CFD convergence. Total six different variables such as (continuity, x-velocity, y-velocity, z-velocity, turbulent kinetic energy, and specific dissipation rate) are observed during the iteration process. The solution convergence criteria is selected as 10^{-4}, which is

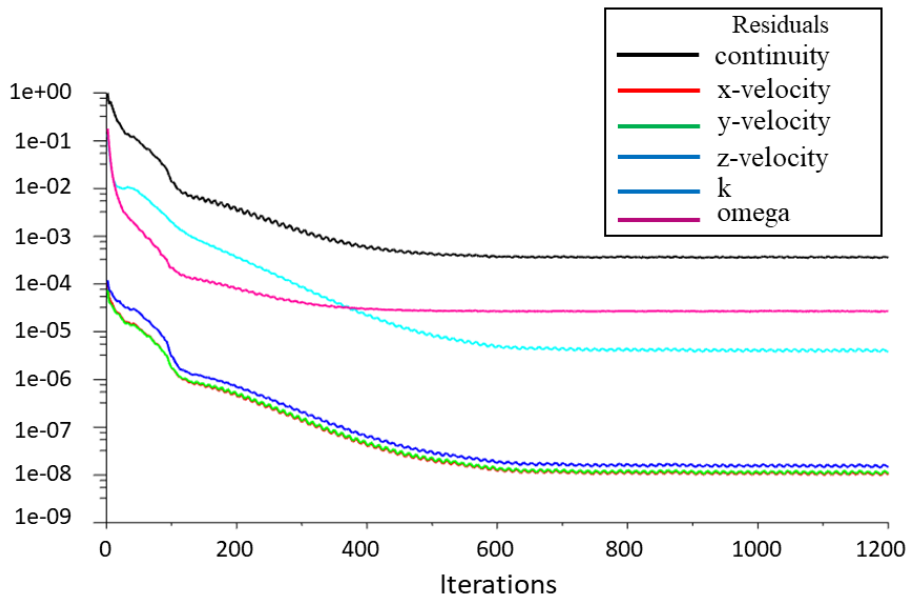

Figure 6.5: Convergence residual for the CFD model.

considered as standard residual convergence value in CFD modelling of wind turbine blades as reported in [215, 216]. The rotor speed, rotational velocity, and pitch angle of the blades are kept at 8 *m/sec*, 50 *rpm*, and 0° respectively. The residual iteration plot for the current wind turbine model is depicted in Fig. 6.5. As seen from the Fig. 6.5, the residual values of all the variables except continuity are less than 10^{-4}, which is assumed as the convergence criteria. The residuals for continuity did not fully converge to the specified criteria, with values plateauing around 10^{-3}. This plateau may be attributed to the complexity of the flow and the use of an unstructured mesh, which can sometimes lead to higher residuals. Despite this, key flow variables, such as velocity, k, omega showed stable behaviour, suggesting that the solution reached an acceptable level of convergence.

6.7 Results and discussion

6.7.1 Pressure distribution and velocity gradient on the domain

After the solution is converged, the aerodynamic pressure acting on the blades and the wind turbine is plotted using the post-processing function in ANSYS-fluent. The pressure distribution contours on each blade front (pressure side), and back (suction side) is displayed in Fig. 6.6. The airflow hits blade 2 at the tip of the trailing edge thus moving the blades in an anticlockwise direction. The blade suction side is shown as the leeward side which displays a negative pressure whereas the pressure side which is the windward side is highly susceptible to maximum pressure. During rotation, the maximum pressure occurred at the pressure side of blade 1 near the leading edge and blade 2 near the trailing edge whereas, for blade 3, the maximum pressure occurred at the suction side where the air hits the blade. Similarly, negative pressure occurred at the top and bottom vertex

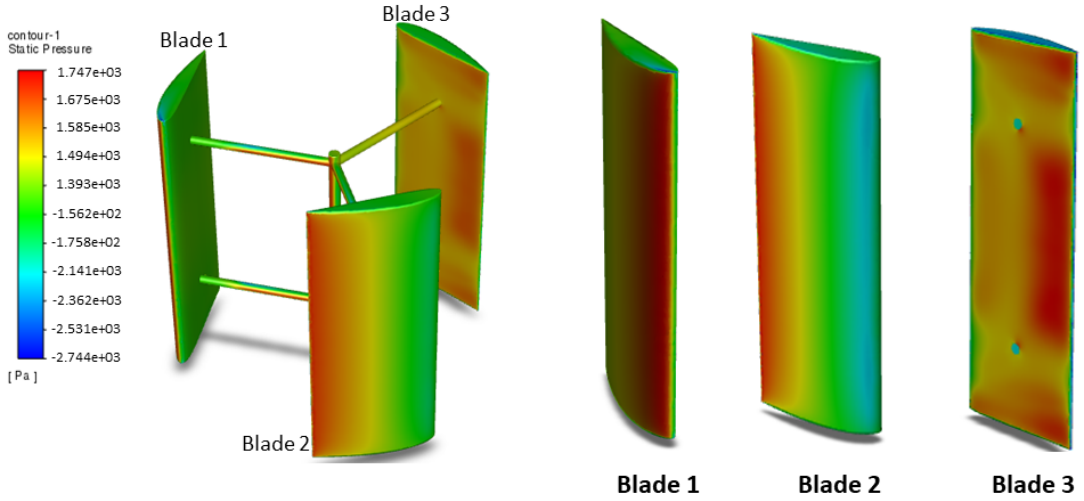

Figure 6.6: Pressure contours on the wind turbine and blades.

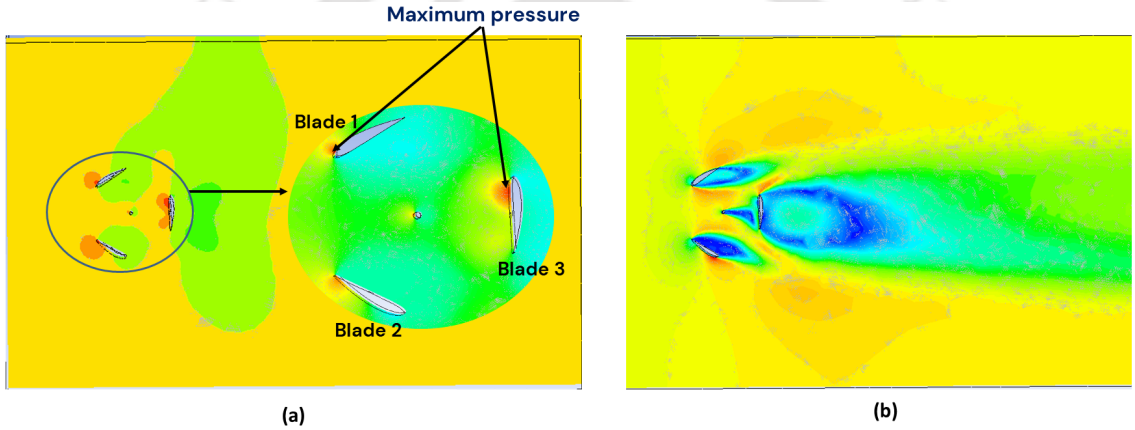

Figure 6.7: Contours on the CFD domain (a) pressure contour, (b) velocity contour.

of the leading edge for blade 1, at the vertex of the leading edge in the pressure side and suction side for blade 2, and the pressure side of blade 3 as shown in Fig. 6.6. The pressure contour and velocity contour of the CFD domain consisting of the wind turbine are displayed in Fig. 6.7. The maximum positive pressure on the blades is 1747.22 *MPa* and the negative pressure is -2744.76 *MPa*.

6.7.2 Static structural analysis

Before performing the static structural analysis, the laminating of the blades with bamboo composite materials is performed in the ACP module. ACP module in Ansys is a

advanced tool used to address the complex mechanical behavior of composites subjected to high temperature and loads. In the ACP module, the hollow blades are developed in the form of the shell which is assigned as a single sheet by adjusting its thickness. The composite fabric is defined with the bamboo-epoxy material properties. Finally, a laminate is created stacking up all the fabrics with different plies from top to bottom as per the angle-ply layup $[45°/90°/0°/\text{-}45°]_S$. The total wall thickness is considered as 4 *mm*. In the blade geometry, the material orientation is determined using geometric attributes such as layup direction, layup area, and reference direction. After the laminates are created, in the next step, orientation element sets are used which defines the reference and orientation of the fiber directions. Finally, a new modelling ply comprising laminated materials is assigned to the blade structure as presented in Fig. 6.8. The green

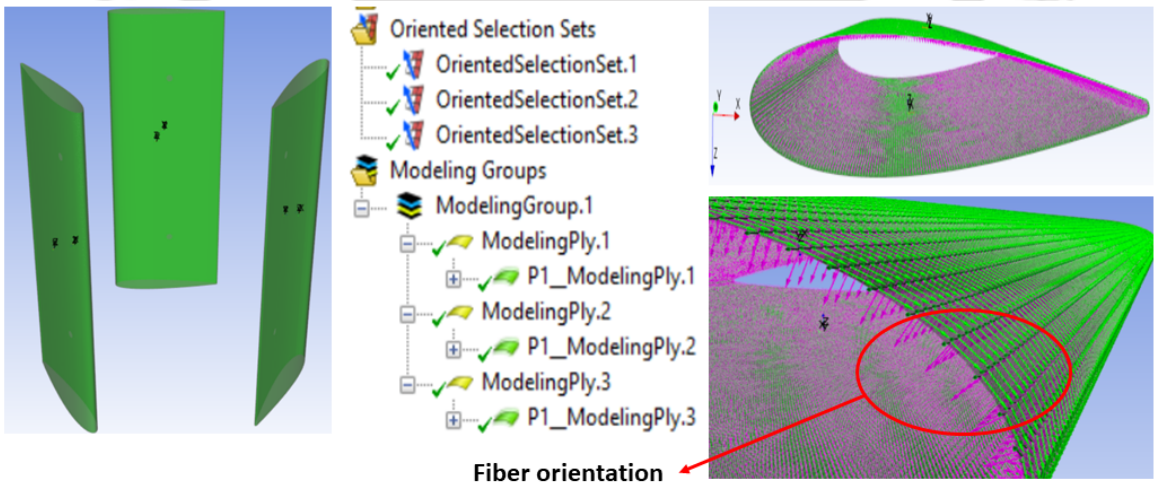

Figure 6.8: Modelling groups and fiber orientation of the turbine blades.

arrows depict the fibers in the x and y directions directing from leading to the trailing edge. The pink arrows depict the fiber orientation in the z-direction. The integration of FE static structural and ACP of the straight Darrieus wind is achieved by transferring the laminated shell structure of the blade and the solid components such as strut, and shaft from ACP to static structural for further analysis.

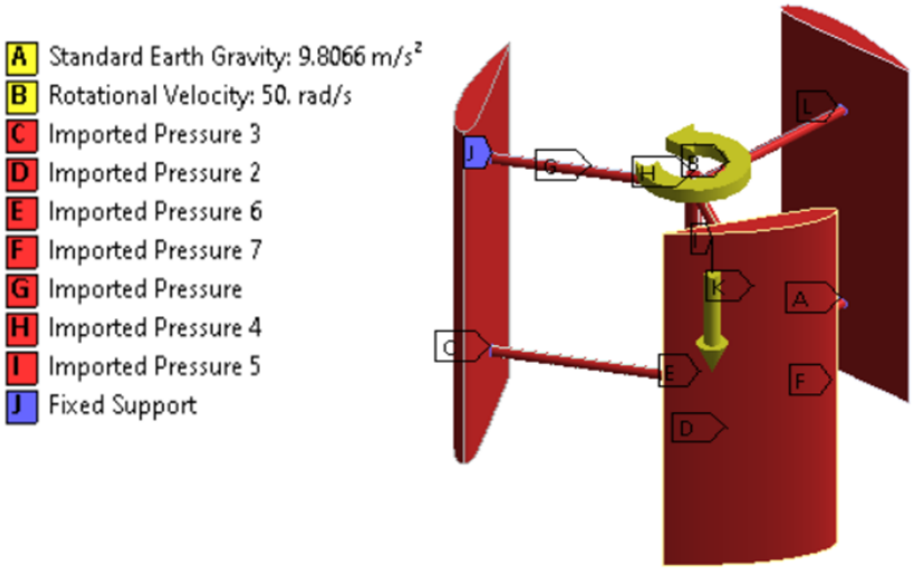

Figure 6.9: Applied loads and boundary conditions.

The FE model of the straight Darrieus wind turbine is imported to the static structural module. Wind turbine blades are mainly subjected to deformations such as bending and torsion [217], therefore proper meshing must be provided to the FE model. For the analysis, the wind turbine model is meshed with 2 *mm* element size and mesh refinement of 0.5 *mm* is provided near the blade strut connectors. The wind turbine is subjected to three types of loading i.e. aerodynamic pressure from the airflow, centrifugal forces, and standard earth gravity. The applied loads and boundary conditions for the analyzed model is shown in Fig. 6.9 The results of the deformation and stresses of the straight Darrieus wind turbine are depicted by the contour plots in Fig. 6.10. The variation of deformation is presented in colors in which the red color is defined as the critical value and the dark blue color is defined as the safest value under the defined aerodynamic load. The total deformation of the wind turbine under the aerodynamic pressure is shown in Fig. 6.10(a). The maximum and minimum deflection of the blades are 0.77 *mm*, and 0.046 *mm* respectively. It is observed that maximum deflection occurred near the leading and trailing edge, and the minimum deflection near the region of the blade fixed supports.

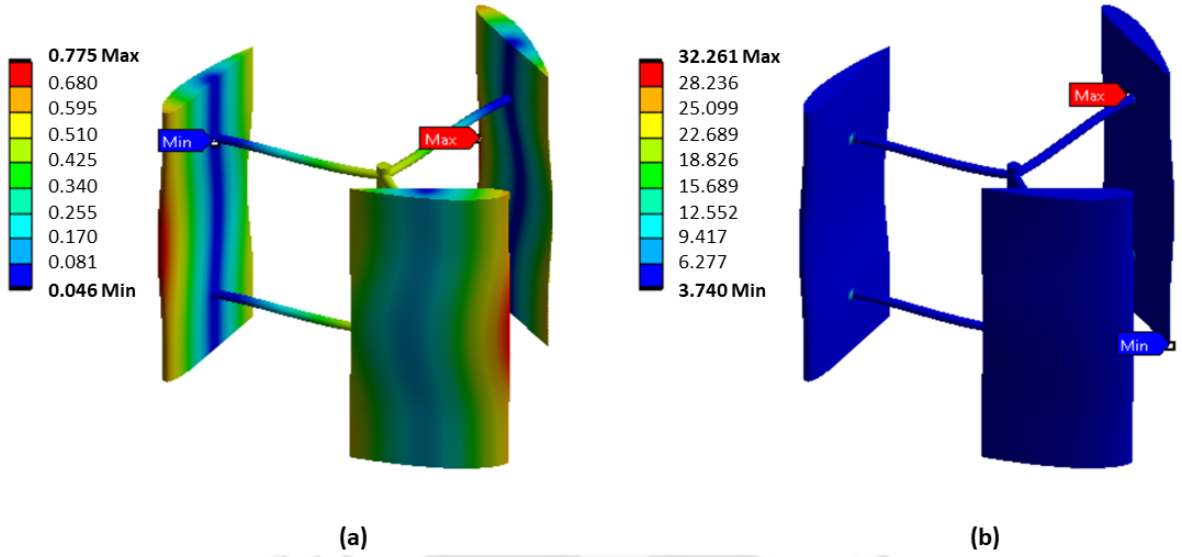

Figure 6.10: Maximum and minimum contours for the turbine (a) Deflection (b) Stress.

The maximum and minimum values of stresses are also evaluated as shown in Fig. 6.10(b). The maximum value of stress on the blades is 32.26 *MPa*. Comparing with the static structural results, the value of stress and deflection of the blade for the same angle-ply layup is 23.89 *MPa* and 6.23 *mm*. A significant difference in the blade deflection is observed due to the reduced length of the blade. However, the value of maximum stress i.e. 32.26 *MPa* is less than the allowable safe stress of the bamboo-epoxy material which is 96.14 *MPa* which indicates safe blade design.

6.8 Blade fabrication

After the detailed performance analysis of the bamboo composite blade, a small blade prototype is fabricated using the hand-layup technique. Firstly, the bamboo culms are procured, and long bamboo strips are extracted. Straightness and uniformity in the bamboo strips have been maintained during the extraction process. The use of thick bamboo strips in epoxy resin could potentially increase the blade weight. However, this increase in weight has been considered during the design phase. The added weight may

affect the starting torque and overall rotational inertia of the Darrieus turbine, but it also provides additional momentum once the turbine is in motion, which can contribute to more stable and efficient energy capture in variable wind conditions. The bamboo fiber composites could be a lighter alternative. However, for the current design and manufacturing capabilities, bamboo strips were preferred. After the extraction process, the procured strips are chemically treated at the laboratory to enhance their structural integrity and compatibility with the epoxy matrix. The chemically treated strips are washed uniformly with distilled water to remove the excess chemicals and oven-dried. In the second stage, a small blade is 3D printed with a standard NACA 4415 profile, and using the dimensions of the 3D printed blade, a metallic mold is prepared as shown in Fig. 6.11(a). The length of the blade is taken as 1000 *mm*, and the chord length of the blade is 200 *mm*. During blade fabrication, a plastic sheet is laid over the whole mold for easy peeling off the fabricated part as shown in Fig. 6.11(b). The extracted bamboo

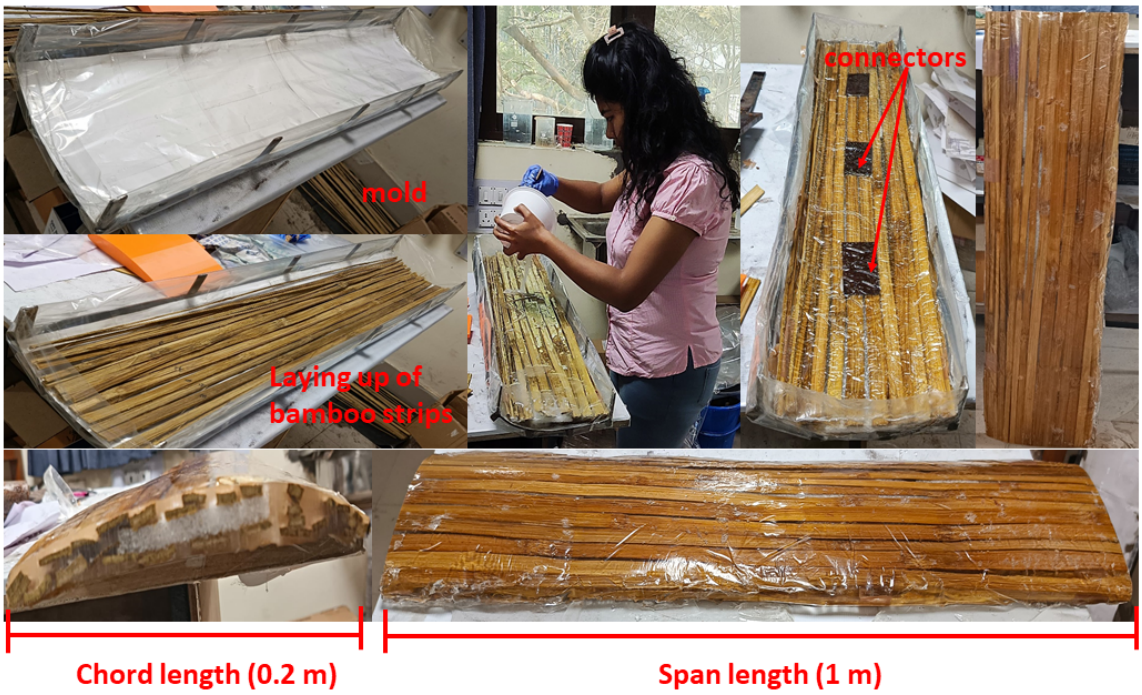

Figure 6.11: Fabrication of blade.

strips are laid over the mold one by one and then the epoxy resin is over the bamboo strips for easy binding. Lastly, the mold is covered with the covering lid and kept for 24 *hours* to set. The final fabricated bamboo composite blade is presented in Fig. 6.11.

6.9 Summary

In this study, the aerodynamic pressure and the structural characteristic of the straight Darrieus wind turbine blade are investigated via Fluid structure-interaction coupling. Straight Darrieus wind turbine is modelled using standard non-symmetrical airfoil NACA 4415. The material for the blades is selected as bamboo composite. From the CFD analysis, it is observed that the maximum pressure occurred at the windward direction of the blades. The evaluated pressure is then imported into the structural model to perform the structural analysis. The laminates of the blade are designed in ANSYS ACP with an angle-ply layup. The stresses and deflection of the bamboo composite blade are evaluated. It is observed that the value of the overall stresses of the wind turbine is less than the allowable safe stress of the bamboo-epoxy material indicating safe structural design.

Chapter 7

Conclusions

For the first time, the study on natural composites for wind turbine blade application is conducted in the North-Eastern region of India. In this research work, bamboo-epoxy composites for wind turbine blades are found to be a promising solution for increasing the sustainability and efficiency of wind energy generation. By harnessing the unique properties like lightweight, durability, and renewability of bamboo fibers, these composite blades offer numerous advantages over traditional materials like glass-fiber and carbon fiber composites. Bamboo composites demonstrate a commendable strength-to-weight ratio reducing the overall weight of the turbine blades. Reducing blade weight further reduces the effect of centrifugal forces which is the dominating factor for failure of VAWT blades. Additionally, the rapid growth cycle and low environmental impact make bamboo an attractive alternative from a sustainable point of view. Apart from these advantages, there are certain challenges such as standardization of the manufacturing processes, lack of design codes and standards, durability and scalability that needs to be addressed in detailed to ensure the safe reliability and widespread adoption of bamboo composite blades in the wind energy industry. The structural integrity and the potential for performance optimization of these composite blades are performed using advanced computational techniques like finite element analysis. The FEA is a powerful tool that enables to simulate the composite blades under different loading conditions to assess the stress distribution, and deflection pattern and identify the areas of improvement in the

blade design. However, its accuracy relies majorly on the quality of input parameters and material properties, highlighting the importance of comprehensive mechanical testing and validation processes. Thus, the incorporation of FEA into the design and optimization process of bio-composite wind turbine blades has enormous stride towards advancing sustainable energy solutions and hastening the transition towards a cleaner, and greener future.

7.1 Chapterwise Synoptic Conclusions From The Present Work

This section summarizes the chapter-wise outcomes of this research work and future research directions. The major conclusions are encapsulated below:

1. The mechanical characterization of three different bamboo species and their composites are successfully carried out. The bamboo strips are successfully extracted from the outer region of the bamboo culm. The following conclusions are drawn from the above investigation:

    - The strength results demonstarted that the bamboo-epoxy composites have a significant increase in strength, modulus, and toughness, compared to the untreated and delignified samples. The tensile strength of the B.Tulda composite is 259 MPa which is 133% higher than untreated bamboo samples.
    - The alkali-treated bamboo samples showed significant reduction in strength due to the swelling of the compact vascular fiber bundles which is confirmed from the FESEM micro-graphs.

- The fiber surface is improved after the chemical treatment which resulted in better impregnation of the epoxy resin between the fiber bundles.
- Bambusa Tulda species showed better performance in terms of mechanical strength compared to Bambusa Balcooa and Bambusa Nutan.
- The tensile strength of the composites (parallel to the fiber direction) is found to be much greater than the strength (perpendicular to the fiber direction).
- The developed composites showed stable behavior towards weight gain, thickness swelling, and width expansion against moisture attack compared to untreated samples. This behavior expands their widespread use in outdoor applications
- The bamboo composites showed almost similar specific strength to glass composites. Hence, it can be summarized that these composites can stand as an promising option offering comparable performance while addressing environmental concerns.
- The fatigue test was performed on raw bamboo and the bamboo composites. For raw bamboo, the fatigue limit is 10^6 at 45% of UTS i.e 57 *MPa*. The composite from the higher fiber density is found to have reached fatigue limit of 10^6 at 65% UTS i.e. 106 *MPa* and composite from less fiber density, the fatigue limit of 10^6 is reached at 80 *MPa* which is 55% of UTS. These values are almost similar to other engineering materials which signify that bamboo composites can sustain dynamic applications like wind turbine blade.

2. A detailed structural investigation, and validation of on the designed bamboo-based straight blade is successfully conducted. The major findings of the study are summarized below -

   - The values of bending stress and deflection of the symmetric NACA 0015 blade is found to be less compared to the non-symmetric NACA 4415 blade under the same loading conditions. The findings implies that the asymmetry in the blade design introduces greater structural weakness resulting in increased deformation and stress concentration.
   - The cross-ply [0°/90°/90°/0°] showed the minimum stress for both blade profiles. It signifies that by increasing the number of layers in the 90° direction, the materials ability to withstand loads in this direction increases leading in reduced maximum stress.
   - The effect of shear webs on the structural performance of the non-symmetric blade is analyzed and it is observed that by using a single shear web the deflection dropped down from 6.23 *mm* to 5.10 *mm*. For double-shear webs, the deflection value further dropped from 5.10 *mm* to 4.45 *mm*. These findings highlights the effectiveness of shear webs in enhancing the structural integrity of bamboo composite blades.
   - The assessment of maximum stress and deflection values for the non-symmetric blade with three shear webs indicates that the addition of these structural components have no discernible impact over the blade with double shear web. Additionally, these extra components increase the overal weight of the blades.
   - The maximum bending stress and deflection of the bamboo-epoxy NACA 4415 profile with the double-shear web are 15.84 *MPa* and 4.45 *mm* for [45°/90°/0°/-

$45°]_S$, and 20.47 MPa and 4.35 mm for $[60°/90°/0°/\text{-}60°]_S$. In comparison to $[45°/90°/0°/\text{-}45°]_S$, $[60°/90°/0°/\text{-}60°]_S$ orientation demonstrated slightly less deflection but higher bending stress. However, to minimize the composite shear effect 45° ply is the desired layup for wind turbine blade design.

- The stress and deflection value of the bamboo-epoxy composite blade is compared with the traditional glass-epoxy for the same composite layup. The significant reduction in maximum stress by 70.98% and deflection by 1.11% demonstrated superior mechanical performance of bamboo-epoxy composites over glass-composites. The comparison results highlights the importance of exploring natural composites to address sustainability concerns.

3. Further investigation is conducted for free and forced vibration of the bamboo-based straight blade. The following conclusions are drawn from the present results:

   - Three airfoil profiles are considered for the study and it is observed that the non-symmetric blade with double shear web obtained the high free-vibrational frequency values for respective four modes compared to the symmetric profile. A high value of natural frequency in blade indicates its resistance to higher frequency excitations thus reducing risk of dynamic instabilities and fatigue failure.

   - The effect of boundary condition is also analyzed for the non-symmetric blade and it is observed that the blade with boundary condition 1 has high frequency values than that with type 1 boundary condition. The findings suggest that the straight blade with two supports exhibited a stiff and compliant structure.

   - The bending and torsional modes are observed in the first three and fifth mode

shapes obtained from the FEM model of the non-symmteric blade. These modes indicates the blade response to the external forces and highlights the interaction between the bending and twisting deformation.

- The harmonic response is evaluated for the non-symmetric blade and it is observed that the maximum amplitude at their respective frequency matches with their natural frequency. This indicates the state of resonance in the wind turbine blade profiles which can lead to increase in vibration amplitude to blade fracture.
- The effect of percentage damping on the resonance frequency amplitude is studied and it is observed that the value of maximum amplitude decreased with the increase in damping percentage.

4. The fluid structure interaction (FSI) is successfully conducted on the 3 dimensional wind turbine blade. The following conclusions are drawn from the present results:

   - The aerodynamic simulation is carried out on the wind turbine and it is observed that maximum value of pressure is 1747.98 Pa which occurred at the windward side(pressure-side) for blade 1 and blade 2, and in the leeward side for blade 3.
   - The values of maximum and minimum deflection on the blades is 0.77 mm and 0.046 mm. These maximum deflection occurred near the leading and trailing edge of the blades. Compared to static structural results, there is a significant difference in the deflection value. This is mainly due to reduction in the length of the blade.
   - Similary, the values of maximum and minimum stress on the blades are

32.261 *MPa* and 3.740 *MPa*. The maximum stress in the blade occurred at the junction of blade strut connectors. The maximum value of stress is found to be comparatively less than allowable safe stress of the bamboo-epoxy material which indicates that the blade is safe from structural integrity.

- Finally, a prototype of the blade is developed using the hand-layup technique.

7.2 Futute Scope of Work

The future studies based on this work can be in following aspects:

- This study is focused on developing bamboo composite wind turbine blades. Further research can be carried out exploring different combinations of bio-based materials, such as flax, bamboo, etc to optimize the mechanical properties, durability, and sustainability of the composite material.
- The static and free vibration of the bamboo-based straight blade with uniform thickness across the blade cross-section is presented. Further analysis can be performed with optimized thicknesses for each section like spar cap, shear webs, etc. to reduce the overall weight of the blade.
- The FSI simulations can be carried out in detailed to access the structural integrity, fatigue life, and dynamic response of the bio-composite blades under different loading conditions.
- The developed prototype need to be tested in the wind tunnel to validate their aerodynamic performance and structural health over extended periods.

Bibliography

[1] Blaabjerg, F., and Ma, K., 2017. "Wind energy systems". *Proceedings of the IEEE,* **105**(11), pp. 2116–2131.

[2] Darwish, A. S., and Al-Dabbagh, R., 2020. "Wind energy state of the art: present and future technology advancements". *Renewable Energy and Environmental Sustainability,* **5**(7), p. 8.

[3] Sutherland, H. J., 2000. "A summary of the fatigue properties of wind turbine materials". *Wind Energy: An International Journal for Progress and Applications in Wind Power Conversion Technology,* **3**(1), pp. 1–34.

[4] Mishnaevsky Jr, L., Branner, K., Petersen, H. N., Beauson, J., McGugan, M., and Sørensen, B. F., 2017. "Materials for wind turbine blades: An overview". *Materials,* **10**(11), p. 1285.

[5] Tong, C., and Tong, C., 2019. "Advanced materials enable renewable wind energy capture and generation". *Introduction to Materials for Advanced Energy Systems*, pp. 379–444.

[6] Liu, P., and Barlow, C. Y., 2017. "Wind turbine blade waste in 2050". *Waste Management,* **62**, pp. 229–240.

[7] Malviya, R. K., Singh, R. K., Purohit, R., and Sinha, R., 2020. "Natural fibre reinforced composite materials: Environmentally better life cycle assessment-a case study". *Materials Today: Proceedings,* **26**(2), pp. 3157–3160.

[8] Miliket, T. A., Ageze, M. B., Tigabu, M. T., and Zeleke, M. A., 2022. "Experimental characterizations of hybrid natural fiber-reinforced composite for wind turbine blades". *Heliyon,* **8**(3), p. e09092.

[9] Ackermann, T., and Söder, L., 2000. "Wind energy technology and current status: a review". *Renewable and sustainable energy reviews,* **4**(4), pp. 315–374.

[10] Müller, G., Jentsch, M. F., and Stoddart, E., 2009. "Vertical axis resistance type wind turbines for use in buildings". *Renewable Energy,* **34**(5), pp. 1407–1412.

[11] Leung, D. Y., and Yang, Y., 2012. "Wind energy development and its environmental impact: A review". *Renewable and sustainable energy reviews,* **16**(1), pp. 1031–1039.

[12] Hepbasli, A., and Ozgener, O., 2004. "A review on the development of wind energy in turkey". *Renewable and Sustainable Energy Reviews,* **8**(3), pp. 257–276.

[13] Rehman, S., Alam, M. M., Alhems, L. M., and Rafique, M. M., 2018. "Horizontal axis wind turbine blade design methodologies for efficiency enhancement—a review". *Energies,* **11**(3), p. 506.

[14] Kumar, R., Raahemifar, K., and Fung, A. S., 2018. "A critical review of vertical axis wind turbines for urban applications". *Renewable and Sustainable Energy Reviews,* **89**, pp. 281–291.

[15] Kavade, R. K., and Ghanegaonkar, P. M., 2017. "Design and analysis of vertical axis wind turbine for household application". *Journal of Clean Energy Technologies,* **5**(5), pp. 353–358.

[16] Hand, B., and Cashman, A., 2020. "A review on the historical development of the lift-type vertical axis wind turbine: From onshore to offshore floating application". *Sustainable Energy Technologies and Assessments,* **38**, p. 100646.

[17] Tjiu, W., Marnoto, T., Mat, S., Ruslan, M. H., and Sopian, K., 2015. "Darrieus vertical axis wind turbine for power generation i: Assessment of darrieus vawt configurations". *Renewable energy,* **75**, pp. 50–67.

[18] Song, C., Wu, G., Zhu, W., Zhang, X., and Zhao, J., 2019. "Numerical investigation on the effects of airfoil leading edge radius on the aerodynamic performance of h-rotor darrieus vertical axis wind turbine". *Energies,* **12**(19), p. 3794.

[19] Santhakumar, S., Palanivel, I., and Venkatasubramanian, K., 2019. "Building a low cost wind turbine in highways for rural house electricity demand". *Environmental Progress & Sustainable Energy,* **38**(1), pp. 278–285.

[20] Bhuyan, S., and Biswas, A., 2014. "Investigations on self-starting and performance characteristics of simple h and hybrid h-savonius vertical axis wind rotors". *Energy Conversion and Management,* **87**, pp. 859–867.

[21] Das, P. P., and Chaudhary, V., 2021. "Moving towards the era of bio fibre based polymer composites". *Cleaner engineering and technology,* **4**, p. 100182.

[22] Šercer, M., Raos, P., and Rujnić-Sokele, M., 2009. "Processing of wood-thermoplastic composites". *International Journal of Material Forming,* **2**, pp. 721–724.

[23] Garcia, M., Hidalgo, J., Garmendia, I., and García-Jaca, J., 2009. "Wood–plastics

composites with better fire retardancy and durability performance". *Composites Part A: Applied Science and Manufacturing,* **40**(11), pp. 1772–1776.

[24] Gholampour, A., and Ozbakkaloglu, T., 2020. "A review of natural fiber composites: Properties, modification and processing techniques, characterization, applications". *Journal of Materials Science,* **55**(3), pp. 829–892.

[25] Ku, H., Wang, H., Pattarachaiyakoop, N., and Trada, M., 2011. "A review on the tensile properties of natural fiber reinforced polymer composites". *Composites Part B: Engineering,* **42**(4), pp. 856–873.

[26] Karimah, A., Ridho, M. R., Munawar, S. S., Adi, D. S., Damayanti, R., Subiyanto, B., Fatriasari, W., Fudholi, A., et al., 2021. "A review on natural fibers for development of eco-friendly bio-composite: characteristics, and utilizations". *Journal of materials research and technology,* **13**, pp. 2442–2458.

[27] Keller, A., Leupin, M., Mediavilla, V., and Wintermantel, E., 2001. "Influence of the growth stage of industrial hemp on chemical and physical properties of the fibres". *Industrial crops and products,* **13**(1), pp. 35–48.

[28] Zhou, Y., Fan, M., and Chen, L., 2016. "Interface and bonding mechanisms of plant fibre composites: An overview". *Composites Part B: Engineering,* **101**, pp. 31–45.

[29] Latif, R., Wakeel, S., Zaman Khan, N., Noor Siddiquee, A., Lal Verma, S., and Akhtar Khan, Z., 2019. "Surface treatments of plant fibers and their effects on mechanical properties of fiber-reinforced composites: A review". *Journal of Reinforced Plastics and Composites,* **38**(1), pp. 15–30.

[30] Herlina Sari, N., Wardana, I., Irawan, Y. S., and Siswanto, E., 2018. "Characteri-

zation of the chemical, physical, and mechanical properties of naoh-treated natural cellulosic fibers from corn husks". *Journal of Natural Fibers,* **15**(4), pp. 545–558.

[31] Sanjay, M. R., Arpitha, G., and Yogesha, B., 2015. "Study on mechanical properties of natural-glass fibre reinforced polymer hybrid composites: A review". *Materials today: proceedings,* **2**(4-5), pp. 2959–2967.

[32] Wang, M., Cai, X., Lu, Y., Noori, A., Chen, F., Chen, L., Jiang, X., and Liu, J., 2021. "Tensile mechanical properties and failure mechanism of bamboo scrimber under different strain rates". *Construction and Building Materials,* **299**(5), p. 124258.

[33] Nkeuwa, W. N., Zhang, J., Semple, K. E., Chen, M., Xia, Y., and Dai, C., 2022. "Bamboo-based composites: A review on fundamentals and processes of bamboo bonding". *Composites Part B: Engineering,* **235**, p. 109776.

[34] Shah, A. U. M., Sultan, M. T. H., Jawaid, M., Cardona, F., and Talib, A. R. A., 2016. "A review on the tensile properties of bamboo fiber reinforced polymer composites". *BioResources,* **11**(4), pp. 10654–10676.

[35] Verma, C. S., Sharma, N. K., Chariar, V., Maheshwari, S., and Hada, M., 2014. "Comparative study of mechanical properties of bamboo laminae and their laminates with woods and wood based composites". *Composites Part B: Engineering,* **60**, pp. 523–530.

[36] Appiah-Kubi, E., Owusu, F., Tekpetey, S., Essien, C., Seidu, H., et al., 2014. "Investigating the mechanical properties of some bamboo species for efficient utilization in ghana". *Journal of Bamboo and Rattan,* **13**(3/4), pp. 81–89.

[37] Yu, Y., Liu, R., Huang, Y., Meng, F., and Yu, W., 2017. "Preparation, physical, mechanical, and interfacial morphological properties of engineered bamboo scrimber". *Construction and Building Materials,* **157**, pp. 1032–1039.

[38] Rassiah, K., Ahmad, M. M., and Ali, A., 2014. "Mechanical properties of laminated bamboo strips from gigantochloa scortechinii/polyester composites". *Materials & Design,* **57**, pp. 551–559.

[39] Al-Rukaibawi, L. S., Omairey, S. L., and Károlyi, G., 2021. "A numerical anatomy-based modelling of bamboo microstructure". *Construction and Building Materials,* **308**(6), p. 125036.

[40] Nahar, S., and Hasan, M., 2013. "Effect of chemical composition, anatomy and cell wall structure on tensile properties of bamboo fiber". *Engineering Journal,* **17**(1), pp. 61–68.

[41] Kaur, P. J., 2018. "Bamboo availability and utilization potential as a building material". *Forestry Research and Engineering: International Journal,* **2**(5), pp. 240–242.

[42] Elejoste, A., Arevalillo, A., Gabilondo, N., Butron, A., and Peña-Rodriguez, C., 2021. "Morphological analysis of several bamboo species with potential structural applications". *Polymers,* **13**(13), p. 2126.

[43] Muhammad, A., Rahman, M. R., Hamdan, S., and Sanaullah, K., 2019. "Recent developments in bamboo fiber-based composites: a review". *Polymer bulletin,* **76**(5), pp. 2655–2682.

[44] Chaowana, P., 2013. "Bamboo: an alternative raw material for wood and wood-based composites". *Journal of Materials Science Research,* **2**(2), p. 90.

[45] Sawarkar, A. D., Shrimankar, D. D., Kumar, A., Kumar, A., Singh, E., Singh, L., Kumar, S., and Kumar, R., 2020. "Commercial clustering of sustainable bamboo species in india". *Industrial Crops and Products,* **154**, p. 112693.

[46] Rampal, T., Chawra, B., Goel, A. M., Taneja, A. R., and Taneja, A. P., 2023. "Potential use of bamboo as a sustainable material in construction in india: A survey of literature". *Journal of the International Society for the Study of Vernacular Settlements,* **10**(9), pp. 90–103.

[47] Zakikhani, P., Zahari, R., Sultan, M., and Majid, D., 2014. "Extraction and preparation of bamboo fibre-reinforced composites". *Materials & Design,* **63**, pp. 820–828.

[48] Okubo, K., Fujii, T., and Yamamoto, Y., 2004. "Development of bamboo-based polymer composites and their mechanical properties". *Composites Part A: Applied science and manufacturing,* **35**(3), pp. 377–383.

[49] Rao, K. M. M., and Rao, K. M., 2007. "Extraction and tensile properties of natural fibers: Vakka, date and bamboo". *Composite structures,* **77**(3), pp. 288–295.

[50] Zhang, X., Fu, J., Paulo, A. C., Yu, C., and Guebitz, G., 2012. "Bioprocessing of bamboo materials". *Fibres and Textiles in Eastern Europe,* **90**(1), pp. 13–19.

[51] Phong, N. T., Fujii, T., Chuong, B., and Okubo, K., 2012. "Study on how to effectively extract bamboo fibers from raw bamboo and wastewater treatment". *Journal of Materials Science Research,* **1**(1), p. 144.

[52] Ashimori, M., Katayama, T., Aoyama, E., and Nagai, S., 2004. "Study on splitting of bamboo fibers due to freezing and tensile strength of frtp using bamboo fibers".

JSME International Journal Series A Solid Mechanics and Material Engineering, **47**(4), pp. 566–569.

[53] Kim, H., Okubo, K., Fujii, T., and Takemura, K., 2013. "Influence of fiber extraction and surface modification on mechanical properties of green composites with bamboo fiber". *Journal of Adhesion Science and Technology,* **27**(12), pp. 1348–1358.

[54] Das, M., and Chakraborty, D., 2008. "Evaluation of improvement of physical and mechanical properties of bamboo fibers due to alkali treatment". *Journal of applied polymer science,* **107**(1), pp. 522–527.

[55] Kaur, V., Chattopadhyay, D., and Kaur, S., 2013. "Study on extraction of bamboo fibres from raw bamboo fibres bundles using different retting techniques". *Text. Light Ind. Sci. Technol,* **2**(4), pp. 174–179.

[56] Rocky, B. P., and Thompson, A. J., 2018. "Production of natural bamboo fibers-1: Experimental approaches to different processes and analyses". *The Journal of the Textile Institute,* **109**(10), pp. 1381–1391.

[57] Verma, Y. K., Singh, A. K., Paswan, M., and Gurmaita, P. K., 2023. "A novel approach to extract and characterize vacuum-pressurized bamboo fibers using mechano-chemical techniques". *Journal of Wood Chemistry and Technology,* **43**(4), pp. 230–242.

[58] Kaur, N., Saxena, S., Gaur, H., and Goyal, P., 2017. "A review on bamboo fiber composites and its applications". In 2017 International Conference on Infocom Technologies and Unmanned Systems (Trends and Future Directions), IEEE, pp. 843–849.

[59] Puttegowda, M., Rangappa, S. M., Jawaid, M., Shivanna, P., Basavegowda, Y., and Saba, N., 2018. "Potential of natural/synthetic hybrid composites for aerospace applications". In *Sustainable composites for aerospace applications*. Elsevier, pp. 315–351.

[60] Sanjay, M., Arpitha, G., Naik, L. L., Gopalakrishna, K., and Yogesha, B., 2016. "Applications of natural fibers and its composites: an overview". *Natural Resources,* **7**(3), pp. 108–114.

[61] Liu, L., Yuan, Z., Fan, X., Pan, C., and Li, X., 2021. "A review of interfacial bonding mechanism of bamboo fiber reinforced polymer composites". *Cellulose,* **29**(3), pp. 1–18.

[62] Suhaily, S. S., Khalil, H. A., Nadirah, W. W., and Jawaid, M., 2013. "Bamboo based biocomposites material, design and applications". In *Materials science-advanced topics*. IntechOpen.

[63] Liu, D., Song, J., Anderson, D. P., Chang, P. R., and Hua, Y., 2012. "Bamboo fiber and its reinforced composites: structure and properties". *Cellulose,* **19**(5), pp. 1449–1480.

[64] Bala, A., and Gupta, S., 2023. "Engineered bamboo and bamboo-reinforced concrete elements as sustainable building materials: A review". *Construction and Building Materials,* **394**(5), p. 132116.

[65] Puri, V., Chakrabortty, P., Anand, S., and Majumdar, S., 2017. "Bamboo reinforced prefabricated wall panels for low cost housing". *Journal of Building Engineering,* **9**, pp. 52–59.

[66] Khan, Z. I., Arsad, A., Mohamad, Z., Habib, U., and Zaini, M. A. A., 2021. "Comparative study on the enhancement of thermo-mechanical properties of carbon fiber and glass fiber reinforced epoxy composites". *Materials Today: Proceedings,* **39**(15), pp. 956–958.

[67] Prasad, V. V., and Talupula, S., 2018. "A review on reinforcement of basalt and aramid (kevlar 129) fibers". *Materials Today: Proceedings,* **5**(2), pp. 5993–5998.

[68] Mengal, A. N., Karuppanan, S., and Wahab, A. A., 2014. "Basalt carbon hybrid composite for wind turbine rotor blades: A short review". *Advanced Materials Research,* **970**, pp. 67–73.

[69] Reddy, S. S. P., Suresh, R., MB, H., and Shivakumar, B., 2021. "Use of composite materials and hybrid composites in wind turbine blades". *Materials Today: Proceedings,* **46**(11), pp. 2827–2830.

[70] Katnam, K., Comer, A., Roy, D., Da Silva, L., and Young, T., 2015. "Composite repair in wind turbine blades: an overview". *The Journal of Adhesion,* **91**(1-2), pp. 113–139.

[71] Heng, H., Meng, F., and McKechnie, J., 2021. "Wind turbine blade wastes and the environmental impacts in canada". *Waste Management,* **133**(19), pp. 59–70.

[72] Fayyaz, S., Lund, K. W., Khoshnevisan, B., Madsen, E. S., and Birkved, M., 2023. "Sustainable end-of-life value chain scenarios for wind turbine blades". In Journal of Physics: Conference Series, Vol. 2507, IOP Publishing, p. 012007.

[73] Rani, M., Choudhary, P., Krishnan, V., and Zafar, S., 2021. "A review on recycling

and reuse methods for carbon fiber/glass fiber composites waste from wind turbine blades". *Composites part B: engineering,* **215**, p. 108768.

[74] Mishnaevsky Jr, L., Freere, P., Sinha, R., Acharya, P., Shrestha, R., and Manandhar, P., 2011. "Small wind turbines with timber blades for developing countries: Materials choice, development, installation and experiences". *Renewable Energy,* **36**(8), pp. 2128–2138.

[75] Astle, C., Burge, I., Chen, M., Herrler, T., Kwan, L., Zibin, N., and Wood, D., 2013. "Timber for small wind turbine blades". *Energy for Sustainable Development,* **17**(6), pp. 671–676.

[76] Pourrajabian, A., Dehghan, M., Javed, A., and Wood, D., 2019. "Choosing an appropriate timber for a small wind turbine blade: A comparative study". *Renewable and Sustainable Energy Reviews,* **100**(11), pp. 1–8.

[77] Peterson, P., and Clausen, P., 2004. "Timber for high efficiency small wind turbine blades". *Wind Engineering,* **28**(1), pp. 87–96.

[78] Sinha, R., Acharya, P., Freere, P., Sharma, R., Ghimire, P., and Mishnaevsky Jr, L., 2010. "Selection of nepalese timber for small wind turbine blade construction". *Wind Engineering,* **34**(3), pp. 263–276.

[79] Jackson, K., Zuteck, M. v., Van Dam, C., Standish, K., and Berry, D., 2005. "Innovative design approaches for large wind turbine blades". *Wind Energy: An International Journal for Progress and Applications in Wind Power Conversion Technology,* **8**(2), pp. 141–171.

[80] Kalagi, G. R., Patil, R., and Nayak, N., 2018. "Experimental study on mechanical

properties of natural fiber reinforced polymer composite materials for wind turbine blades". *Materials Today: Proceedings,* **5**(1), pp. 2588–2596.

[81] Batu, T., Lemu, H. G., and Sirhabizuh, B., 2020. "Study of the performance of natural fiber reinforced composites for wind turbine blade applications". *Advances in Science and Technology. Research Journal,* **14**(2).

[82] Boria, S., Santulli, C., Raponi, E., Sarasini, F., and Tirillò, J., 2019. "Evaluation of a new green composite solution for wind turbine blades". *Multiscale and Multidisciplinary Modeling, Experiments and Design,* **2**(4), pp. 141–150.

[83] Holmes, J. W., Brøndsted, P., Sørensen, B. F., Jiang, Z., Sun, Z., and Chen, X., 2009. "Development of a bamboo-based composite as a sustainable green material for wind turbine blades". *Wind Engineering,* **33**(2), pp. 197–210.

[84] Huang, X.-D., Hse, C.-Y., and Shupe, T. F., 2015. "Evaluation of the performance of the composite bamboo/epoxy laminated material for wind turbine blades technology". *BioResources,* **10**(1), pp. 660–671.

[85] Shah, D. U., Schubel, P. J., and Clifford, M. J., 2013. "Can flax replace e-glass in structural composites: A small wind turbine blade case study". *Composites Part B: Engineering,* **52**, pp. 172–181.

[86] Asim, M., Paridah, M. T., Chandrasekar, M., Shahroze, R. M., Jawaid, M., Nasir, M., and Siakeng, R., 2020. "Thermal stability of natural fibers and their polymer composites". *Iranian Polymer Journal,* **29**(7), pp. 625–648.

[87] Mohanty, S., and Nayak, S. K., 2010. "Short bamboo fiber-reinforced hdpe com-

posites: influence of fiber content and modification on strength of the composite". *Journal of Reinforced Plastics and Composites,* **29**(14), pp. 2199–2210.

[88] Lokesh, P., Kumari, T. S., Gopi, R., and Loganathan, G. B., 2020. "A study on mechanical properties of bamboo fiber reinforced polymer composite". *Materials Today: Proceedings,* **22**(8), pp. 897–903.

[89] Saba, N., Jawaid, M., Alothman, O. Y., Paridah, M., and Hassan, A., 2016. "Recent advances in epoxy resin, natural fiber-reinforced epoxy composites and their applications". *Journal of Reinforced Plastics and Composites,* **35**(6), pp. 447–470.

[90] Samanta, B., Maity, T., Dalai, S., and Banthia, A., 2006. "Mechanical properties of modified epoxy: effect of chain length". *Pigment & resin technology,* **35**(4), pp. 216–223.

[91] Chin, S. C., Tee, K. F., Tong, F. S., Ong, H. R., and Gimbun, J., 2020. "Thermal and mechanical properties of bamboo fiber reinforced composites". *Materials Today Communications,* **23**, p. 100876.

[92] Hou, Y., Zhang, K., Noori, A., Lu, Y., Zhang, Y., Chen, J., and Ke, J., 2023. "Experimental investigation on mechanical properties of aged bamboo fiber-reinforced composites under quasi-static loading". *Journal of the Mechanical Behavior of Biomedical Materials,* **143**(5), p. 105869.

[93] Barman, P., Dutta, P. P., Bardalai, M., and Dutta, P. P., 2023. "Experimental investigation on bamboo fiber reinforced epoxy polymer composite materials developed through two different techniques". *Proceedings of the Institution of Mechanical Engineers, Part C: Journal of Mechanical Engineering Science,* **0**(0), p. 09544062231195474.

[94] Osorio, L., Trujillo, E., Van Vuure, A. W., and Verpoest, I., 2011. "Morphological aspects and mechanical properties of single bamboo fibers and flexural characterization of bamboo/epoxy composites". *Journal of reinforced plastics and composites,* **30**(5), pp. 396–408.

[95] Awalluddin, D., Ariffin, M. A. M., Osman, M. H., Hussin, M. W., Ismail, M. A., Lee, H.-S., and Lim, N. H. A. S., 2017. "Mechanical properties of different bamboo species". In MATEC web of conferences, Vol. 138, EDP Sciences, p. 01024.

[96] Kumar, P., Gautam, P., Kaur, S., Chaudhary, M., Afreen, A., and Mehta, T., 2021. "Bamboo as reinforcement in structural concrete". *Materials Today: Proceedings,* **46**, pp. 6793–6799.

[97] Fadlelmola, A. B. F. A., Chen, Z., Du, Y., Ma, R., and Ma, J., 2021. "Experimental investigations and design method on a lightweight bamboo-concrete sandwich panel under axial load". *Journal of Building Engineering,* **42**, p. 103077.

[98] Wang, C., Song, W., Cheng, H., Yu, X., Li, W., and Zhang, S., 2016. "Dipping modification with nano-caco3 to improve tensile properties of individual bamboo fiber for developing bamboo–plastic composite". *Journal of Natural Fibers,* **13**(6), pp. 737–748.

[99] Chen, H., Yu, Y., Zhong, T., Wu, Y., Li, Y., Wu, Z., and Fei, B., 2017. "Effect of alkali treatment on microstructure and mechanical properties of individual bamboo fibers". *Cellulose,* **24**(1), pp. 333–347.

[100] Manalo, A. C., Wani, E., Zukarnain, N. A., Karunasena, W., and Lau, K.-t., 2015. "Effects of alkali treatment and elevated temperature on the mechanical proper-

ties of bamboo fibre–polyester composites". *Composites Part B: Engineering,* **80**, pp. 73–83.

[101] Behera, S., Prasad, N., and Kumar, S., 2018. "Study of mechanical properties of bamboo fibers before and after alkali treatment". *International Journal of Applied Engineering Research,* **13**(7), pp. 5251–5255.

[102] Wang, F., Zhou, S., Li, L., and Zhang, X., 2018. "Changes in the morphological–mechanical properties and thermal stability of bamboo fibers during the processing of alkaline treatment". *Polymer Composites,* **39**(S3), pp. E1421–E1428.

[103] Kaima, J., Preechawuttipong, I., Peyroux, R., Jongchansitto, P., and Kaima, T., 2023. "Experimental investigation of alkaline treatment processes (naoh, koh and ash) on tensile strength of the bamboo fiber bundle". *Results in Engineering,* **18**(5), p. 101186.

[104] Zhang, K., Wang, F., Liang, W., Wang, Z., Duan, Z., and Yang, B., 2018. "Thermal and mechanical properties of bamboo fiber reinforced epoxy composites". *Polymers,* **10**(6), p. 608.

[105] Asif, M., Rahman, K. A., Faisal, M. O., and Islam, M. S., 2020. "Comparative study on mechanical properties of bamboo and bamboo-glass fiber reinforced hybrid composites". *Journal of Engineering Advancements,* **1**(01), pp. 06–10.

[106] Bako, R., Djafar, Z., Renreng, I., Wullur, C., et al., 2019. "Analysis of mechanical strength of woven strip composite at petung bamboo (dendrocalamus asper) epoxy resin tape: tensile strength properties of bamboo strips". In IOP Conference Series: Earth and Environmental Science, Vol. 343, IOP Publishing, p. 012192.

[107] Sumardi, I., Dungani, R., Sulastiningsih, I., and Amalia, D., 2020. "Effect of combined strip and zephyr laminated bamboo composite on physical and mechanical properties". In IOP Conference Series: Materials Science and Engineering, Vol. 935, IOP Publishing, p. 012010.

[108] Keogh, L., O'Hanlon, P., O'Reilly, P., and Taylor, D., 2015. "Fatigue in bamboo". *International Journal of Fatigue,* **75**, pp. 51–56.

[109] Song, J., Surjadi, J. U., Hu, D., and Lu, Y., 2017. "Fatigue characterization of structural bamboo materials under flexural bending". *International Journal of Fatigue,* **100**, pp. 126–135.

[110] Ali, A., Rassiah, K., Othman, F., Lee, H. P., Tay, T. E., Hazin, M. S., and Ahmad, M. M. H. M., 2016. "Fatigue and fracture properties of laminated bamboo strips from gigantochloa scortechinii polyester composites". *BioResources,* **11**(4), pp. 9142–9153.

[111] Onche, E. O., Oyewole, O. K., Obayemi, J. D., Ekwe, N. B., Rahbar, N., and Soboyejo, W. O., 2021. "Fracture and fatigue behavior of bambusa vulgaris-schrad bamboo". *Cogent Engineering,* **8**(1), p. 1914289.

[112] Amada, S., and Untao, S., 2001. "Fracture properties of bamboo". *Composites Part B: Engineering,* **32**(5), pp. 451–459.

[113] Mannan, S., Parameswaran, V., and Basu, S., 2018. "Stiffness and toughness gradation of bamboo from a damage tolerance perspective". *International Journal of Solids and Structures,* **143**, pp. 274–286.

[114] Khan, Z., Yousif, B., and Islam, M., 2017. "Fracture behaviour of bamboo fiber reinforced epoxy composites". *Composites Part B: Engineering,* **116**, pp. 186–199.

[115] Wong, K., Zahi, S., Low, K., and Lim, C., 2010. "Fracture characterisation of short bamboo fibre reinforced polyester composites". *Materials & Design,* **31**(9), pp. 4147–4154.

[116] Scherer, J. F., Bom, R. P., and Barbieri, R., 2020. "Torsional fatigue in bamboo fibers reinforced epoxy resin composites". *Engineering Research Express,* **2**(1), p. 015018.

[117] Thwe, M. M., and Liao, K., 2003. "Durability of bamboo-glass fiber reinforced polymer matrix hybrid composites". *Composites science and technology,* **63**(3-4), pp. 375–387.

[118] Subramanian, A., Yogesh, S. A., Sivanandan, H., Giri, A., Vasudevan, M., Mugundhan, V., and Velamati, R. K., 2017. "Effect of airfoil and solidity on performance of small scale vertical axis wind turbine using three dimensional cfd model". *Energy,* **133**, pp. 179–190.

[119] Mohamed, M., 2012. "Performance investigation of h-rotor darrieus turbine with new airfoil shapes". *Energy,* **47**(1), pp. 522–530.

[120] Wang, Y., Shen, S., Li, G., Huang, D., and Zheng, Z., 2018. "Investigation on aerodynamic performance of vertical axis wind turbine with different series airfoil shapes". *Renewable energy,* **126**, pp. 801–818.

[121] Kanyako, F., and Janajreh, I., 2014. "Numerical investigation of four commonly

used airfoils for vertical axis wind turbine". In ICREGA'14-Renewable Energy: Generation and Applications, Springer, pp. 443–454.

[122] Mohamed, M., Ali, A., and Hafiz, A., 2015. "Cfd analysis for h-rotor darrieus turbine as a low speed wind energy converter". *Engineering Science and Technology, an International Journal,* **18**(1), pp. 1–13.

[123] Maleki Dastjerdi, S., HormoziNejad, A., Gharali, K., and Nathwani, J., 2021. "Numerical investigation of vawt airfoil shapes on power extraction and self-starting purposes". In Recent Developments in Mathematical, Statistical and Computational Sciences: The V AMMCS International Conference, Waterloo, Canada, August 18–23, 2019, Springer, pp. 383–392.

[124] Kumar, R., and Sarkar, S., 2022. "Effect of design parameters on the performance of helical darrieus hydrokinetic turbines". *Renewable and Sustainable Energy Reviews,* **162**, p. 112431.

[125] Liu, Q., Miao, W., Ye, Q., and Li, C., 2022. "Performance assessment of an innovative gurney flap for straight-bladed vertical axis wind turbine". *Renewable Energy,* **185**(117), pp. 1124–1138.

[126] Tong, H., and Wang, Y., 2021. "Experimental study on unsteady aerodynamic characteristics of deformed blades for vertical axis wind turbine". *Renewable energy,* **173**(8), pp. 808–826.

[127] Butbul, J., MacPhee, D., and Beyene, A., 2015. "The impact of inertial forces on morphing wind turbine blade in vertical axis configuration". *Energy Conversion and Management,* **91**, pp. 54–62.

[128] Eriksson, S., Bernhoff, H., and Leijon, M., 2008. "Evaluation of different turbine concepts for wind power". *Renewable and sustainable energy reviews,* **12**(5), pp. 1419–1434.

[129] Raj, E. F. I., Appadurai, M., Ram, V., Gnaniah, A. M., and Salkuti, S. R., 2023. "Natural-fibre-reinforced composite-based micro-size wind turbines: Numerical analysis and feasibility study". *Journal of Composites Science,* **7**(5), p. 197.

[130] Hameed, M. S., Afaq, S. K., and Shahid, F., 2015. "Finite element analysis of a composite vawt blade". *Ocean Engineering,* **109**, pp. 669–676.

[131] Hand, B., Kelly, G., and Cashman, A., 2021. "Structural analysis of an offshore vertical axis wind turbine composite blade experiencing an extreme wind load". *Marine Structures,* **75**, p. 102858.

[132] Muggiasca, S., Taruffi, F., Fontanella, A., Di Carlo, S., Giberti, H., Facchinetti, A., and Belloli, M., 2021. "Design of an aeroelastic physical model of the dtu 10mw wind turbine for a floating offshore multipurpose platform prototype". *Ocean Engineering,* **239**(9), p. 109837.

[133] Wang, L., Liu, X., Guo, L., Renevier, N., and Stables, M., 2014. "A mathematical model for calculating cross-sectional properties of modern wind turbine composite blades". *Renewable Energy,* **64**, pp. 52–60.

[134] Wang, L., Kolios, A., Nishino, T., Delafin, P.-L., and Bird, T., 2016. "Structural optimisation of vertical-axis wind turbine composite blades based on finite element analysis and genetic algorithm". *Composite Structures,* **153**, pp. 123–138.

[135] Barnes, R., and Morozov, E., 2016. "Structural optimisation of composite wind

turbine blade structures with variations of internal geometry configuration". *Composite Structures,* **152**, pp. 158–167.

[136] Guo, J., Zeng, P., and Lei, L., 2020. "Structure analysis of an innovative vertical axis wind turbine with inclined pitch axes using finite element method". In IOP Conference Series: Materials Science and Engineering, Vol. 825, IOP Publishing, p. 012004.

[137] Lin, J., Xu, Y.-l., and Xia, Y., 2019. "Structural analysis of large-scale vertical axis wind turbines part ii: Fatigue and ultimate strength analyses". *Energies,* **12**(13), p. 2584.

[138] Brown, K., and Brooks, R., 2010. "Design and analysis of vertical axis thermoplastic composite wind turbine blade". *Plastics, rubber and composites,* **39**(3-5), pp. 111–121.

[139] Shohag, M. A. S., Hammel, E. C., Olawale, D. O., and Okoli, O. I., 2017. "Damage mitigation techniques in wind turbine blades: A review". *Wind Engineering,* **41**(3), pp. 185–210.

[140] Finnegan, W., Jiang, Y., Dumergue, N., Davies, P., and Goggins, J., 2021. "Investigation and validation of numerical models for composite wind turbine blades". *Journal of Marine Science and Engineering,* **9**(5), p. 525.

[141] Ferroudji, F., Khelifi, C., and Meguellati, F., 2016. "Modal analysis of a small h-darrieus wind turbine based on 3d cad, fea". *International Journal of Renewable Energy Research,* **6**(2), pp. 637–643.

[142] Maalawi, K. Y., and Negm, H. M., 2002. "Optimal frequency design of wind

turbine blades". *Journal of Wind Engineering and Industrial Aerodynamics,* **90**(8), pp. 961–986.

[143] Verkinderen, E., and Imam, B., 2015. "A simplified dynamic model for mast design of h-darrieus vertical axis wind turbines (vawts)". *Engineering structures,* **100**(4), pp. 564–576.

[144] Alaimo, A., Iacono, F. L., Navarra, G., and Pipitone, G., 2016. "Numerical and experimental comparison between two different blade configurations of a wind generator". *Composite Structures,* **136**, pp. 526–537.

[145] Wang, Y., Lu, W., Dai, K., Yuan, M., and Chen, S.-E., 2018. "Dynamic study of a rooftop vertical axis wind turbine tower based on an automated vibration data processing algorithm". *Energies,* **11**(11), p. 3135.

[146] Mabrouk, I. B., El Hami, A., Walha, L., Zghal, B., and Haddar, M., 2017. "Dynamic vibrations in wind energy systems: Application to vertical axis wind turbine". *Mechanical Systems and Signal Processing,* **85**, pp. 396–414.

[147] Tong, M., Zhu, W., Zhao, X., Yu, M., Liu, K., and Li, G., 2020. "Free and forced vibration analysis of h-type and hybrid vertical-axis wind turbines". *Energies,* **13**(24), p. 6747.

[148] Dey, S., Mukhopadhyay, T., Spickenheuer, A., Adhikari, S., and Heinrich, G., 2016. "Bottom up surrogate based approach for stochastic frequency response analysis of laminated composite plates". *Composite Structures,* **140**, pp. 712–727.

[149] Wang, L., Quant, R., and Kolios, A., 2016. "Fluid structure interaction modelling

of horizontal-axis wind turbine blades based on cfd and fea". *Journal of Wind Engineering and Industrial Aerodynamics,* **158**, pp. 11–25.

[150] Liu, X., Wang, L., and Tang, X., 2013. "Optimized linearization of chord and twist angle profiles for fixed-pitch fixed-speed wind turbine blades". *Renewable Energy,* **57**, pp. 111–119.

[151] Shourangiz-Haghighi, A., Haghnegahdar, M. A., Wang, L., Mussetta, M., Kolios, A., and Lander, M., 2020. "State of the art in the optimisation of wind turbine performance using cfd". *Archives of Computational Methods in Engineering,* **27**(5), pp. 413–431.

[152] Masters, I., Malki, R., Williams, A. J., and Croft, T. N., 2013. "The influence of flow acceleration on tidal stream turbine wake dynamics: A numerical study using a coupled bem–cfd model". *Applied Mathematical Modelling,* **37**(16-17), pp. 7905–7918.

[153] Zhang, P., and Huang, S., 2011. "Review of aeroelasticity for wind turbine: Current status, research focus and future perspectives". *Frontiers in Energy,* **5**(4), pp. 419–434.

[154] Bazilevs, Y., Korobenko, A., Deng, X., Yan, J., Kinzel, M., and Dabiri, J., 2014. "Fluid–structure interaction modeling of vertical-axis wind turbines". *Journal of Applied Mechanics,* **81**(8), p. 081006.

[155] MacPhee, D. W., and Beyene, A., 2016. "Fluid–structure interaction analysis of a morphing vertical axis wind turbine". *Journal of Fluids and Structures,* **60**, pp. 143–159.

[156] Arora, P., Parmeshwar Atkale, P., Prasad Patel, B., and Ahmad, S., 2023. "Response analysis of composite blades of offshore vawt using cfd and fsi for the indian ocean". In International Conference on Offshore Mechanics and Arctic Engineering, Vol. 86847, American Society of Mechanical Engineers, p. V002T02A047.

[157] Marzec, Ł., Buliński, Z., Krysiński, T., and Tumidajski, J., 2023. "Structural optimisation of h-rotor wind turbine blade based on one-way fluid structure interaction approach". *Renewable Energy,* **216**, p. 118957.

[158] Madapur, A., Malge, A., and Pawar, P. M., 2020. "Fluid-structure interaction analysis of multi-storey vertical axis wind turbine". In Techno-Societal 2018: Proceedings of the 2nd International Conference on Advanced Technologies for Societal Applications-Volume 2, Springer, pp. 693–703.

[159] Huda, S., Reddy, N., and Yang, Y., 2012. "Ultra-light-weight composites from bamboo strips and polypropylene web with exceptional flexural properties". *Composites Part B: Engineering,* **43**(3), pp. 1658–1664.

[160] Asim, M., Jawaid, M., Fouad, H., and Alothman, O., 2021. "Effect of surface modified date palm fibre loading on mechanical, thermal properties of date palm reinforced phenolic composites". *Composite Structures,* **267**(2), p. 113913.

[161] Zhao, X., Tu, W., Chen, Q., and Wang, G., 2021. "Progressive modeling of transverse thermal conductivity of unidirectional natural fiber composites". *International Journal of Thermal Sciences,* **162**, p. 106782.

[162] Greszczuk, L., 1969. "Theoretical studies of the mechanics of the fiber-matrix interface in composites".

[163] Wu, Y., Zheng, Y., Yang, F., and Yang, L., 2021. "Preparation process and characterization of mechanical properties of twisted bamboo spun fiber bundles". *Journal of Materials Research and Technology,* **14**(1), pp. 2131–2139.

[164] Abdullah, C. K., Jawaid, M., Khalil, H. A., Zaidon, A., and Hadiyane, A., 2012. "Oil palm trunk polymer composite: morphology, water absorption, and thickness swelling behaviours". *BioResources,* **7**(3), pp. 2948–2959.

[165] Sukmawan, R., Takagi, H., and Nakagaito, A. N., 2016. "Strength evaluation of cross-ply green composite laminates reinforced by bamboo fiber". *Composites Part B: Engineering,* **84**, pp. 9–16.

[166] Cai, Q., Fan, Z., Chen, J., Guo, W., Ma, F., Sun, S., Hu, L., and Zhou, Q., 2018. "Dissolving process of bamboo powder analyzed by ft-ir spectroscopy". *Journal of Molecular Structure,* **1171**, pp. 639–643.

[167] Xu, G., Wang, L., Liu, J., and Wu, J., 2013. "Ftir and xps analysis of the changes in bamboo chemical structure decayed by white-rot and brown-rot fungi". *Applied Surface Science,* **280**(2), pp. 799–805.

[168] Li, Z., Chen, C., Mi, R., Gan, W., Dai, J., Jiao, M., Xie, H., Yao, Y., Xiao, S., and Hu, L., 2020. "A strong, tough, and scalable structural material from fast-growing bamboo". *Advanced Materials,* **32**(10), p. 1906308.

[169] Liang, R., Zhu, Y.-H., Wen, L., Zhao, W.-W., Kuai, B.-B., Zhang, Y.-L., and Cai, L.-P., 2020. "Exploration of effect of delignification on the mesopore structure in poplar cell wall by nitrogen absorption method". *Cellulose,* **27**, pp. 1921–1932.

[170] Md Shah, A. U., Sultan, M. T., and Jawaid, M., 2021. "Sandwich-structured

bamboo powder/glass fibre-reinforced epoxy hybrid composites–mechanical performance in static and dynamic evaluations". *Journal of Sandwich Structures & Materials,* **23**(1), pp. 47–64.

[171] Kushwaha, P. K., and Kumar, R., 2011. "Influence of chemical treatments on the mechanical and water absorption properties of bamboo fiber composites". *Journal of Reinforced Plastics and Composites,* **30**(1), pp. 73–85.

[172] Yang, D., Li, H., Xiong, Z., Mimendi, L., Lorenzo, R., Corbi, I., Corbi, O., and Hong, C., 2020. "Mechanical properties of laminated bamboo under off-axis compression". *Composites Part A: Applied Science and Manufacturing,* **138**, p. 106042.

[173] Jawaid, M., Khalil, H. A., Bakar, A. A., Hassan, A., and Dungani, R., 2013. "Effect of jute fibre loading on the mechanical and thermal properties of oil palm–epoxy composites". *Journal of Composite Materials,* **47**(13), pp. 1633–1641.

[174] Mylsamy, K., and Rajendran, I., 2011. "Influence of alkali treatment and fibre length on mechanical properties of short agave fibre reinforced epoxy composites". *Materials & Design,* **32**(8-9), pp. 4629–4640.

[175] Sharma, B., and van der Vegte, A., 2020. "Engineered bamboo for structural applications". In *Nonconventional and vernacular construction materials*. Elsevier, pp. 597–623.

[176] Verma, C., Purohit, R., Rana, R., and Mohit, H., 2017. "Mechanical properties of bamboo laminates with other composites". *Materials Today: Proceedings,* **4**(2), pp. 3380–3386.

[177] Lou, Z., Han, X., Liu, J., Ma, Q., Yan, H., Yuan, C., Yang, L., Han, H., Weng, F.,

and Li, Y., 2021. "Nano-fe3o4/bamboo bundles/phenolic resin oriented recombination ternary composite with enhanced multiple functions". *Composites Part B: Engineering,* **226**, p. 109335.

[178] Wang, Q., Han, H., Lou, Z., Han, X., Wang, X., and Li, Y., 2022. "Surface property enhancement of bamboo by inorganic materials coating with extended functional applications". *Composites Part A: Applied Science and Manufacturing,* **155**, p. 106848.

[179] Zhang, H., Li, H., Li, Y., Xiong, Z., Zhang, N., Lorenzo, R., and Ashraf, M., 2021. "Effect of nodes on mechanical properties and microstructure of laminated bamboo lumber units". *Construction and Building Materials,* **304**(6), p. 124427.

[180] Guo, W., Kalali, E. N., Wang, X., Xing, W., Zhang, P., Song, L., and Hu, Y., 2019. "Processing bulk natural bamboo into a strong and flame-retardant composite material". *Industrial Crops and Products,* **138**(1), p. 111478.

[181] Kalali, E. N., Hu, Y., Wang, X., Song, L., and Xing, W., 2019. "Highly-aligned cellulose fibers reinforced epoxy composites derived from bulk natural bamboo". *Industrial Crops and Products,* **129**, pp. 434–439.

[182] Gu, F., Zheng, Y., Zhang, W., Yao, X., Pan, D., Wong, A. S. M., Guo, J., Hall, P., and Sharmin, N., 2018. "Can bamboo fibres be an alternative to flax fibres as materials for plastic reinforcement: A comparative life cycle study on polypropylene/flax/bamboo laminates". *Industrial Crops and Products,* **121**, pp. 372–387.

[183] Qian, D., Bao, L., Takatera, M., Kemmochi, K., and Yamanaka, A., 2010. "Fiber-reinforced polymer composite materials with high specific strength and excellent solid particle erosion resistance". *Wear,* **268**(3-4), pp. 637–642.

[184] Rajmohan, T., Palanikumar, K., and Ranganathan, S., 2013. "Evaluation of mechanical and wear properties of hybrid aluminium matrix composites". *Transactions of nonferrous metals society of China,* **23**(9), pp. 2509–2517.

[185] Lakkad, S., and Patel, J., 1981. "Mechanical properties of bamboo, a natural composite". *Fibre science and technology,* **14**(4), pp. 319–322.

[186] Awad, Z. K., Aravinthan, T., and Manalo, A., 2012. "Geometry effect on the behaviour of single and glue-laminated glass fibre reinforced polymer composite sandwich beams loaded in four-point bending". *Materials & Design,* **39**, pp. 93–103.

[187] Venkatesha, B., Kumar, S. P., Saravanan, R., and Ishak, A., 2020. "Tension fatigue behaviour of woven bamboo and glass fiber reinforced epoxy hybrid composites". In IOP conference series: materials science and engineering, Vol. 1003, IOP Publishing, p. 012087.

[188] Harries, K. A., Bumstead, J., Richard, M., and Trujillo, D., 2017. "Geometric and material effects on bamboo buckling behaviour". *Proceedings of the Institution of Civil Engineers-Structures and Buildings,* **170**(4), pp. 236–249.

[189] Shah, D. U., Schubel, P. J., Clifford, M. J., and Licence, P., 2013. "Fatigue life evaluation of aligned plant fibre composites through s–n curves and constant-life diagrams". *Composites Science and Technology,* **74**(12), pp. 139–149.

[190] Bianchini, A., Ferrara, G., and Ferrari, L., 2015. "Design guidelines for h-darrieus wind turbines: Optimization of the annual energy yield". *Energy Conversion and Management,* **89**, pp. 690–707.

[191] Islam, M., Fartaj, A., and Carriveau, R., 2008. "Analysis of the design parameters related to a fixed-pitch straight-bladed vertical axis wind turbine". *Wind engineering,* **32**(5), pp. 491–507.

[192] Hameed, M. S., and Afaq, S. K., 2013. "Design and analysis of a straight bladed vertical axis wind turbine blade using analytical and numerical techniques". *Ocean Engineering,* **57**(3), pp. 248–255.

[193] Ahmadi-Baloutaki, M., Carriveau, R., and Ting, D. S., 2014. "Straight-bladed vertical axis wind turbine rotor design guide based on aerodynamic performance and loading analysis". *Proceedings of the Institution of Mechanical Engineers, Part A: Journal of Power and Energy,* **228**(7), pp. 742–759.

[194] Atlaschian, O., and Metzger, M., 2021. "Numerical model of vertical axis wind turbine performance in realistic gusty wind conditions". *Renewable Energy,* **165**, pp. 211–223.

[195] Rezaeiha, A., Montazeri, H., and Blocken, B., 2018. "Towards optimal aerodynamic design of vertical axis wind turbines: Impact of solidity and number of blades". *Energy,* **165**, pp. 1129–1148.

[196] Hand, B., and Cashman, A., 2017. "Conceptual design of a large-scale floating offshore vertical axis wind turbine". *Energy Procedia,* **142**, pp. 83–88.

[197] Raju, B., Hiremath, S., and Mahapatra, D. R., 2018. "A review of micromechanics based models for effective elastic properties of reinforced polymer matrix composites". *Composite Structures,* **204**, pp. 607–619.

[198] Zhou, X.-Y., Gosling, P., Pearce, C., Ullah, Z., and Kaczmarczyk, L., 2016.

"Perturbation-based stochastic multi-scale computational homogenization method for woven textile composites". *International Journal of Solids and Structures,* **80**, pp. 368–380.

[199] Omairey, S. L., Dunning, P. D., and Sriramula, S., 2019. "Development of an abaqus plugin tool for periodic rve homogenisation". *Engineering with Computers,* **35**, pp. 567–577.

[200] Cheng, G.-D., Cai, Y.-W., and Xu, L., 2013. "Novel implementation of homogenization method to predict effective properties of periodic materials". *Acta Mechanica Sinica,* **29**(4), pp. 550–556.

[201] Mohammed, Y., Hassan, M. K., El-Ainin H, A., and Hashem, A., 2014. "Effect of stacking sequence and geometric scaling on the brittleness number of glass fiber composite laminate with stress raiser". *Science and Engineering of Composite Materials,* **21**(2), pp. 281–288.

[202] Belfkira, Z., Mounir, H., and El Marjani, A., 2021. "Structural optimization of a horizontal axis wind turbine blade made from new hybrid composites with kenaf fibers". *Composite Structures,* **260**(1), p. 113252.

[203] Cox, K., and Echtermeyer, A., 2014. "Effects of composite fiber orientation on wind turbine blade buckling resistance". *Wind Energy,* **17**(12), pp. 1925–1943.

[204] Singh, R., Sharma, S., and Singh, S., 2018. "Effect of blade thickness on the natural frequency of h-rotor vertical axis wind turbine". *International Journal of Mechanical and Production Engineering Research and Development*, pp. 187–193.

[205] Santo, G., Peeters, M., Van Paepegem, W., and Degroote, J., 2019. "Dynamic

load and stress analysis of a large horizontal axis wind turbine using full scale fluid-structure interaction simulation". *Renewable energy,* **140**, pp. 212–226.

[206] El Chazly, N., 1993. "Static and dynamic analysis of wind turbine blades using the finite element method". *Renewable energy,* **3**(6-7), pp. 705–724.

[207] Jokar, H., Mahzoon, M., and Vatankhah, R., 2020. "Dynamic modeling and free vibration analysis of horizontal axis wind turbine blades in the flap-wise direction". *Renewable Energy,* **146**, pp. 1818–1832.

[208] Spears, R., and Jensen, S., 2012. "Approach for selection of rayleigh damping parameters used for time history analysis". *Journal of pressure vessel technology,* **134**(6), p. 061801.

[209] Murray, R. E., Beach, R., Barnes, D., Snowberg, D., Berry, D., Rooney, S., Jenks, M., Gage, B., Boro, T., Wallen, S., et al., 2021. "Structural validation of a thermoplastic composite wind turbine blade with comparison to a thermoset composite blade". *Renewable Energy,* **164**(4), pp. 1100–1107.

[210] Zhang, J., Guo, L., Wu, H., Zhou, A., Hu, D., and Ren, J., 2014. "The influence of wind shear on vibration of geometrically nonlinear wind turbine blade under fluid–structure interaction". *Ocean engineering,* **84**, pp. 14–19.

[211] Popelka, D., 1982. Aeroelastic stability analysis of a darrieus wind turbine. Tech. rep., Sandia National Lab.(SNL-NM), Albuquerque, NM (United States).

[212] Cheng, Z., Madsen, H. A., Gao, Z., and Moan, T., 2016. "Numerical study on aerodynamic damping of floating vertical axis wind turbines". In Journal of Physics: Conference Series, Vol. 753, IOP Publishing, p. 102001.

[213] Jones, W. P., and Launder, B. E., 1972. "The prediction of laminarization with a two-equation model of turbulence". *International journal of heat and mass transfer,* **15**(2), pp. 301–314.

[214] Wilcox, D. C., 2008. "Formulation of the kw turbulence model revisited". *AIAA journal,* **46**(11), pp. 2823–2838.

[215] Kim, B., Kim, W., Bae, S., Park, J., and Kim, M., 2011. "Aerodynamic design and performance analysis of multi-mw class wind turbine blade". *Journal of Mechanical Science and Technology,* **25**(8), pp. 1995–2002.

[216] Yelmule, M. M., and Vsj, E. A., 2013. "Cfd predictions of nrel phase vi rotor experiments in nasa/ames wind tunnel". *International journal of renewable energy research,* **3**(2), pp. 261–269.

[217] Lipian, M., Czapski, P., and Obidowski, D., 2020. "Fluid–structure interaction numerical analysis of a small, urban wind turbine blade". *Energies,* **13**(7), p. 1832.

Brief Biodata of the Author

The author, Mridusmita Bora, was born in the year 1993 in the Guwahati city of Assam State. She graduated in Civil Engineering in the year 2016 from Royal School of Engineering and Technology, Guwahati affiliated with Gauhati University, Guwahati (Assam). She worked as an employee in the consultancy, "ADMECA Design and Engineering Solutions, LLP" as an structural engineer. In July, 2018 she joined the Ph.D program at IIT Guwahati in the School of Energy Science and Engineering and this research work is carried out during this period.

List of Publications from the Thesis

List of Publications in International Journals

1. **Journal Publications:**

   - Bora, M., Kumari, P. and Sahoo, N., 2022. Mechanical properties of Assam's bamboo-epoxy composite laminates - An experimental investigation. Industrial Crops and Products, 188, p.115556. DOI -:10.1016/j.indcrop.2022.115556
   - Bora, M., Sharma, A.V., Kumari, P. and Sahoo, N., 2023. Investigation of bamboo-based vertical axis wind turbine blade under static loading. Ocean Engineering, 285, P.115317. DOI -:10.1016/j.oceaneng.2023.115317
   - Bora, M., Kumari, P. and Sahoo, N. Dynamic vibration analysis of bamboo composite vertical axis wind turbine blades. (Submitted to the journal, Ocean engineering, Elsevier)

2. **Conferences:**

   - Bora, M., Sharma, A.V., Kumari, P. and Sahoo, N. Investigation of the mechanical behavior of the treated and untreated bamboo fiber reinforced epoxy composites – Assam's Bamboo, at ICCS24 – 24th International Conference on Composite Structure, Porto 14 -16th June. (International conference)
   - Bora, M., Kumari, P. and Sahoo, N. Mechanical strength evaluation of bamboo-composites for its use in low to medium scale structural components, North East Research Conclave, NERC 2022, IIT Guwahati, 20-22nd May, 2022. (National Conference)

- Bora, M., Kumari, P. and Sahoo, N. Study on strength evaluation of bamboo-epoxy composite laminates for different stacking combinations, International conference on 67th congress of the Indian Society of Theoretical and Applied Mechanics (ISTAM), IIT Mandi 14-16th December, 2022. (International Conference)

- Bora, M., Kumari, P. and Sahoo, N. A numerical investigation on the structural design and analysis of bamboo wind turbine blade, 11th International conference on Materials for Advanced Technologies, ICMAT-2023, Singapore 26–30th June, 2023 (International conference).